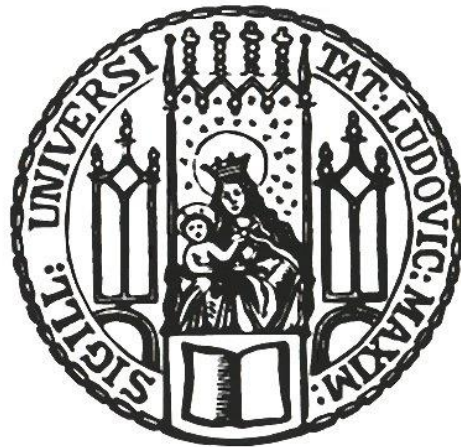


**Neurotransmitters in the neuronal  
circuit for motion vision in  
*Drosophila melanogaster***

Katarina Pankova



Dissertation

Graduate School of Systemic Neurosciences

Ludwig-Maximilians-Universität München

Submitted on May 12<sup>th</sup>, 2017

**First reviewer (supervisor):** Prof. Dr. Alexander Borst

**Second reviewer:** Prof. Dr. Ilona Grunwald Kadow

**Oral defense:** October 20<sup>th</sup>, 2017



# SUMMARY

Understanding how neuronal circuits perform computations on the cellular and molecular level is a crucial step towards deciphering how brains function. Yet, the complete elucidation of mechanisms underlying simple computations such as the visual detection of movement is still missing. In this dissertation, I employ genetically accessible model organism *Drosophila melanogaster* to investigate the neurotransmitter systems that are used by cells in the neuronal circuit for motion vision.

The contribution of this dissertation to current knowledge about the neuronal circuit for motion vision in *D. melanogaster* is as follows:

In the publication “Neural circuit to integrate opposing motions in the visual field”, together with my colleagues, we identify two new types of neurons in the motion vision circuit termed LPi3-4 and LPi4-3 cells that receive input from the local motion detectors, the T4 and T5 neurons and provide inhibitory input to wide-field motion-selective lobula plate tangential cells. Using antibody immunostainings and single-cell transcriptome analysis, we show that the neurotransmitter used by the LPi3-4 and LPi4-3 neurons is glutamate. Glutamate released from the LPi3-4 neurons opens a chloride channel GluCl $\alpha$  on the dendrites of the LPTCs and thus, its role at this synapse is inhibitory. In addition, we demonstrate that the LPi3-4 neurons are necessary for tuning of the lobula plate tangential cells to movement in a specific direction in naturalistic situations where competing visual stimuli moving in various directions are present.

In the publication “RNA-seq transcriptome analysis of direction-selective T4/T5 neurons in *Drosophila*”, I provide the first genome - wide transcriptome analysis of the T4 and T5 neurons. The obtained gene expression database characterizes the expression levels of all neurotransmitter receptors in T4 and T5 neurons and thus, gives information on which neurotransmitters provide input to T4 and T5 neurons. Moreover, the transcriptome analysis reveals the co-existence of the cholinergic and GABAergic markers in *D. melanogaster* neurons that has not been described previously. This study also analyzes the

biophysical implementation of the computations performed by the T<sub>4</sub> and T<sub>5</sub> neurons on the molecular level.

In the publication “Transgenic line for the identification of cholinergic release sites in *Drosophila melanogaster*”, using the newly generated FRT-STOP-FRT-VAcH<sub>T</sub>::HA allele, I show that the Mi<sub>1</sub> and Tm<sub>3</sub> neurons possess cholinergic release sites in their axons and thereby likely provide cholinergic input to the local motion detectors, the T<sub>4</sub> neurons. The FRT-STOP-FRT-VAcH<sub>T</sub>::HA allele described in this study is a universal tool that can serve for the identification of cholinergic cells also in other neuronal circuits in *D. melanogaster*.

# ACKNOWLEDGEMENT

I would like to thank my supervisor Axel Borst for giving me the opportunity to discover the beauty of fly brains and freedom to choose what I wanted to work on. I would also like to thank Wolfgang Essbauer for his help with cloning, embryo injections and fly work, Michi Sauter for countless brain dissections and Romina Kutlesa and Christian Theile for running the behavioral tests. I appreciate the help with calcium imaging I got from Alexander Arenz and Michi Drews and I am thankful to Alex Mauss for letting me use his e-phys rig.

I am grateful to the members of Oliver Griesbeck's lab for sharing their tips and tricks on the molecular biology techniques and cloning. In particular, I would like to thank Arne Fabritius for all his advice and willingness to troubleshoot. I am also grateful to Robert Kasper for introducing me to super-resolution microscopy techniques and for his enthusiastic support. I would also like to thank my colleague Ines Ribeiro for the help with data analysis and for providing useful comments on the first draft of this dissertation.

# CONTENT

## 1| INTRODUCTION 1

- 1.1 *DROSOPHILA MELANOGASTER* AS A MODEL ORGANISM 1
  - 1.1.1 *Genetic manipulations in D. melanogaster* 1
  - 1.1.2 *D. melanogaster in circuit neuroscience* 4
- 1.2 NEUROTRANSMITTERS IN *D. MELANOGASTER* 5
  - 1.2.1 *Acetylcholine* 6
  - 1.2.2 *Glutamate* 7
  - 1.2.3 *GABA* 7
  - 1.2.4 *Monoamines* 8
  - 1.2.5 *Assessment of the neurotransmitter phenotype* 9
- 1.3 VISUAL SYSTEM OF *D. MELANOGASTER* 12
  - 1.3.1 *Neuronal circuit for motion vision* 13
- 1.4 COMPUTATIONS UNDERLYING DIRECTION SELECTIVITY 18
- 1.5 AIMS OF THIS DISSERTATION 20

## 2| PUBLICATIONS 21

- 2.1 NEURAL CIRCUIT TO INTEGRATE OPPOSING MOTIONS IN THE VISUAL FIELD 21
- 2.2 RNA-SEQ TRANSCRIPTOME ANALYSIS OF DIRECTION-SELECTIVE T4/T5 NEURONS IN *DROSOPHILA* 48
- 2.3 TRANSGENIC LINE FOR THE IDENTIFICATION OF CHOLINERGIC RELEASE SITES IN *DROSOPHILA MELANOGASTER* 61

## 3| DISCUSSION 68

- 3.1 MECHANISM UNDERLYING DIRECTION SELECTIVITY IN THE T4 AND T5 NEURONS 68
- 3.2 VGAT IN T4 AND T5 NEURONS 2
  - 3.2.1 *Approach to generate a conditional knock-in of the VGAT gene* 70
  - 3.2.2 *Approach to visualize VGAT using super-resolution microscopy* 70
  - 3.2.3 *Possible roles of VGAT* 71
- 3.3 INHIBITORY ROLE OF GLUTAMATE IN NEURONAL CIRCUITS 73
- 3.4 PROS AND CONS OF THE FRT-STOP-FRT-VACHT::*HA* ALLELE 75
- 3.5 CONCLUSION 77

## 4| BIBLIOGRAPHY 78

# 1 | INTRODUCTION

## 1.1 *DROSOPHILA MELANOGASTER* AS A MODEL ORGANISM

The first use of a common fruit fly *Drosophila melanogaster* in scientific experiments can be traced back to early 1900s. Owing to pioneering work of Thomas H. Morgan on the chromosomal mapping of genes using fruit fly mutants, *D. melanogaster* became the experimental organism of choice for the generations of geneticists to follow. When compared to vertebrate model organisms, the key advantage for using fruit flies in research is that they are easy and inexpensive to rear and maintain. In addition, their short life cycle, sequenced genome (Adams et al., 2000) and variety of genetic tools available make them ideal candidates to tackle almost any biological question.

Several influential findings that have broadened our understanding of the molecular mechanisms of human biology and disease processes have been made with *D. melanogaster*. Among the most significant are the discovery of homeotic genes that regulate embryonic development (Lewis, 1978; Nüsslein-Volhard and Wieschaus, 1980) and the elucidation of the role of Toll receptors family in innate immunity (Lemaitre et al., 1996).

### 1.1.1 *Genetic manipulations in D. melanogaster*

The earliest approaches to genetic manipulation of fruit flies involved use of X-rays (Muller, 1927) and chemical mutagens such as ethyl methanesulfonate (EMS) (Alderson, 1965) that produced a substantial number of loss-of-function mutant strains. A revolutionary tool to perform not only gene disruptions but also to introduce transgenes into fruit fly genome emerged after the discovery of P element transposons in 1970s (Kidwell et al., 1977). The P elements are DNA sequences that can change their position within genome by their excision and re-insertion. Interestingly, the excision and reinsertion of P elements is mediated by the enzyme transposase which is encoded in the P element sequence. This



arrangement allows a P element to autonomously “jump” within a genome. An elegant way for using P elements to generate transgenic flies came with an idea for the separation of the two functional components of a P element, the gene for transposase enzyme and the recognition sequences for transposase action (Rubin and Spradling, 1982). By attaching the P element recognition sites to a foreign DNA and by providing a source of transposase, the foreign DNA can easily be incorporated into the fly genome.

Another important milestone in the development of genetic tools in *D. melanogaster* was the recruitment of two of the yeast binary gene regulatory systems: the GAL4/UAS expression system (Brand and Perrimon, 1993) and the FLP/FRT recombination system (Golic and Lindquist, 1989; Golic, 1991) (Figure 1).

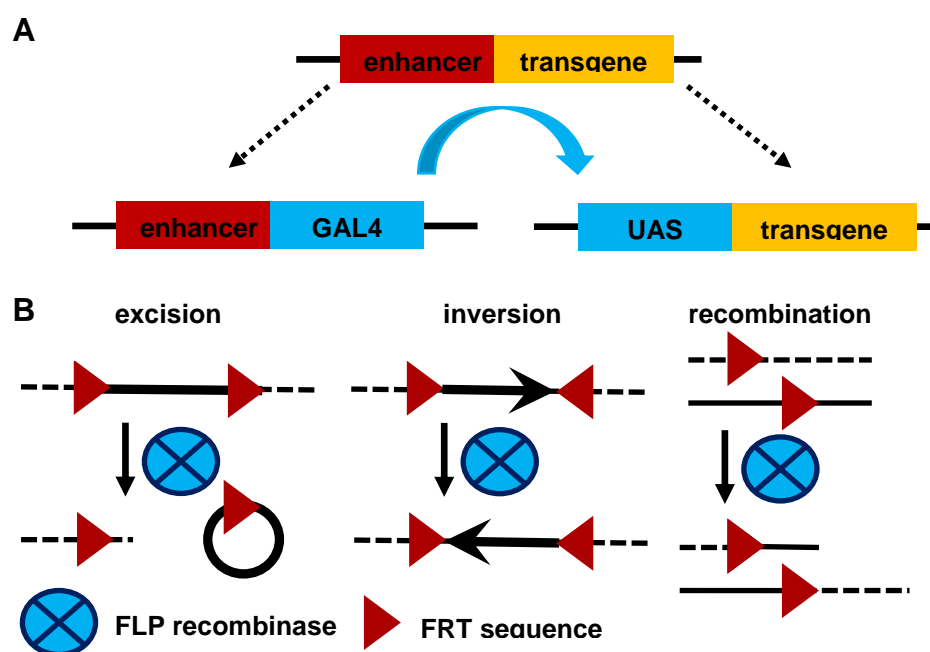


**Figure 1. The Gal4/UAS and the FRT/FLP systems.** A) The earliest approaches to a tissue-specific transgene expression involved the fusion of a genomic enhancer to a transgene of choice (upper illustration). The binary expression systems such as GAL4/UAS separate the enhancer and transgene components allowing for the versatile combinatorial expression of transgenes. The genomic enhancer that is active in a specific tissue or a set of cells triggers the expression of a GAL4 transcription factor. The GAL4 protein in turn binds to the UAS sequence and initiates the transcription of a transgene. B) The flippase (FLP) recognizes the FRT sequences and mediates recombination between them. Depending on the organization of the FRT sites in the genome, various genetic modifications such as sequence excision, inversion or chromosomal recombination are possible.

Subsequent and still ongoing expansion of the genetic tools in *Drosophila* is largely based on the refinement and combinatorial use of the GAL4/UAS, FRT/FLP and other binary expression systems.

A relatively new technique for genome editing in flies relies on CRISPR/Cas9-induced single- or double-break cleavages in defined genomic locations (Gratz et al., 2013) (Figure 2). Due to its simplicity and versatility, this approach holds a promise to engineer flies on demand in a timely manner with virtually any sort of genome modification ranging from inactivation of a selected gene to insertion of complex engineered foreign sequences.

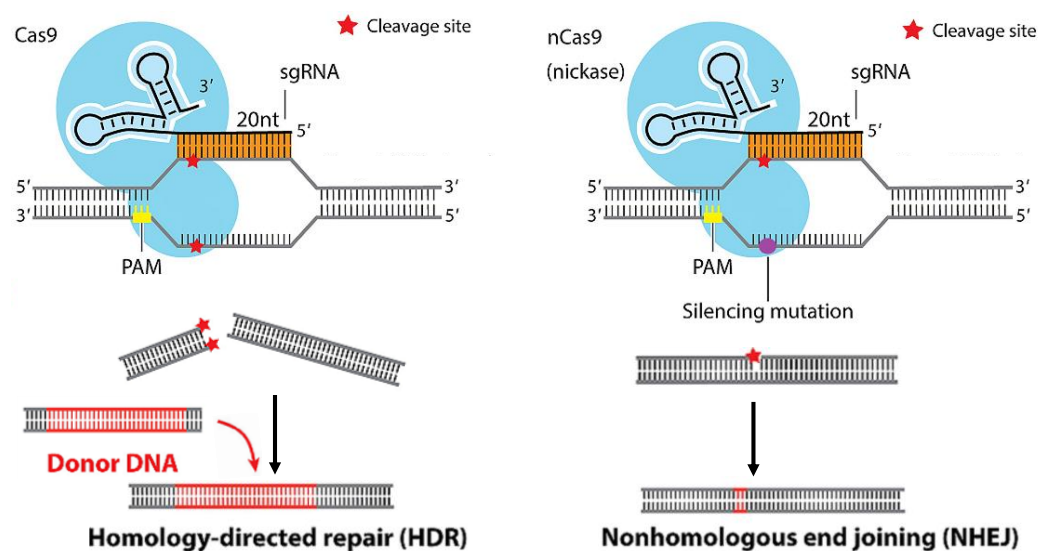


**Figure 2. Mechanism of the site-specific DNA cleavage mediated by the CRISPR/Cas9 system.** (Adapted from Wang et al., 2016). The sequence of 20 nucleotides in the 5' of the sgRNA pairs with the complementary sequence in the genomic DNA. In order for the Cas9-mediated DNA digestion to occur, a specific three-nucleotide sequence called PAM must be present on the DNA strand opposite to the target strand. Cas9 (left) digests both DNA strands while its mutated version nCas9 (right) only cleaves one DNA strand.

The CRISPR (clustered regularly interspaced short palindromic repeats) are segments in the prokaryotic DNA that together with Cas proteins create adaptive immunity system of bacteria and archaea (Barrangou et al., 2007). The Cas9 protein from *Streptococcus pyogenes* is a DNA endonuclease that interacts with RNA molecules which navigate the Cas9 protein to a specific DNA sequence that are then cut by Cas9 (Jinek et al., 2012). For the genome editing purposes, the RNA molecules that interact with Cas9 can be reduced to a single RNA molecule (termed single-guide

RNA or sgRNA) that consists of a constant region which interacts with the Cas9 protein and a variable 20-nucleotide region that binds to the complementary DNA (Jinek et al., 2012).

In order for the DNA to be cut by the Cas9 protein, a specific three-nucleotide sequence called PAM must be present in the DNA sequence adjacent to the sgRNA binding site but on the opposite strand (Figure 2). The key advantage for using the Cas9-mediated approach to induce breaks in the DNA is that the site-specificity of the Cas9-induced cleavages is based on the easily interchangeable 20 nucleotide recognition sequence of the sgRNA.

The Cas9 protein causes double-strand breaks in the DNA (Jinek et al., 2012). These breaks can be used as a site for the insertion of a donor DNA which is incorporated to the genome by the homology-directed repair (HDR) mechanism. The insertion of the donor DNA can be used to generate gene knock-ins, correct genes or introduce any other sequence of choice. A mutated version of Cas9 called nCas9 (or nickase) only digests one DNA strand (Jinek et al., 2012). Single-strand DNA breaks can be repaired by the non-homologous end joining (NHEJ) mechanism which leads to random deletions or insertions and, as a result, shifts the reading frame giving rise to loss-of-function alleles.

### 1.1.2 *D. melanogaster* in circuit neuroscience

The relation between the brain structure and function at the cellular and molecular levels is the subject of study of circuit (or systems) neuroscience. One advantage of using *D. melanogaster* as a model for studying neuronal circuits is the relative simplicity of its nervous system. The nervous system of a fly consists of two ganglia, one located in head and one in thorax, and peripheral nerves extending from these ganglia. The head ganglion, commonly referred to as brain, comprises an estimated 100 000 – 150 000 neurons. In addition, apart from certain experience-triggered synaptic plasticity (Kanamori et al., 2015; Yaniv and Schuldiner, 2016), the fly brain is to substantial extent hard-wired allowing for a reproducible identification of every neuron in every individual (Chiang et al., 2011). Yet, despite the relative simplicity of the fly brain, fruit flies still display variety of complex behaviors making them an attractive system to study. As the basic principles of how neuronal circuits function are largely shared across the species, findings

from studying the nervous system of a fruit fly can often be transferred to mammalian systems.

As for the drawbacks of using *D. melanogaster* as a model organism in circuit neuroscience, it is mainly the small size of neurons that makes it difficult to perform electrophysiological recordings from single neurons. To overcome this issue, several tools for the optical recording from *Drosophila* neurons have been developed. In comparison to electrophysiological recordings, the genetically encoded calcium reporters and voltage sensors allow for monitoring of neuronal activity with higher throughput and spatial precision, although not with the same temporal acuity (Cao et al., 2013; Chen et al., 2013, Gong et al., 2015; Yang et al., 2016).

Functional dissection of neuronal circuits in fruit flies is greatly facilitated by the possibility to precisely manipulate the activity of neurons within a circuit. Currently, several thousands of GAL4 lines with the expression in various neuronal populations are available (Pfeiffer et al., 2008; Jenett et al., 2012; Kvon et al., 2014). In combination with the sophisticated tools for activation and silencing of neurons in a temporally defined way, the role of individual neurons within a circuit can be relatively easily examined.

## **1.2 NEUROTRANSMITTERS IN *D. MELANOGASTER***

Neurotransmitters are small molecules that are stored in synaptic vesicles and released to the extracellular environment upon activation of a neuron. Once released, neurotransmitter diffuses through the synaptic cleft and binds to membrane receptors on the postsynaptic neuron. Binding of a neurotransmitter to its receptor leads to direct opening of ion channels or activation of second messenger signaling cascade in the postsynaptic neuron. The type of neurotransmitter receptor defines what action will take place in the postsynaptic neuron. Fast ionotropic receptors are ligand-gated ion channels with different degree of selectivity for sodium, potassium, calcium or chloride that cause immediate depolarization or hyperpolarization of a neuron. The other group of neurotransmitter receptors, the slow metabotropic G protein-coupled receptors, trigger a variety of second messenger-induced events that in general affect membrane permeability on a larger timescale. A single neuron can express both, ionotropic and metabotropic receptors for several neurotransmitters simultaneously and thus, integrate a

variety of incoming signals. Understanding of which neurotransmitters and receptors participate at a synapse is therefore crucial for deciphering the computations taking place in neuronal circuits.

In *D. melanogaster*, eight different neurotransmitters have been identified so far: acetylcholine, glutamate, GABA, dopamine, serotonin, octopamine, tyramine and histamine (Martin and Krantz, 2014). In comparison to vertebrates, there is no evidence for the use of ATP or nitric oxide as neurotransmitters. Another distinction between *D. melanogaster* and vertebrate neurotransmitter systems is that no co-release of two or more neurotransmitters from a single neuron has been documented in fruit flies so far.

A neurotransmitter is either synthesized in a neuron or enters a neuron via a dedicated membrane transporter. From the cytosolic space, a neurotransmitter is loaded into synaptic vesicles with a vesicular neurotransmitter transporter. Depending on the type of neurotransmitter, the degradation of a neurotransmitter can take place either in the extracellular milieu or intracellularly, in a neuron or a glial cell. The neurotransmitter synthesizing and degrading enzymes as well as the vesicular and membrane transporters can serve as markers of the neurotransmitter phenotype of a neuron, assuming that their function is restricted to neurotransmitter metabolism or transport.

### *1.2.1 Acetylcholine*

Acetylcholine is a major excitatory neurotransmitter in the fly nervous system. The biosynthesizing enzyme of acetylcholine is choline acetyltransferase (ChAT) that catalyzes the fusion of choline with acetylcoenzyme A (Figure 3) (Salvaterra and McCaman, 1985). Loading of the acetylcholine to synaptic vesicles is mediated by the vesicular acetylcholine transporter (VACHT) (Kitamoto et al., 1998). Degradation of acetylcholine occurs extracellularly in the synaptic cleft by the separation of the acetyl residue from choline by the enzyme acetylcholine esterase (AChE) that is found in the synaptic cleft (Haas et al., 1988). Choline is then transported into the presynaptic neuron via a dedicated membrane choline transporter and re-used for the further synthesis of acetylcholine. The choline transporter has already been studied extensively in mammals (Parikh et al., 2013; Traiffort et al., 2013).

However, in fruit flies, the function of the homologue gene, the CG7708, has not been experimentally confirmed yet.

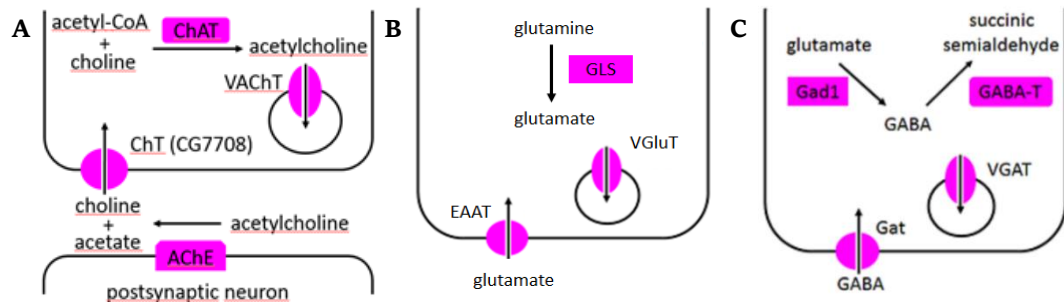


**Figure 3. Metabolism of acetylcholine, glutamate and GABA in a presynaptic neuron.** (A) The markers of the cholinergic neurons in fruit flies are ChAT and VAcHT. The *D. melanogaster* gene CG7708 is a structural homologue of choline transporter, however, its role in the transport of choline in fruit flies has not been confirmed experimentally, yet. (B) Glutamatergic neurons can be identified by the presence of VGLuT. The GLS and EAAT have not been identified as necessary for the glutamatergic transmission in *D. melanogaster*, yet. (C) The known markers of the GABAergic neurons are Gad1, VGAT, Gabat and Gat.

### 1.2.2 Glutamate

Glutamate in fruit flies can have either an excitatory or inhibitory effect on the postsynaptic neuron, depending on the type of receptors it expresses (Liu and Wilson, 2013). Glutamate is an amino acid, a building block of proteins, and therefore is abundantly present in all cells. The most common biosynthetic precursor of glutamate is glutamine that can be converted to glutamate by enzyme glutaminase (GLS) (Chase and Kankel, 1987). The packaging of glutamate into synaptic vesicles is mediated by the vesicular glutamate transporter (VGLuT) (Daniels et al., 2004) (Figure 3). Glutamate is removed from the synaptic cleft by the excitatory amino acid transporters (EAATs) that are present either on neurons or glia (Besson et al., 1999).

### 1.2.3 GABA

The main inhibitory neurotransmitter in *D. melanogaster* is GABA. So far, the only described metabolic pathway to synthesize GABA in fruit flies is from glutamate with the enzyme glutamate decarboxylase (Gad1) (Featherstone et al., 2000) (Figure 3). The transport of GABA into synaptic vesicles is achieved by the vesicular GABA transporter (VGAT)

(Fei et al., 2010). GABA released into the synaptic cleft is cleared by its re-uptake into neurons or glia with the membrane GABA transporter (Gat) (Neckameyer and Cooper, 1998). Degradation of GABA in GABAergic neurons is performed by GABA transaminase (GabaT) that converts GABA to succinic semialdehyde which is in turn further metabolized in the Krebs cycle (Balazs et al., 1970; Chen et al., 2015).

#### *1.2.4 Monoamines*

The neurotransmitters serotonin, dopamine, octopamine, tyramine and histamine have in common that from the chemical point of view, they are all derived from aromatic amino acids and contain one amino residue. In addition, all monoamine neurotransmitters in a fruit fly are loaded into synaptic vesicle with the same type of transporter: the vesicular monoamine transporter (Vmat) (Greer et al., 2005; Romero-Calderón et al., 2008).

The precursor for the synthesis of histamine is histidine that is converted to histamine by the action of histidine decarboxylase (Hdc) (Burg et al., 1993). From the synaptic cleft, histamine is re-uptaken by glial cells that convert histamine into carcinine. Carcinine is then transported back into neurons via CarT transporter and converted to histamine with tan hydrolase (Borycz et al., 2002; Stenesen et al., 2015).

For the synthesis of dopamine, octopamine and tyramine, the starting substrate is the amino acid tyrosine. Tyrosine is converted in one-step reaction into tyramine with an enzyme tyrosine decarboxylase (Tdc) (Livingstone and Tempel, 1983). Tyramine can in turn be transformed into octopamine with an enzyme tyramine beta-hydroxylase (Tbh) (Monastirioti et al., 1996). For the synthesis of dopamine, the tyrosine is first converted to L-DOPA with tyrosine hydroxylase (ple or also known as TH) (Friggi-Grelin et al., 2003). In the next step, dopa decarboxylase (Ddc) catalyzes conversion of L-DOPA to dopamine (Livingstone and Tempel, 1983). Serotonin is in fruit flies synthesized from amino acid tryptophan that is converted to 5-hydroxytryptophan with tryptophan hydroxylase (Trh). The 5-hydroxytryptophan is subsequently turned into serotonin in a reaction catalyzed by Ddc (Livingstone and Tempel, 1983).

From the synaptic cleft, dopamine and serotonin are removed with dedicated transporters, DAT and SerT, respectively (Corey et al., 1994; Demchyshyn et al., 1994; Pörzgen et al., 2001). In mammals, the crucial

enzyme involved in the degradation of dopamine and serotonin is monoamine oxidase (MAO). Based on the sequence similarity, the predicted homologue of MAO in *D. melanogaster* is the CG5653 gene. However, the function of CG5653 in the neurotransmitter metabolism has not been confirmed yet.

A plasma membrane transporters of octopamine and tyramine have not been identified in fruit flies so far, neither are understood the pathways that lead to degradation of these neurotransmitters. Interestingly, octopamine transporter has been already described in other insect species (Malutan et al., 2002).

### *1.2.5 Assessment of the neurotransmitter phenotype*

The neurotransmitter phenotype of a cell is commonly examined by scrutinizing the expression of the transporters or enzymes involved in the neurotransmitter life-cycle. The expression of neurotransmitter marker genes (or any protein-encoding gene in general) can be examined on three distinct levels: 1.) presence of a protein, 2.) presence of mRNA or 3.) transcription level of the relevant genomic region. Available methods for addressing the presence of the neurotransmitter markers on each of these three levels are outlined below.

Proving the expression of proteins which are localized to the presynaptic release sites such as neurotransmitter transporters on the synaptic vesicles is not trivial in *Drosophila* neurons. The small diameter of the dendrites and axons does not allow for a reliable cell-type specific detection of the synaptically localized proteins using whole-brain staining with antisera and traditional confocal microscopy. The super-resolution microscopy techniques such as STED or STORM might provide a solution to this issue, nevertheless, reaching the satisfactory resolution in a three-dimensional tissue blocks such as fly brain is, has not been demonstrated yet. The detection of neurotransmitter markers on the protein level is thus restricted to the examination of their presence in the neuronal cell bodies. This approach, however, might lead to false negative interpretation of the results: the inability to detect a marker protein in the soma does not necessarily mean that it is not present in other neuronal compartments. For several neurotransmitter markers either specific antibodies or tagged gene knock-ins in the endogenous loci are available (Takagawa and Salvaterra, 1996; Kitamoto et al., 1998;



Featherstone et al., 2000; Daniels et al., 2004; Greer et al., 2005; Romero-Calderón et al., 2008; Fei et al., 2010; Sarov et al., 2016).

Detection of markers at the level of mRNA requires isolation of cell type-specific mRNA. This can be done either by manual or FACS-based sampling of the labelled neuronal somata or, alternatively, by immunoprecipitation of the tagged nuclei or ribosomes from many fly brains simultaneously. Depending on the amount of mRNA collected, the transcripts can be analyzed either by RT-PCR or with high-throughput approaches such as microarrays or RNA-seq (Figure 4).

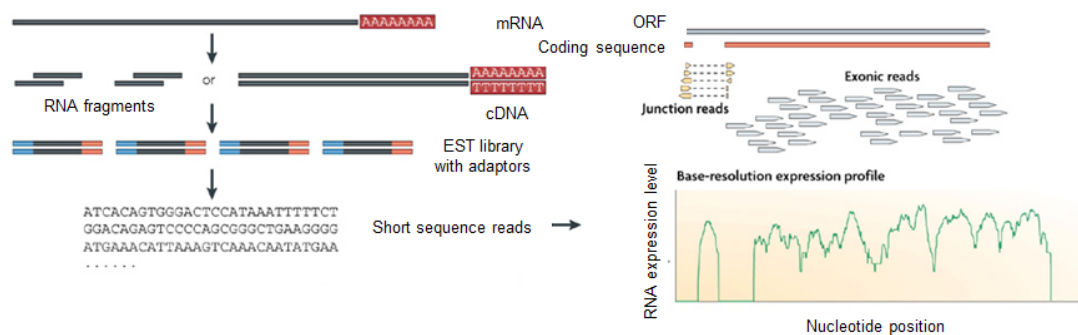


**Figure 4. RNA-seq workflow.** (Adapted from Wang et al., 2009 with permission). The isolated mRNA is converted into a library in a process that involves fragmentation and cDNA synthesis (the order of these two steps is interchangeable). The result of sequencing are short reads that are aligned to a genome (or a transcriptome). The information about expression strength of every protein-encoded gene is obtained.

The main advantages of transcriptome profiling with RNA-seq over RT-PCR and microarrays are the increased dynamic range, higher selectivity and ability to detect also weakly expressed genes. Although RNA-seq can be performed with a variety of platforms, in practice, sequencing with Illumina technology dominates the field. Illumina technology is based on sequencing by synthesis using reversible terminator bases with fluorescent dyes attached. A complementary strand to the examined sequence is synthesized using fluorescently labelled bases that contain a removable terminator. One base at a time is added, imaged and the terminator is removed so the cycle can be repeated. As hundreds of millions of short sequences can be imaged simultaneously, the method yields large amounts of data in a short time. The obtained reads are then aligned to the genome and the gene expression is analyzed.

The major concern when isolating the cell type-specific mRNA is the contamination with transcripts from other cell types what may compromise the results. Detection of mRNA is possible also directly in tissues with the method known as in situ hybridization. However, due to laborious process of the probe optimization, this is not a commonly used approach to detect neurotransmitter markers in fruit fly brain tissue.

Visualization of the expression pattern of any gene can be performed by inserting a reporter gene sequence into the transcribed portion of the gene locus. Using this approach, the presence of the reporter protein marks all the cells throughout the brain that express the studied gene. The MiMIC library (Venken et al., 2011; Diao et al., 2015) of gene-trap cassette insertions provides a major source for visualization of gene expression patterns with the inserted reporters such as green fluorescent protein (GFP) or transcription factors of binary expression systems. However, the MiMIC collection of lines was generated by random genomic insertions and therefore not every gene contains the insertional cassette. Recently, the generation of the LexA knock-ins into the VACHT, VGluT and VGAT genes expanded the available toolbox for the determination of the neuronal neurotransmitter identity (Simpson, 2016).

The earlier approaches to reveal the expression pattern of genes were based on so-called “enhancer trapping” that involved cloning of an artificial construct consisting of the gene enhancer sequence fused to a reporter protein that was introduced into genome (Figure 1). Even though this approach provided some useful transgenic lines for revealing the neurotransmitter phenotype, it is often difficult to estimate the sequence that constitutes a gene enhancer, therefore, the expression pattern of many enhancer trap lines does not reliably copy the expression pattern of the gene that the enhancer region belongs to (Simpson, 2016).

In addition to detecting neurotransmitter markers, the presence of neurotransmitter in neuronal cell bodies can be directly visualized with immunostaining. In *D. melanogaster*, specific antibodies against several neurotransmitters have been used successfully (Monastirioti et al., 1995; Yuan et al., 2005; Kolodziejczyk et al., 2008). Nevertheless, the same issue as with the detection of synaptically localized proteins applies: to visualize a neurotransmitter which is synthesized locally at the synapse, the resolution achievable by traditional confocal microscopy is not sufficient.

### 1.3 VISUAL SYSTEM OF *D. MELANOGASTER*

Judging from the portion of brain devoted to visual processing, the vision is an important source of sensory information about the surrounding world for fruit flies. The optic lobes occupy in total almost two thirds of the fly brain volume. Anatomically, the optic lobe is located beneath the retina and consists of the four neuropils: lamina, medulla, lobula and lobula plate (Figure 5).

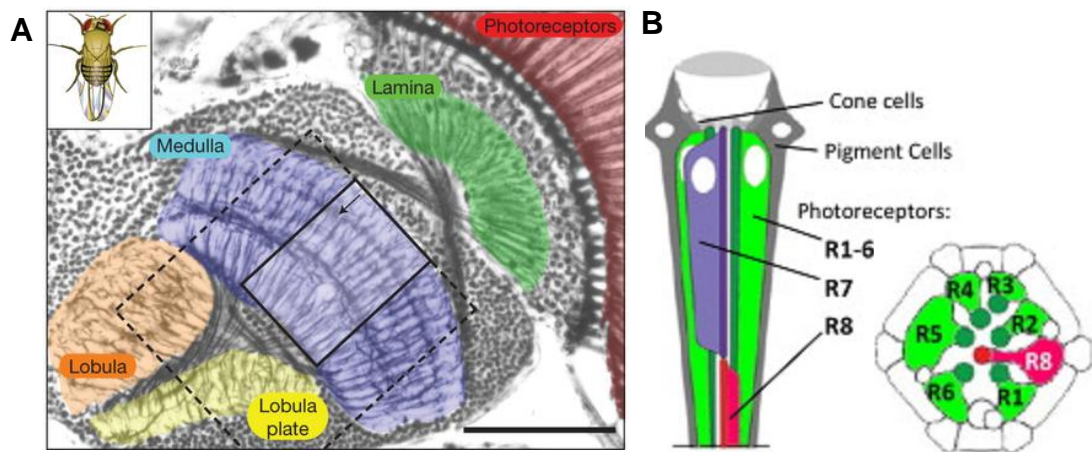


**Figure 5. Visual system of a fruit fly.** A) (Reprinted from Takemura et al., 2013 with permission). The optic lobe comprises of photoreceptors in retina that provide input to the underlying neuropils called lamina and medulla. The visual information is then further processed in the lobula and the lobula plate. B) (Adapted from Wernet et al., 2015 with permission). Vertical (left) and horizontal (right) cross-section through a single ommatidium found in retina. The function of the cone cells and the pigment cells ensures the effective collection of photons by photoreceptors from a single point in space.

The retina comprises light-sensitive photoreceptors organized in hexagonal units called ommatidia (Figure 5). In total, there are approximately 750 ommatidia in each eye of a fruit fly. Each ommatidium contains eight photoreceptors arranged in a stereotyped manner. Depending on the position in ommatidium, the photoreceptors are termed as R1, R2, R3, R4, R5, R6, R7 and R8 cells. The ‘outer’ photoreceptors R1-R6 provide the major input to the contrast and motion vision circuit (Yamaguchi et al., 2008) while the “inner” photoreceptors R7 and R8 are involved in color discrimination (Yamaguchi et al., 2010). The photoreceptor types vary with respect to the class of light-absorbing pigment rhodopsin that they express and the projection pattern of their axons. The photoreceptors R1-R6 send their axons to the lamina whereas

the axons of the photoreceptors R7 and R8 project through the lamina and only form synapses in the medulla.

Downstream of photoreceptors, the visual signal is passed onto neurons that are organized in parallel units termed visual columns. This arrangement preserves the retinotopy of the visual information processing by precisely mapping each region of the visual field onto one of the distinct columns in the lamina and medulla. The types of neurons, their number and connectivity is identical in each column. The lamina is a relatively simple neuropil consisting of only 12 classes of neurons with well-studied connectivity and at least partially understood function (Meinertzhagen and O'Neil, 1991; Joesch et al., 2010; Rivera-Alba et al., 2011; Tuthill et al., 2013; Tuthill et al., 2014). In contrast, the medulla is a larger and more complicated neuropil with more than 70 distinct types of neurons (Morante and Desplan, 2008). The function in the visual processing and the synaptic connections of the neurons in medulla have been established only for a small portion of the medullar cells (Takemura et al., 2011; Takemura et al., 2013; Behnia et al., 2014; Karupudurai et al., 2014; Serbe et al., 2016; Shinomiya et al., 2014; Strother et al., 2014; Yang et al., 2016; Strother et al., 2017; Takemura et al., 2017). At the level of lobula and lobula plate, the columnar structure of neuropil is largely lost. Various tangential types of neurons with more elaborate response properties that integrate signals from several visual columns or even larger regions of the visual field are found at this stage of the visual system (Fischbach and Dittrich, 1989).

### *1.3.1 Neuronal circuit for motion vision*

The visual detection of motion is a classic example of a simple neuronal computation that has been studied for decades, yet, is still not fully understood neither in mammals nor in fruit flies. Motion vision in *Drosophila* begins at the level of the R1-R6 photoreceptors. Similar to mammals, the fly visual system also processes the information about local light increments and decrements separately, in two parallel streams – the ON and OFF channels (Joesch et al., 2010). The signal from R1-R6 photoreceptors splits into ON and OFF channels very early in the visual processing, already at the level of the first postsynaptic neurons in lamina (Joesch et al., 2010; Eichner et al., 2011; Joesch et al., 2013). Two types of the columnar laminar neurons are central to motion vision processing: the L1 neurons representing the first component of the ON

pathway and the L2 neurons that give rise to the OFF pathway (Joesch et al., 2010).

Fly photoreceptors release from their axons neurotransmitter histamine which opens chloride channels on the L1 and L2 neurons and hyperpolarizes them (Hardie 1989, Gisselmann et al., 2002; Zheng et al., 2002). Just as vertebrate photoreceptors, fly photoreceptors also release their neurotransmitter continuously over time. Due to a different molecular mechanism of the photoconversion in vertebrates and arthropods, the mammalian photoreceptors are constantly depolarized in the dark whereas fly photoreceptors, on contrary, depolarize in response to light and are hyperpolarized in the dark. The information about light decrement is translated in flies into less histamine released from the photoreceptors and as a result, transient depolarization of the postsynaptic L1 and L2 cells (Yang et al., 2016). On the contrary, light increment leads to more of the histamine released and consequently to hyperpolarization of the L1 and L2 neurons (Yang et al., 2016).

For the L1 and L2 neurons to act as a point of splitting of the signal from photoreceptors to the ON and OFF channel, the signal must be half-wave rectified, meaning, that one laminar cell type only spreads the information about its depolarization while the other one only relays information about its hyperpolarization to the downstream neurons. Indeed, the half-wave rectification has been observed in both, the L1 and L2 cells (Reiff et al., 2010; Yang et al., 2016). The L2 cells depolarize and release neurotransmitter acetylcholine as a response to light decrements but not to light increments (Reiff et al., 2010; Takemura et al., 2011). On the other hand, the glutamatergic L1 neurons have been shown to relay the information about light increments represented as their membrane potential hyperpolarization and, interestingly, invert the sign of the signal such that the neurons postsynaptic to L1 cells depolarize as a response to the hyperpolarization of the L1 neurons (Yang et al., 2016). It has been already speculated that this sign inversion is achieved by the continuous release of glutamate from the L1 neurons causing hyperpolarization of the postsynaptic neurons via inhibitory glutamate-gated chloride channel (Liu and Wilson, 2013), nevertheless, this has not been proven experimentally, yet.

The splitting of the channels at the level of the L1 and L2 cells is not perfectly segregated. Along with the L2 cells, the laminar L3 neurons also

provide input to the OFF pathway via Tm9 neuron (Silies et al., 2013; Fisher (a) et al., 2015) (Figure 6).

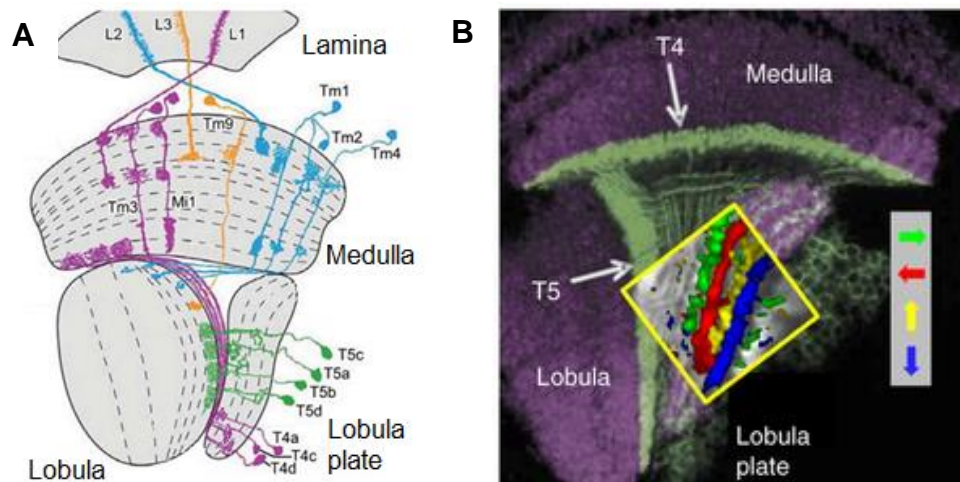


**Figure 6. Neurons in the motion vision circuit.** (A) (Adapted from Shinomiya et al., 2014 with permission). Morphology of the neuronal cell types underlying processing of the visual motion. (B) (Adapted from Borst and Helmstaedter, 2015 with permission). In vivo calcium imaging of the axon terminals of the T4 and T5 neurons in the lobula plate reveals the directional tuning map in the lobula plate. Each of the four layers of the lobula plate is innervated by the T4 and T5 neurons that respond to the same direction of motion.

The main downstream components of the ON pathway are the medullar columnar neurons Mi1 and Tm3 cells which synapse on the T4 neurons, the first identified motion- and direction-sensitive cells in the ON pathway of the fly visual system (Maisak et al., 2013; Takemura et al., 2013; Behnia et al., 2014; Strother et al., 2014; Strother et al., 2017; Takemura et al., 2017) (Figure 6). The Mi1 and Tm3 neurons respond specifically to light increments but not in a direction-selective manner (Behnia et al., 2014; Strother et al., 2014; Yang et al., 2016). Silencing of the Mi1 and Tm3 neurons reduces the ability of flies to behaviorally respond to moving increments of light, further confirming the role of these cells in the motion vision circuit (Ammer et al., 2015). Nevertheless, the neurotransmitter of the Mi1 and Tm3 neurons has not been described until recently (Strother et al., 2017; Takemura et al., 2017), neither has it been known whether the input that the Mi1 and Tm3 neurons provide to the direction-selective T4 neurons is excitatory or inhibitory.

In the OFF pathway, the downstream elements of L2 neurons are medullar cells Tm1, Tm2, Tm4 and Tm9 (Shinomiya et al., 2014; Serbe et al., 2016) (Figure 6). The first direction-selective cell type in the OFF channel are T5 neurons (Maisak et al., 2013) which receive the input from all of the four types of the columnar medulla neurons (Shinomiya et al., 2014). All of the identified neurons that provide input to T5 cells, the Tm1, Tm2, Tm4 and Tm9 cells, appear to be cholinergic (Raghu et al., 2011; Shinomiya et al., 2014).

The T4 and T5 cells are the elementary motion detector neurons in a fruit fly, representing the first stage in the visual system where direction selectivity arises (Maisak et al., 2013; Fisher (b) et al., 2015). Both, the T4 and T5 neurons, comprise of four subtypes, termed T4a, T4b, T4c, T4d and T5a, T5a, T5b, T5c, T5d. Each of the a-d subtypes of the T4 and T5 neurons responds preferentially to one of the four cardinal directions: front-to-back, back-to-front, upwards and downwards (Maisak et al., 2013.). In addition to different physiological responses, the T4a-d and T5a-d neuronal subtypes differ also in their morphology: each subtype has a dendritic tree prolonged in a direction opposite to its preferred direction of response (Takemura et al., 2013). Moreover, the axonal projections of the a-d subtypes of the T4 and T5 neurons separate in the lobula plate such that each subtype projects to one of the four layers depending on its preferred direction (Maisak et al., 2013) (Figure 6).

The neurotransmitter phenotypes of neurons involved in the processing of visual motion including the type of marker detected and the method used are summarized in the Table 1.

The T4 and T5 neurons have been shown to synthesize and release acetylcholine onto their downstream postsynaptic partners, the lobula plate tangential cells (LPTCs) (Mauss et al., 2014; Shinomiya et al., 2014). The LPTCs are wide-field motion-sensitive neurons that integrate signal about motion from larger areas of the visual field and receive input from both processing streams, ON and OFF (Joesch et al., 2008; Schnell et al., 2010). In comparison to the local motion detectors, the T4 and T5 neurons, LPTCs show biphasic response properties to visual motion: depolarization to the motion in the preferred direction and hyperpolarization to the motion in the opposite, null direction (Figure 7).

Neuron	Neurotransmitter	Marker	Method used	Reference
<b>R1-R6</b>	Histamine	-	Histamine applied on postsynaptic cells	Hardie, 1989
<b>L1</b>	Glutamate	VGluT	RT-PCR of RNA from isolated cells	Takemura et al., 2011
<b>L2</b>	Acetylcholine	ChAT	RT-PCR of RNA from isolated cells	Takemura et al., 2011
<b>Tm1</b>	Acetylcholine	ChAT	anti-ChAT staining	Shinomiya et al., 2014
<b>Tm2</b>	Acetylcholine	ChAT	RT-PCR of RNA from isolated cells	Takemura et al., 2011
<b>Tm4</b>	Acetylcholine (?)	ChAT (?)	ChAT-GAL4 expression pattern	Raghu et al., 2011
<b>Tm9</b>	Acetylcholine	ChAT	RT-PCR of RNA from isolated cells	Shinomiya et al., 2014
<b>T4</b>	Acetylcholine	ChAT	RT-PCR of RNA from isolated cells; anti-ChAT staining	Shinomiya et al., 2014; Mauss et al., 2014
<b>T5</b>	Acetylcholine	ChAT	RT-PCR of RNA from isolated cells; anti-ChAT staining	Shinomiya et al., 2014; Mauss et al., 2014

**Table 1. Neurons in the motion vision circuit with identified neurotransmitter.** The neurons in the fruit fly motion vision circuit with known neurotransmitters are listed. The Tm4 neurons were identified as cholinergic, however, it is not clear whether the ChAT-GAL4 line used for the identification labels exclusively cholinergic neurons.

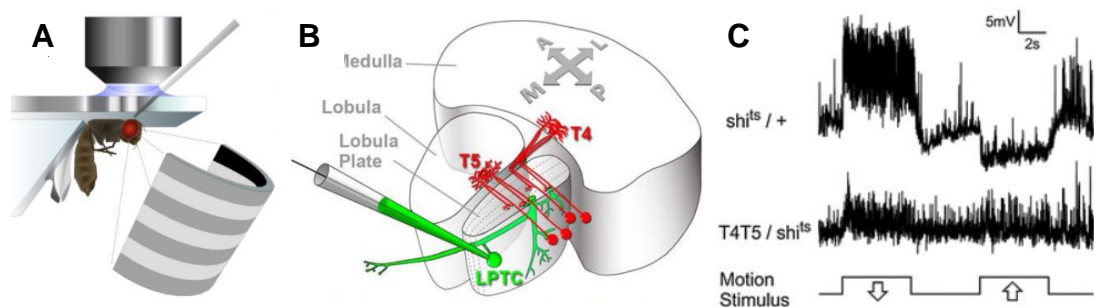


**Figure 7. Response properties of the LPTCs.** (A) (Reprinted from Joesch et al., 2008 with permission). Schematics of the fly preparation for the *in vivo* electrophysiological recordings combined with simultaneous visual stimulation. (B) (Reprinted from Mauss et al., 2014). Illustration of the optic lobe depicts the position of the LPTCs in the fruit fly visual system. (C) (Reprinted from Schnell et al., 2012). *In vivo* intracellular recordings from LPTCs show depolarization as a response to visual stimulus moving upwards and hyperpolarization to downward motion (upper trace). In flies with the T4 and T5 neurons synaptically silenced by the overexpression of shibire<sup>ts</sup>, the LPTCs do not show any motion-specific responses (lower trace).



The input of the T4 and T5 neurons is necessary for direction-specific responses of the LPTCs (Schnell et al., 2012) (Figure 7). As all the T4 and T5 neurons have been shown to synthesize acetylcholine (Mauss et al., 2014), the following question arises: How does the activity of the cholinergic T4 and T5 neurons translate into hyperpolarization of the postsynaptic LPTCs?

#### 1.4 COMPUTATIONS UNDERLYING DIRECTION SELECTIVITY

In the research field of motion vision, two prevalent algorithmic models have been used to describe the mechanism of direction selectivity: the Hassenstein-Reichardt (HR) model (Hassenstein and Reichardt, 1956) and the Barlow-Lewick (BL) model (Barlow and Levick, 1965). Both models predict existence of a simple, hypothetical circuit which responds to motion in a direction-specific fashion by combining two inputs from the neighboring points in the visual field that are temporally offset. The HR model was inspired by the behavioral experiments performed on the beetle *Chlorophanus* (Hassenstein and Reichardt, 1956) and has been dominating the field of insect motion vision. The HR model assumes that the visual input from two adjacent points in space is differentially filtered in time. The two excitatory inputs then converge on the direction-selective detector that produces supralinear response if the two inputs arrive simultaneously (Figure 8). Peculiarly, the two inputs only reach the detector simultaneously if the visual movement is presented in a specific direction.

The other influential model of direction selectivity, the BL model, was inspired by the work on rabbit retina (Barlow and Levick, 1965). Like the HR model, the BL model also assumes that the direction selective unit receives two temporally offset inputs from two neighboring points in the visual field (Figure 9). In comparison to the HR model which assumes the multiplication of two excitatory inputs, the BL detector acts on the subtraction principle by deducting the inhibitory input from the excitatory one.

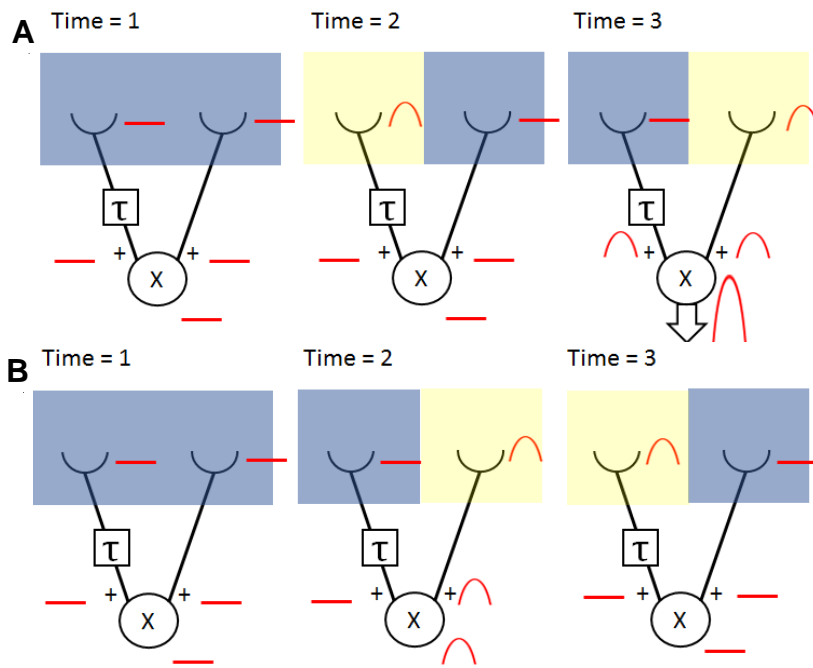


**Figure 8. The HR model of direction selectivity and its responses to preferred- and null- direction stimuli.** The illustration shows an HR model that responds specifically to left-to-right motion of light increments. Three subsequent points in time are illustrated. The model consists of two light detectors

(depicted as half-circles) that collect light from two adjacent points in space and convey the signal to the direction-selective unit (depicted as circle). One of the inputs is temporally delayed (square with  $\tau$ ). Red traces show signal at the level of light detectors, inputs lines and at the level of direction-selective unit. Left-to-right motion (preferred direction) of a single bright point (yellow square) and the corresponding responses of the HR model are depicted in (A) and the opposite, null-direction right-to-left motion of an ON stimulus is in (B). The direction-selective unit performs multiplicative non-linear summation of the inputs and conveys the signal further only if the two inputs arrive simultaneously.

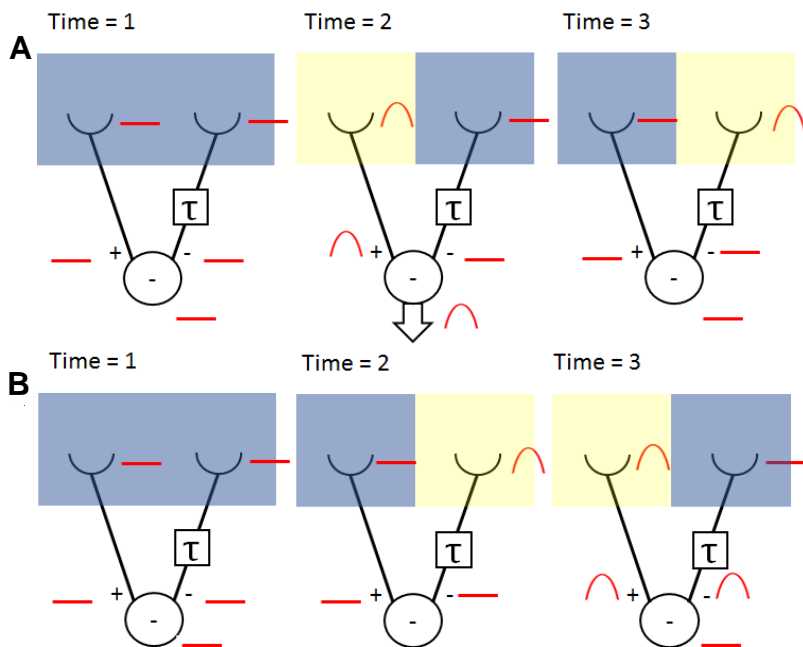


**Figure 9. The BL model of direction selectivity and its responses to preferred- and null- direction stimuli.** The BL model of direction selectivity with left-to-right ON motion as a preferred stimulus. In (A), the responses to preferred direction of motion are depicted. (B) shows null-direction movement.

The computation that underlies direction selectivity of the T4 and T5 neurons is still not fully understood. Recent works suggested, that the response properties of the T4 and T5 neurons are a mixture of the both theoretical models outlined above (Fisher (b) et al., 2015; Haag et al., 2016; Leong et al., 2016; Strother et al., 2017.). To elucidate how direction selectivity in the T4 and T5 neurons arises, several questions need to be fully answered: Which neurons provide input to the T4 and T5 cells? What neurotransmitters do neurons providing input to T4 and T5 cells use? Where and how is the temporal delay represented in the motion vision circuit? On the level of input neurons, on the level of the synapses between the input neurons and the T4 and T5 neurons or on the level of the dendrites of the T4 and T5 neurons? How do the T4 and T5 neurons perform the supralinear summation and what is the molecular substrate for the null-direction inhibition?

## **1.5 AIMS OF THIS DISSERTATION**

The aim of this dissertation is to elucidate the biophysical implementation of computations that underlie the direction-specific response of the local motion detectors, the T4 and T5 neurons as well as their downstream partner, the wide-field motion-sensitive LPTCs.

By applying a whole genome transcriptome analysis to investigate gene expression of the T4 and T5 cells, I examine the neurotransmitter input that the T4 and T5 neurons receive as well as the molecular substrate for their supralinear summation response to visual motion in a preferred direction.

Furthermore, in order to map the known neuronal components of the motion vision pathway onto proposed theoretical circuits, I develop and describe a new tool for the identification of cholinergic neurons and use this tool to analyze the neurotransmitter phenotype of neurons in the ON-channel of motion vision, the Mi1 and Tm3 cells.

In addition, this dissertation also describes the morphology and function of the previously uncharacterized class of interneurons that receive input from the T4 and T5 neurons and convey the information about the null direction movement to the hyperpolarization of the LPTCs.

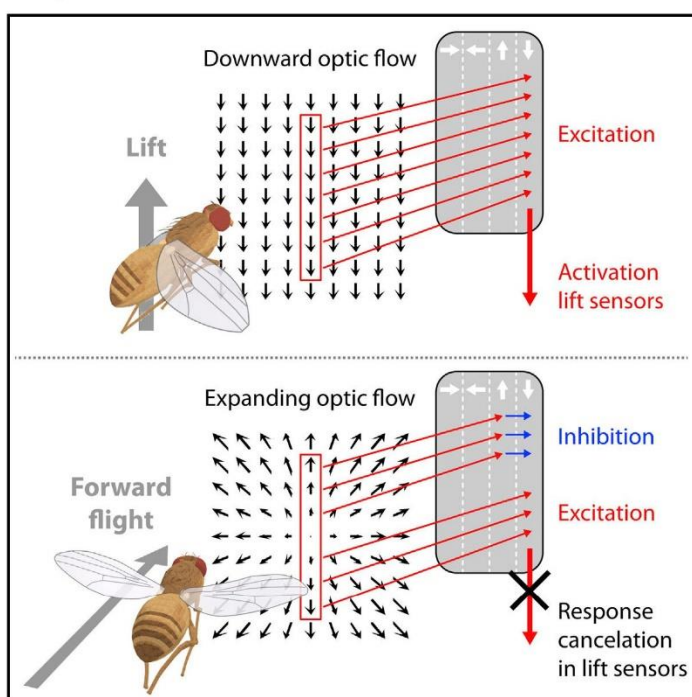
## 2 | PUBLICATIONS

### **2.1 NEURAL CIRCUIT TO INTEGRATE OPPOSING MOTIONS IN THE VISUAL FIELD**

The article “Neural circuit to integrate opposing motions in the visual field” (<http://dx.doi.org/10.1016/j.cell.2015.06.035>) was originally published in the journal Cell in July 2015 and is reprinted here with the publisher’s permission. The following authors contributed to this work: Alex S. Mauss performed and analyzed electrophysiological recordings. Katarina Pankova carried out and analyzed immunostainings (except multicolor labeling and TNT-E expression), transcript profiling, and GRASP experiments. Alexander Arenz performed and analyzed two-photon calcium imaging experiments. Alexander Borst did computer simulations. Gerald M. Rubin and Aljoscha Nern generated the LPi driver lines and performed multicolor stochastic labeling. Alex S. Mauss and Alexander Borst designed the study. Alex S. Mauss, Alexander Arenz, and Alexander Borst wrote the paper with the help of all authors.

# Neural Circuit to Integrate Opposing Motions in the Visual Field

## Graphical Abstract



## Highlights

- Discovery of bi-stratified glutamatergic lobula plate-intrinsic (LPi) interneurons
- LPi neurons provide visual null direction inhibition to wide-field tangential cells
- Blocking LPi activity leads to target neurons responding to inadequate motion cues
- Motion opponency thus increases flow-field selectivity

## Authors

Alex S. Mauss, Katarina Pankova, Alexander Arenz, Aljoscha Nern, Gerald M. Rubin, Alexander Borst

## Correspondence

amauss@neuro.mpg.de

## In Brief

Newly identified inhibitory neurons are central to an integrative circuit that enables *Drosophila* to process visual cues with opposite motions generated during flight. The neurons are required to discriminate between distinct complex motion patterns, indicating that neural processing of opposing cues can yield outcomes beyond the simple sum of two inputs.



Mauss et al., 2015, Cell 162, 351–362  
 July 16, 2015 ©2015 Elsevier Inc.  
<http://dx.doi.org/10.1016/j.cell.2015.06.035>

# Neural Circuit to Integrate Opposing Motions in the Visual Field

Alex S. Mauss,<sup>1,\*</sup> Katarina Pankova,<sup>1</sup> Alexander Arenz,<sup>1</sup> Aljoscha Nem,<sup>2</sup> Gerald M. Rubin,<sup>2</sup> and Alexander Borst<sup>1</sup>

<sup>1</sup>Max-Planck-Institute of Neurobiology, 82152 Martinsried, Germany

<sup>2</sup>Janelia Research Campus, Howard Hughes Medical Institute, Ashburn, VA 20147, USA

\*Correspondence: [amauss@neuro.mpg.de](mailto:amauss@neuro.mpg.de)

<http://dx.doi.org/10.1016/j.cell.2015.06.035>

## SUMMARY

When navigating in their environment, animals use visual motion cues as feedback signals that are elicited by their own motion. Such signals are provided by wide-field neurons sampling motion directions at multiple image points as the animal maneuvers. Each one of these neurons responds selectively to a specific optic flow-field representing the spatial distribution of motion vectors on the retina. Here, we describe the discovery of a group of local, inhibitory interneurons in the fruit fly *Drosophila* key for filtering these cues. Using anatomy, molecular characterization, activity manipulation, and physiological recordings, we demonstrate that these interneurons convey direction-selective inhibition to wide-field neurons with opposite preferred direction and provide evidence for how their connectivity enables the computation required for integrating opposing motions. Our results indicate that, rather than sharpening directional selectivity per se, these circuit elements reduce noise by eliminating non-specific responses to complex visual information.

## INTRODUCTION

Diverse sensory experiences can result in largely overlapping patterns of activation within sensory circuits yet require fundamentally different behavioral responses. An underlying key operation is the extraction of features relevant for specific behaviors by hierarchical layers of neuronal networks with increasing selectivity. A well-studied example of such feature extraction is the computation of the optic flow associated with self-motion—that is, the feedback motion cues created by an animal progressing through its environment. Across many animals studied, motion-sensitive neurons covering large receptive fields (those that receive input from cues spanning the visual field) tend to be motion opponent, i.e., are excited by motion along one and inhibited along the opposite direction (Collett and Blest, 1966; Duffy and Wurtz, 1991; Hausen, 1984; Ibbotson, 1991; Krapp and Hengstenberg, 1996; Wylie et al., 1998). However, the functional significance of motion opponency is unclear and has to date not been experimentally challenged. Here, we address this problem in *Drosophila*, which has emerged as a

powerful model system to study the mechanisms underlying motion vision (Borst et al., 2010).

The *Drosophila* optic lobe consists of four neuropiles called lamina, medulla, lobula, and lobula plate. Each of these neuropiles is built from about 750 repetitive columns arranged in a retinotopic way. Monopolar L1 and L2 cells, among others, receive photoreceptor input in the lamina and feed into two motion pathways (Bausenwein et al., 1992; Bausenwein and Fischbach, 1992; Clark et al., 2011; Joesch et al., 2010; Rister et al., 2007; Shinomiya et al., 2014; Silies et al., 2013; Takemura et al., 2013; Tuthill et al., 2013). Within each pathway, the direction of motion is computed separately, with the L1-pathway selectively processing motion of brightness increments (ON) and the L2-pathway motion of brightness decrements (OFF) (Eichner et al., 2011; Joesch et al., 2010, 2013). The outputs of the ON and OFF pathways are represented by arrays of small-field T4 and T5 cells, respectively. Each T4 and T5 cell is tuned to one of four cardinal directions and terminates in one of the four layers of the lobula plate such that opposite directions are represented in adjacent layers (Maisak et al., 2013) (layer 1: front to back; layer 2: back to front; layer 3: upward; layer 4: downward). These directions match the preferred directions of wide-field motion-sensitive tangential cells that extend their dendrites in the respective layers: horizontal system cells with dendrites in layer 1 depolarize during front-to-back motion and hyperpolarize during back-to-front motion, Hx cells in layer 2 exhibit the opposite tuning, and vertical system (VS) cells with dendrites mostly in layer 4 depolarize primarily during downward and hyperpolarize during upward motion (Hausen et al., 1980; Hopp et al., 2014; Schnell et al., 2010; Scott et al., 2002; Wasserman et al., 2015). With T4/T5 cells blocked, tangential cells lose all of their motion sensitivity (Schnell et al., 2012), and flies become completely motion blind (Bahl et al., 2013). Combining optogenetic stimulation of T4/T5 cells with various pharmacological antagonists, the connections between T4/T5 and tangential cells have recently been characterized as monosynaptic, excitatory, and cholinergic (Mauss et al., 2014). T4/T5 cells thus account for the depolarization of the tangential cells during preferred direction motion. What remains unclear is the mechanism and functional role of subtracting information about motion in the opposite or null direction.

Here, we characterize a hitherto unknown class of vertical system lobula plate intrinsic (LPI) neurons and demonstrate how they contribute to motion opponency. First, our anatomical and molecular characterization, as well as combined optogenetic stimulation and electrophysiological recordings, reveal that LPI



neurons are bi-stratified and inhibit tangential cells in single lobula plate layers via glutamatergic synapses. Second, we demonstrate by two-photon calcium imaging that LPi neurons are activated in response to motion directions similar to their presumed T4/T5 inputs and opposite to their postsynaptic targets. Third, genetically silencing LPi cell output selectively abolishes null direction inhibitory potential changes in tangential cells. We therefore conclude that LPi neurons hyperpolarize tangential cells during null direction motion through sign-inverting layer interactions, thus forming the cellular basis of motion opponency in the fly. As a final point, the identification of LPi neurons enabled us to experimentally address the long-sought functional relevance of motion opponency. As blocking the activity of LPi neurons renders their postsynaptic wide-field motion-sensitive neurons responsive to a variety of moving patterns, our experiments suggest that motion opponency is essential for flow-field selectivity, thereby improving the ability to reliably estimate self-motion trajectories based on complex visual information.

## RESULTS

### Anatomy of Lobula Plate Intrinsic Neurons

Previous work suggested the existence of yet unidentified lobula plate neurons underlying null direction responses in tangential cells (Mauss et al., 2014). Candidate neurons to fulfill this role are expected to possess a bi-stratified morphology covering either both horizontal (1 and 2) or both vertical (3 and 4) layers. To identify such cell types, we screened the *Janelia Drosophila* driver line collection (Jenett et al., 2012; Pfeiffer et al., 2008) and discovered two independent lines (R20D01, R38G02) containing neurons that exclusively innervate the two layers of the lobula plate vertical system. Moreover, putative presynaptic varicosities for each line are located in either layer 3 (R38G02) or 4 (R20D01), suggesting two distinct functional cell types. We confirmed the presynaptic nature of these varicosities by co-expressing GFP and the presynaptic reporter Synaptotagmin (Sytx), which correspondingly localized to layer 3 (R38G02) and layer 4 (R20D01; Figures 1A–1B’). This anatomical layout indicates a complementary directed signal transfer from layer 3 to 4 in one and from layer 4 to 3 in the other cell type. Accordingly, these two new neuron types are termed LPi3-4 (lobula plate intrinsic) and LPi4-3, respectively. To reveal single-cell morphologies, we performed stochastic multicolor labeling of LPi cells (Figures 1C–1I) (Nern et al., 2015). Neurons in each line have vertically elongated arbors covering the lobula plate in partly segregated patches. While individual LPi neurons occupy lobula plate layers 3 and 4, their potential postsynaptic targets, the VS cells, have dendrites restricted to layer 4 only (Figures 1J and 1J’).

### Transmitter Phenotype and Connectivity

We next investigated the transmitter phenotype of the LPi cells by immunostaining (LPi3-4 and LPi4-3) and mRNA profiling (Takemura et al., 2011) (LPi3-4). Both approaches revealed that LPi neurons express vesicular glutamate transporter (vGluT; Figures 2A–2C), while cholinergic and GABAergic markers could not be detected (Figures 2C and S1). Aply, tangential cells express glutamate-gated chloride channel  $\alpha$  (GluCl $\alpha$ ; Figure 2C), in line with their hyperpolarizing responses to glutamate applica-

tion (Mauss et al., 2014). These results suggest that tangential cells receive inhibitory glutamatergic input from LPi neurons. To directly explore the synaptic connectivity between LPi neurons and tangential cells, we focused on LPi3-4 neurons, which provide putative synaptic input to the experimentally accessible VS cells in lobula plate layer 4 (Figure 1J). First, we labeled membrane contacts using the GRASP method (Feinberg et al., 2008) by expressing membrane-targeted CD4-spGFP1-10 and CD4-spGFP11 independently in LPi3-4 and VS cells using four different driver line combinations. In all cases, reconstituted fluorescence signal could be detected exclusively in lobula plate layer 4, indicating contact between LPi3-4 terminals and VS cell dendrites (Figures 2D and S2). To functionally determine the synaptic connectivity, we took an optogenetic approach previously used to establish connectivity between T4/T5 and tangential cells (Mauss et al., 2014): brief optogenetic stimulation of T4/T5 cells in blind, *norpA*<sup>7</sup> mutant flies evoked biphasic synaptic responses in VS cells with direct cholinergic excitation and delayed indirect inhibition (Figure 2E, red trace), the latter being sensitive to the GABA/glutamate receptor antagonist picrotoxinin (Mauss et al., 2014). To test whether this inhibitory component could be conveyed by LPi3-4 cells, we optogenetically stimulated LPi3-4 cells expressing ChR2-H134R in blind flies while performing patch-clamp recordings from VS cells. VS cells responded to optogenetic LPi stimulation with picrotoxinin-sensitive inhibitory potential changes (Figures 2E–2H) and onset latencies comparable to T4/T5-evoked excitation (Figure 2E). We conclude that LPi3-4 neurons provide fast inhibitory glutamatergic input to VS cells in layer 4 of the lobula plate.

### Visual Response Properties of LPi Neurons

Cholinergic T4/T5 cells represent the major motion-sensitive input to the lobula plate (Schnell et al., 2012), and their axons segregate into four layers according to their directional tuning (Maisak et al., 2013). LPi cells of a single type are thus expected to acquire direction selectivity by receiving excitatory input from T4/T5 cells in one of the two motion-opponent layers. To probe the LPi cells’ visual response properties, we expressed the genetically encoded calcium indicator GCaMP5G (Akerboom et al., 2012) and recorded calcium signals (Denk et al., 1990; Maisak et al., 2013; Reiff et al., 2010) from putative presynaptic boutons in the lobula plate while stimulating flies with pattern motion (Figures 3A and 3B). Both LPi cell types responded in a strictly direction-selective way to moving square-wave gratings. Importantly, LPi3-4 cells were tuned to upward motion and LPi4-3 cells to the opposite, i.e., downward direction (Figures 3C and 3D). Thus, the preferred direction of LPi3-4 cells matches the one of T4/T5 cells terminating in layer 3, and the preferred direction of LPi4-3 cells corresponds to the one of T4/T5 cells terminating in layer 4. We next tested LPi responses to gratings moving with different velocities. A correlation type motion detector as implemented in flies results in a velocity tuning as a linear function of the spatial pattern wavelength. This feature is reflected in the T4/T5 and tangential cell responses, which exhibit an optimal temporal frequency of  $\sim 1$  Hz in quiescent flies (Joesch et al., 2008; Maisak et al., 2013; Schnell et al., 2010). Likewise, LPi3-4 and LPi4-3 cells both had velocity tuning peaks at  $24^\circ \text{ s}^{-1}$  for gratings with a spatial wavelength of  $24^\circ$

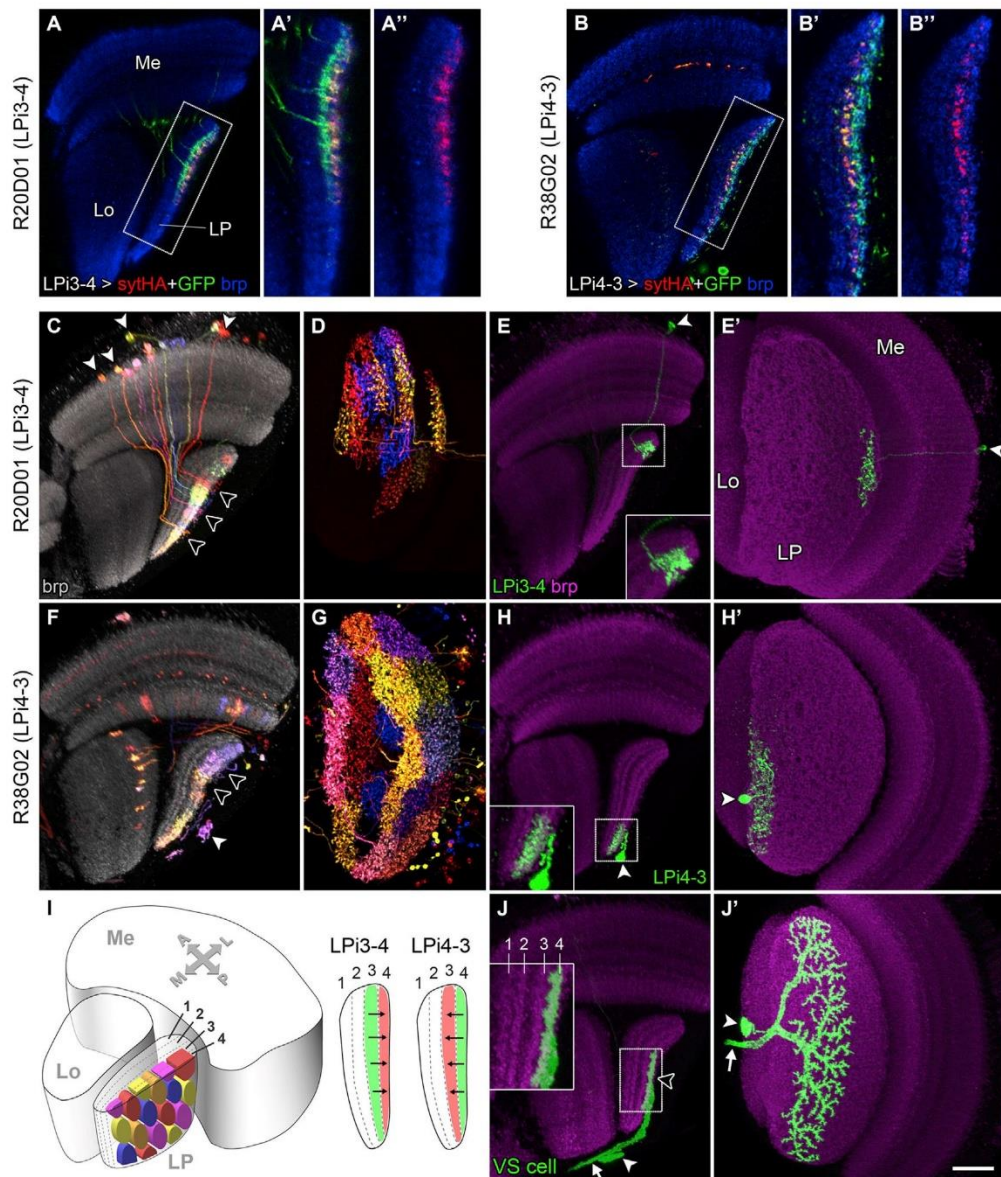


**Figure 1. Anatomical Characterization of Lobula Plate Intrinsic Neurons**

(A–B'') Co-expression of GFP and the presynaptic marker synaptotagmin by LPI-specific Gal4 driver lines (A, R20D01; B, R38G02) reveals the bi-stratified morphology and polarity of LPI neurites in lobula plate layers 3 and 4 in the horizontal confocal cross section (lateral up, anterior to the left). LPI3-4 neurons exhibit synaptic output sites only in layer 4 (A–A''), while LPI4-3 neurons (B–B'') with synaptotagmin in layer 3 show the opposite polarity. Postsynaptic sites are presumably restricted to the respective synaptotagmin-negative layers. Counterstaining with anti-bruchpilot (brp) highlights the synaptic neuropiles of the fly optic. (C–H') In two different views, stochastic multicolor labelings of LPI3-4 (C and D) and LPI4-3 neurons (E and G) are shown as well as individual neurons segmented from multicolor samples (F and H). Five stacks each with ~50 labeled cells for R38G02 and ~100 labeled cells for R20D01 were analyzed in detail. The layer positions and cell body locations were highly reproducible for each LPI type.

(I) Schematic representation of the fly optic lobe highlighting anatomical LPI neuron properties. LPI neurons cover lobula plate layers 3 and 4 in partly segregated patches. Since the lobula plate is organized in a retinotopic fashion, individual LPI neurons represent different points in visual space. Lobula plate cross-sections illustrate the inferred directed signal transfer. A, anterior; P, posterior; M, medial; L, lateral.

(J and J') Wide-field VS tangential cell segmented from a multicolor sample with its large dendrite restricted to layer 4.

Me, medulla; Lo, lobula; LP, lobula plate; white arrow heads, somata; black arrow heads, ramifications within the lobula plate; white arrows, VS cell axon. Scale bar, 20  $\mu$ m and 10  $\mu$ m for magnified views.



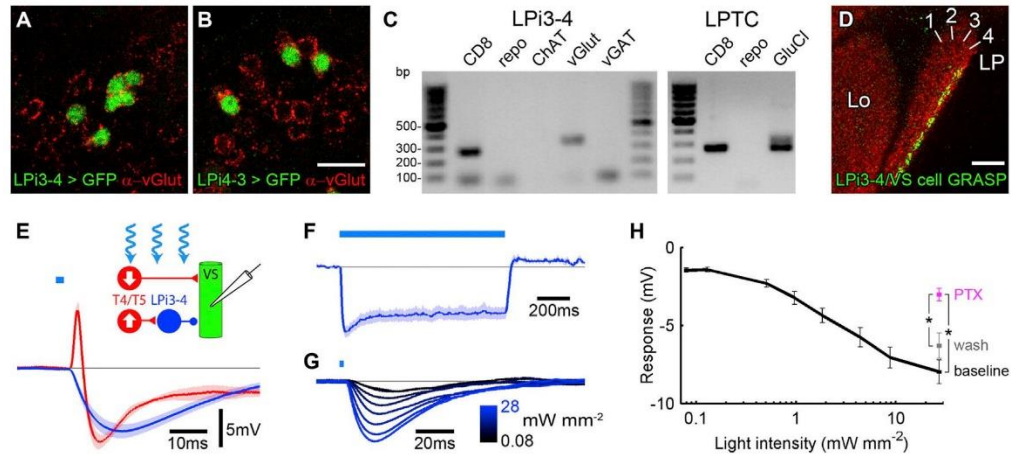


**Figure 2. LPI Neurons Provide Glutamatergic Inhibitory Input to Tangential Cells**

(A and B) Co-localization of antibodies against the vesicular glutamate transporter (vGlut) with GFP-expressing LPI neurons indicates that LPI3-4 (A) and LPI4-3 (B) both release the neurotransmitter glutamate (see also Figure S1). Scale bar, 10  $\mu\text{m}$ .

(C) Consistently, transcript profiling shows that mCD8-GFP-labeled LPI3-4 cells express vGlut (gel band with expected size of 339 bp), but neither choline acetyltransferase (ChAT) nor vesicular GABA transporter (vGAT). The bands detected in the repo and vGAT lanes do not match the predicted sizes of products from cDNA templates (137 and 151 bp, respectively) and probably correspond to primers. Transcript amplification of mCD8 and the glial marker repo were included as positive and negative control, respectively. Lobula plate tangential cells (LPTCs) express glutamate-gated chloride channel  $\alpha$  (GluCl $\alpha$ ), expected size 265 bp, indicating an inhibitory synaptic connection between LPI neurons and LPTCs.

(D) GFP reconstitution across synaptic partners (GRASP) reveals contacts between LPI3-4 cells and VS tangential cells in layer 4 (see also Figure S2). Lo, lobula; LP, lobula plate. Scale bar, 20  $\mu\text{m}$ .

(E) Optogenetic activation of Channelrhodopsin-2-H134R-expressing T4/T5 cells in blind flies using a 2 ms pulse of blue light (472/30 nm,  $\sim 3 \text{ mW mm}^{-2}$ ) leads to a biphasic excitatory/inhibitory synaptic response in VS cells (red trace,  $n = 4$ ; data taken from Mauss et al., 2014). Optogenetic activation of LPI3-4 cells ( $\sim 30 \text{ mW mm}^{-2}$ ) in contrast causes a purely inhibitory response in VS cells with a similar onset latency (blue trace,  $n = 7$ ). The schematic depicts the inferred connectivity between T4/T5, LPI3-4, and VS cells supported by the data, with excitatory cholinergic and inhibitory glutamatergic synapses marked by red triangles and a blue circle, respectively.

(F) Sustained hyperpolarizing VS cell response to 1 s optogenetic LPI3-4 activation ( $n = 6$ ;  $\sim 1 \text{ mW mm}^{-2}$ ).

(G) VS cell responses to 2 ms optogenetic LPI3-4 activation with varying light intensities.

(H) Quantification of data shown in (G) as baseline-subtracted response minima. For the highest light intensity and  $n = 4$  cells, responses were also quantified after 10 min bath perfusion with 25  $\mu\text{M}$  PTX and after another 30 min wash.

Significant differences were established using a two-tailed Wilcoxon rank-sum test, with asterisk indicating  $p < 0.05$ . Data in (E) to (H) are represented as mean  $\pm$  SEM.

corresponding to a temporal frequency of 1 Hz (Figures 3E and 3F). Finally, to assess how T4/ON and T5/OFF signals are integrated by LPI cells, we imaged individual presynaptic LPI boutons in the lobula plate and stimulated flies by moving ON and OFF edges separately. Most LPI3-4 boutons showed mixed but also ON and OFF edge-selective responses (Figure 3G). In LPI4-3 cells, mixed and ON edge-selective responses dominated (Figure 3H). These results indicate that both T4 and T5 cells at least partly converge onto individual LPI cells. Taken together, the anatomical overlap between T4/T5 output and LPI cell input arbors as well as their precisely matching visual response properties strongly suggests that LPI cells receive directionally tuned excitatory inputs from T4 and T5 cells.

#### Tangential Cell Motion Responses without LPI Input

Our data so far show that LPI3-4 neurons provide inhibitory input to VS cells and depolarize to opposite motion directions. To test directly whether LPI3-4 neurons convey null direction inhibition to VS cells, we performed patch-clamp recordings from VS cells (Joersch et al., 2008) in flies with LPI3-4 neurons silenced by

expression of tetanus toxin (Sweeney et al., 1995) (Figure 4A; “block flies”: *LPI3-4-Gal4 > UAS-TNT-E*), as well as in parental control flies. In control flies, stimulating the eye with gratings moving in the VS cells’ preferred direction (downward) produced graded depolarizations, while null direction stimulation (upward motion) hyperpolarized VS cells (Figure 4B, black and gray traces/bars). In block flies, preferred direction responses were similar to the controls. However, in sharp contrast, null direction responses were almost entirely absent (Figure 4B, red traces/bars). VS cell responses to individual ON and OFF edges were also strongly diminished in LPI3-4 block flies selectively for null direction motion (Figure 4C).

We next aimed to determine whether LPI activity might shape preferred direction response properties in VS cells. It has been suggested that the subtraction of oppositely tuned antagonistic inputs sharpens directional tuning in postsynaptic neurons (Levick et al., 1969; Oyster et al., 1971; Sato et al., 1991; Single et al., 1997). In *Drosophila* however, this might not be a vital requirement since the directional tuning of T4/T5 cells seems already sufficiently narrow to avoid significant overlap at orthogonal

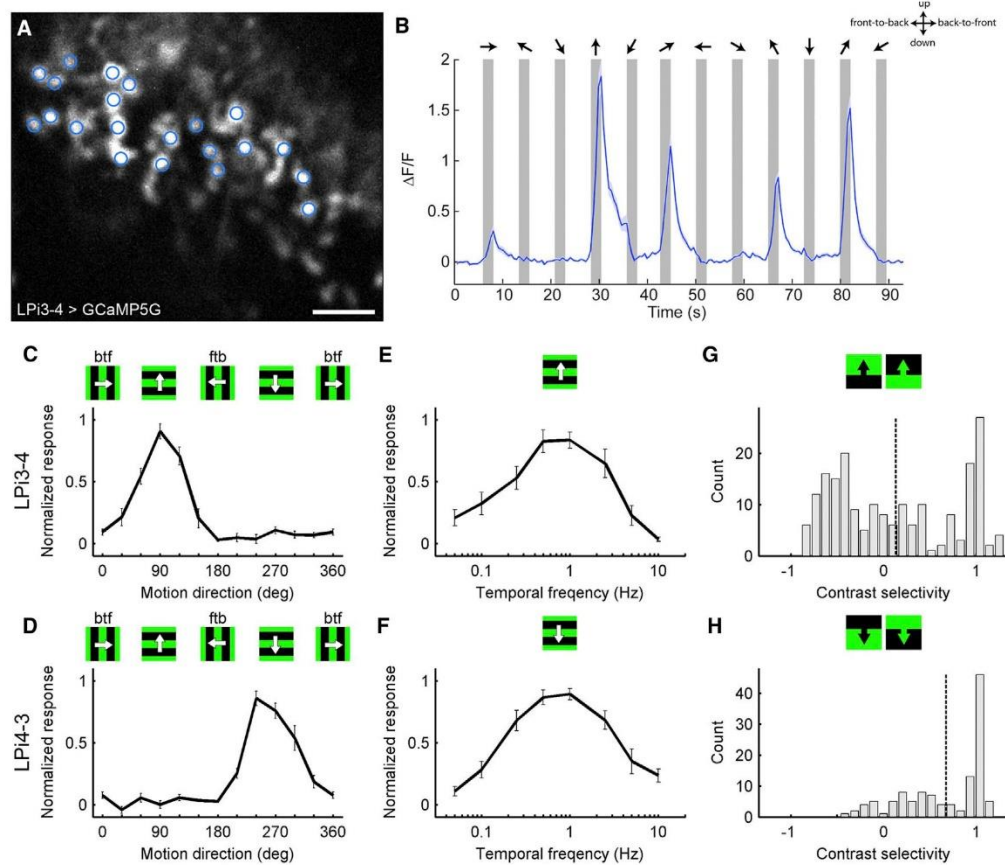


**Figure 3. LPI Neurons Are Direction Selective in Agreement with Layer-Specific Input from T4/T5 Terminals**

(A) Representative frame from a two-photon calcium imaging experiment (LPI3-4 expressing GCaMP5G) with ROIs indicated with blue circles. Scale bar, 5  $\mu\text{m}$ . (B) Average time-varying fluorescence ( $\Delta F/F$ ) across all ROIs in response to square-wave gratings moving in the above indicated directions.

(C and D) LPI3-4 ( $n = 7$ ) and LPI4-3 ( $n = 10$ ) neurons respond specifically to upward and downward motion, respectively (btf, back to front; ftb, front to back). (E and F) Both LPI cell types respond optimally to gratings moving at a temporal frequency of 1 Hz (E,  $n = 5$ ; F,  $n = 7$ ).

(G) Individual LPI3-4 neuron boutons can show preferences for moving ON or OFF edges or mixed responses to both contrast polarities ( $n = 10$  flies,  $n = 198$  boutons).

(H) Calcium signals from individual LPI4-3 boutons ( $n = 8$ ,  $n = 120$ ) indicate an average preference for ON over OFF edges.

Contrast selectivity =  $(R_{\text{ON}} - R_{\text{OFF}})/(R_{\text{ON}} + R_{\text{OFF}})$ . Dashed vertical lines indicate the population mean. Data in (B) to (F) are represented as mean  $\pm$  SEM.

directions (Maisak et al., 2013). We directly tested this by measuring VS cell responses in control and LPI block flies as a function of motion direction. The directional tuning curve of VS cells in control flies reveals a sinusoidal dependence on motion direction, with negative potential changes around  $90^\circ$  (upward) and positive potential changes around  $270^\circ$  (downward) (Figure 5A, black curve). Polarity and tuning width of the positive and negative parts of the curve closely match those obtained from calcium signals of T4d/T5d cells terminating in layer 4 and the inverse signals from T4c/T5c innervating layer 3 (Maisak et al., 2013), respectively, further indicating that VS cells integrate antagonistic inputs from oppositely tuned T4/T5 cells. As expected, in LPI3-4 block flies, directions around  $90^\circ$  on average did not evoke hyperpolarizing potential changes in VS cells (Fig-

ure 5A, red curve). The tuning curve for preferred directions around  $270^\circ$ , however, resembled that of the control condition. To test for a potential function in gain control, we presented gratings at different contrasts (Figure 5B). The resulting response functions showed lack of null direction inhibition selectively in LPI3-4 block flies but were indistinguishable between both experimental conditions for preferred directions. Last, we asked whether LPI input might influence the dynamics of the depolarizing VS cell responses to coherent pattern motion. To this end, we tested a dynamic motion stimulus consisting of a sine-wave grating changing velocity and direction according to a pseudo-random velocity distribution. In control flies, the VS cells' potential followed the pattern velocity with graded hyper- and depolarizations (Figures 5C–5E, black). In contrast, the responses in LPI

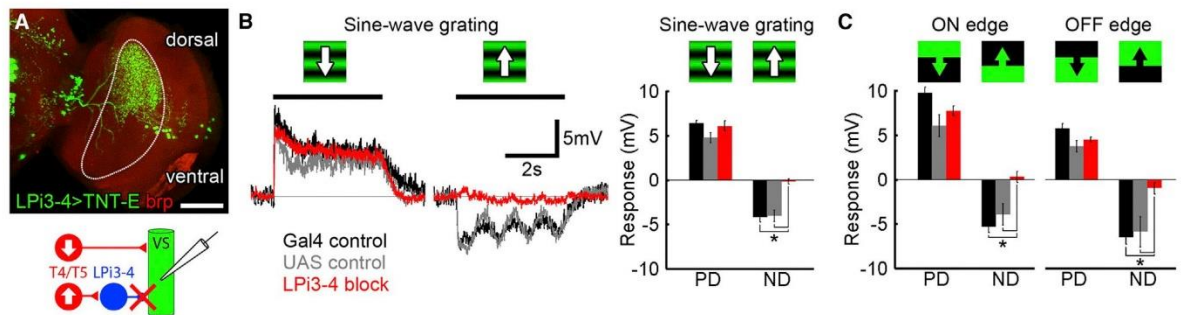


**Figure 4. LPI Neurons Convey Null Direction Responses to Tangential Cells**

(A) Tetanus toxin light chain (TNT-E) is expressed in LPI3-4 neurons to silence synaptic release. Since expression by the driver line is confined to the dorsal part of the lobula plate (demarked by white line), visual stimuli to test LPI3-4 function were partly confined to the upper half of the visual field. Scale bar, 50  $\mu$ m. The schematic depicts the experimental approach to probe LPI3-4 cell function by whole-cell voltage recordings from VS cells.

(B) Visual stimulation of flies with sine-wave gratings moving down (preferred direction [PD]) or up (null direction [ND]) evokes de- and hyperpolarization in control flies (Gal4, n = 9; UAS, n = 5). In LPI3-4 block flies (n = 10), hyperpolarizing responses to ND motion are selectively abolished. Voltage traces represent averaged data, with SEM omitted for clarity.

(C) VS cell responses to moving ON and OFF edges are similarly affected with ND responses to both edge contrasts abolished in LPI3-4 block flies (Gal4, n = 9; UAS n = 4; LPI3-4 block, n = 10).

Significant differences were established using a two-tailed Wilcoxon rank-sum test, with asterisk indicating  $p < 0.0001$ . Data are represented as mean  $\pm$  SEM.

block flies were largely clipped for negative velocities (upward motion), while positive velocities (downward motion) were still encoded in membrane depolarizations with no obviously different dynamics (Figures 5C–5E, red).

Taken together, these data demonstrate that LPI3-4 neurons integrate direction-selective information from T4 and T5 cells in lobula plate layer 3 and convey this information to VS cells via inhibitory synapses in layer 4, giving rise to the VS cells' null direction responses. However, the absence of inhibitory LPI3-4 input does not noticeably alter the direction tuning, gain, or dynamics of the remaining depolarizing tangential cell potential changes in response to coherently moving patterns (Figures 4, 5, and S3).

#### Functional Implications of Motion Opponency

Since tangential cell dendrites—the postsynaptic targets of LPI neurons—integrate inputs over large receptive fields (Figure 1J'), we reasoned that motion opponency might serve to cancel out incoherent motion signals impinging on different parts of the dendritic tree. To test this, we devised three visual stimuli containing opponent motion information (Figures 6A–6C): (1) 100 dots with random motion trajectories, reflecting independent object motion (“motion noise”); (2) a radially expanding pattern simulating flight through a tunnel (“expanding flow”); and (3) an expanding black square as perceived during object approach on a collision course (“looming square”). We presented these patterns to control and LPI block flies while recording from VS cells. Average responses in control flies were consistently subtle for all patterns (Figures 6D–6G, black traces and bars). In contrast, VS cells in LPI block flies showed robust depolarizations (Figures 6D–6G, red traces and bars). These differences were largely captured by model simulations of a motion detection circuit (for details, see Supplemental Experimental Procedures) subjected to the same kind of stimuli (Figures 6H–6J). We therefore conclude that, in the absence of motion opponent

inhibition, VS cells are rendered sensitive to incoherent motion signals and that the integration of motion opponent inputs serves to reduce noise sensitivity and to increase flow-field selectivity in wide-field neurons.

#### DISCUSSION

Motion detection is a fundamental function of all higher visual systems. It is a paradigmatic model for sensory feature extraction since motion information is not explicitly encoded in the single receptor response but has to be computed by downstream neural circuits. Motion detection can be described as a two-stage process (Borst and Egelhaaf, 1990; Egelhaaf et al., 1989; Reichardt, 1987; van Santen and Sperling, 1985): In the first stage, direction-selective signals are generated by correlating the output from neighboring photoreceptors after asymmetric temporal filtering. Neural substrates corresponding to these correlators are, for instance, the T4/T5 cells of the fly optic lobes (Maisak et al., 2013) and the dendrites of starburst amacrine cells in the mammalian retina (Euler et al., 2002; Kim et al., 2014). In the second stage, signals from oppositely tuned correlators are subtracted from each other, giving rise to a fully opponent output. This processing step is implemented in the fly optic lobe on the dendrites of the lobula plate tangential cells (Borst et al., 1995; Joesch et al., 2008), which receive two kinds of inputs: (1) a direct excitatory input from T4/T5 cells terminating within the same lobula plate layer, giving rise to depolarization during preferred direction motion (Maisak et al., 2013; Mauss et al., 2014; Schnell et al., 2012); and (2) as shown here, an indirect inhibitory input via bi-stratified LPI neurons from T4/T5 cells terminating in the adjacent layer, causing hyperpolarization during null direction motion (Figure 7).

GABAergic inhibition has been shown to shape response properties of interneurons in early visual processing by mediating lateral antagonistic effects in *Drosophila* (Freifeld et al.,

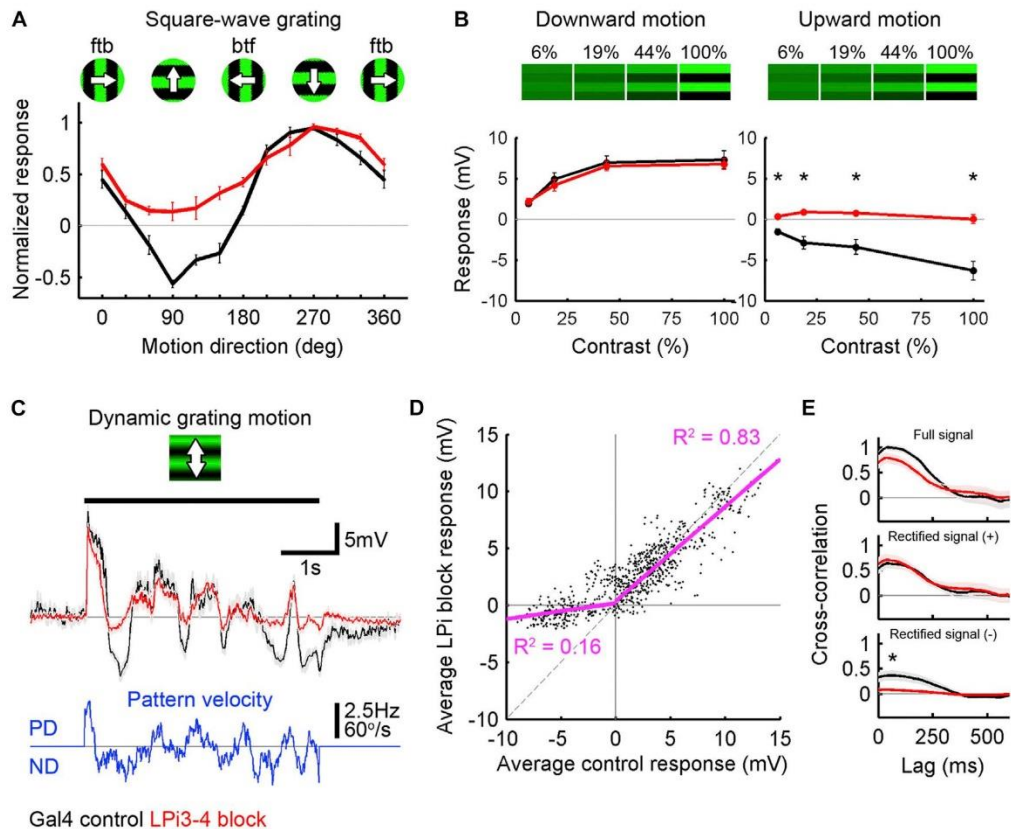


**Figure 5. Directional Tuning, Gain, and Dynamics of Preferred Direction Responses to Coherent Wide-Field Motion Are Normal in Absence of LPI Input**

(A) The directional tuning curve of VS cells in control flies ( $n = 6$ ) shows a sinusoidal dependence on motion direction. Blocking LPI3-4 neurons ( $n = 6$ ) selectively clips all hyperpolarizing responses. ftb, front to back; btf, back to front.

(B) Preferred direction excitation as a function of pattern contrast is indistinguishable between control ( $n = 7$ ) and LPI3-4 block conditions ( $n = 7$ ). Null direction inhibition is selectively abolished for all contrasts in absence of LPI3-4 activity.

(C) Averaged VS cell voltage responses to sine-wave gratings dynamically moving up and down with velocities following a pseudo-random temporal profile (blue, upward deflection represents downward motion). While the voltage responses in VS cells in control flies (black,  $n = 7$ ) followed the velocity in both directions, the VS cell membrane voltage in LPI3-4 block flies (red,  $n = 6$ ) predominantly encoded PD (downward) motions.

(D) Scatter plot of average membrane voltage from VS cells in LPI block against control flies obtained from dynamic motion stimulation (blue trace in C; played forward and backward). For positive control values, the distribution follows a positive linear relationship well described by  $y = 0.83x + 0.35$  ( $R^2 = 0.83$ ), revealing little differences between the two conditions. For negative control values, this relationship breaks down ( $y = 0.14x + 0.17$ ;  $R^2 = 0.16$ ), due to the clipped hyperpolarizing responses in LPI block flies.

(E) Cross-correlation of full, positively, and negatively rectified control and LPI block VS cell signals with the velocity profile of the dynamic motion stimulus (blue trace in C; played forward and backward). Peak correlation for negatively rectified signals is significantly smaller in LPI block compared to control flies since hyperpolarizing potentials are largely missing in the absence of LPI input. For the positively rectified signals, no significant difference is observed. Hence, the lack of inhibitory LPI3-4 input to VS cells does not alter the dynamics of their depolarizing responses.

Significant differences were established using a two-tailed Wilcoxon rank-sum test, with asterisk indicating  $p < 0.001$ . Data are represented as mean  $\pm$  SEM. See also Figure S3.

2013). Work in the *Calliphora* visual system has ascribed a more specialized role for GABAergic transmission in mediating null direction inhibition, based on experiments using picrotoxinin as a GABA receptor antagonist (Brotz and Borst, 1996; Egelhaaf et al., 1990). Unexpectedly, in the same context, we have identified glutamate as the underlying neurotransmitter in *Drosophila*. This discrepancy is perhaps due to neglecting the action of the

pharmacologic compound as a rather unspecific chloride channel blocker (Liu and Wilson, 2013; Marder and Paupardin-Tritsch, 1978; Mauss et al., 2014) in earlier work. It should also be noted that, in *Calliphora*, picrotoxinin application was shown to have two effects on tangential cell motion processing: preferred direction depolarization was enlarged, and null direction hyperpolarization was replaced by noticeable depolarization

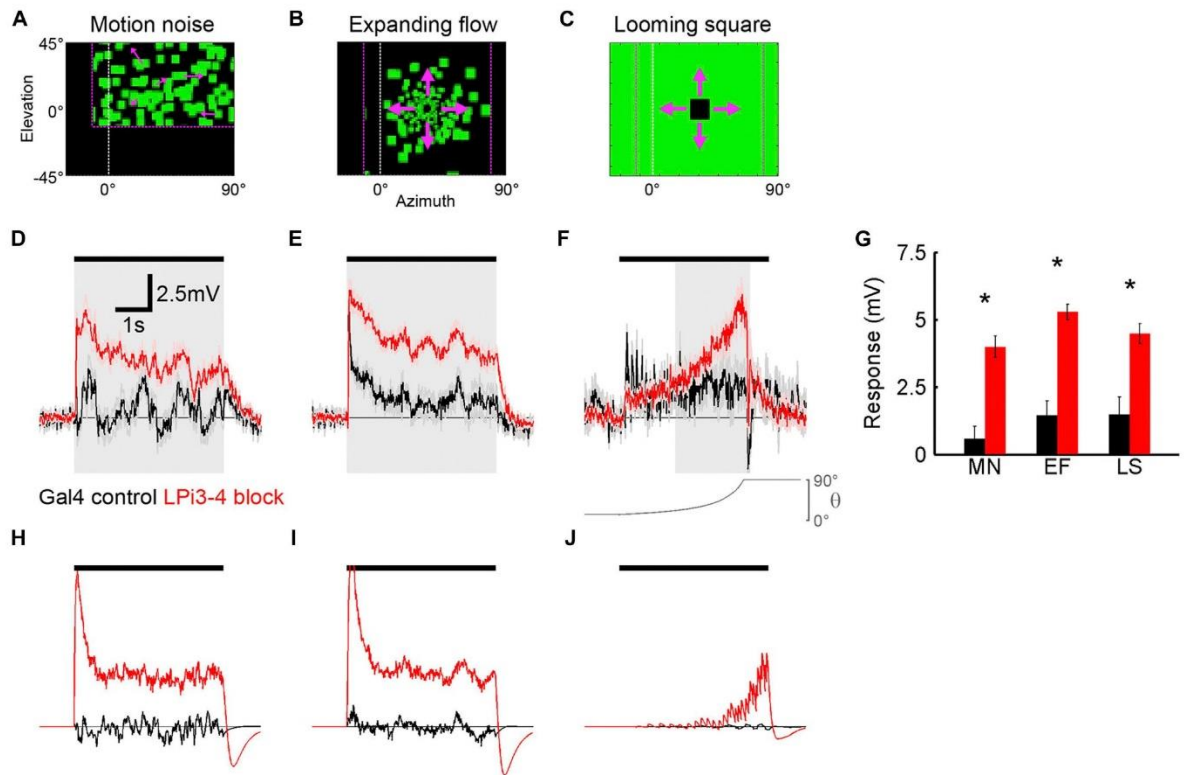


**Figure 6. Silencing Inhibitory Motion-Opponent Input to Tangential Cells Increases Responses to Motion Noise and Non-uniform Flow-Field Patterns**

(A–C) Stimulation arena showing images from visual patterns used to probe VS cell responses in control and LPI3-4 block flies. Independent motion of 100 dots following random two-dimensional trajectories (A); expanding flow field simulating flight through a tunnel (B); and looming black square (C) with angular size as a function of time shown in (F).

(D–F) Averaged recording traces ( $n = 6$ ) from Gal4 control (black) and LPI3-4 block (red) flies subjected to the above shown visual patterns (four independent patterns for each D and E).

(G) Bars represent average baseline-subtracted responses. Shaded gray areas in (D) to (F) demarcate the response time window used for quantification. VS cell responses in control flies were small for all stimuli with average depolarizations of  $< 1.5$  mV. In contrast, VS cells without motion-opponent inhibitory input (LPI3-4 block flies) showed significantly higher depolarizations ( $> 4$  mV).

(H to J) Tangential cell responses could be largely captured by a computational model incorporating spatial integration of elementary motion detectors with and without motion-opponent subtraction (see Supplemental Experimental Procedures for details).

Significant differences were established using a two-tailed Wilcoxon rank-sum test, with asterisk indicating  $p < 0.005$ . Data are represented as mean  $\pm$  SEM.

(Single et al., 1997). This was interpreted as evidence for weak directional tuning of the inputs, i.e., the later identified T4/T5 cells. A similar result was observed in *Drosophila* (A.S.M., unpublished data). The LPI3-4 block in *Drosophila*, however, did not produce a prominent null direction depolarization, and preferred direction excitation was indistinguishable from the control condition (Figures 4, 5, and S3). Since a recent study demonstrated narrow directional tuning of the T4/T5 cells (Maisak et al., 2013), rendering postsynaptic directional response sharpening unnecessary, we suggest that picrotoxinin off-target effects on glutamate or GABA receptors in the upstream circuit are responsible for this inconsistency, and genetic LPI block represents a more suitable approach to eliminate null direction inhibition.

We have focused our analysis on the LPI3-4 neurons and their postsynaptic partners in layer 4, the VS cells, because of their

experimental accessibility. However, our findings can be most likely extended to the other layers. Tangential cells with dendrites in layer 3 have been identified in other fly species (Hausen, 1976, 1984; Wertz et al., 2008). Such so-called V2 cells are motion opponent with preference to upward flow, in agreement with their presumed inputs from excitatory layer 3 T4/T5 cells. Since our data indicate that the LPI4-3 neurons convey glutamatergic signals selective for downward motion to lobula plate layer 3, it seems plausible that a motion-opponent wiring complementary to the LPI3-4/V2 cell connectivity exists as well (Figure 7). The preference of LPI4-3 cells to ON over OFF edges is unexpected because in contrast to tangential cells, LPI4-3 neurons appear to be able to differentiate between T4/ON and T5/OFF input. Whether this finding hints toward an ON-selective null direction inhibition in layer 3 postsynaptic cells, perhaps dictated by

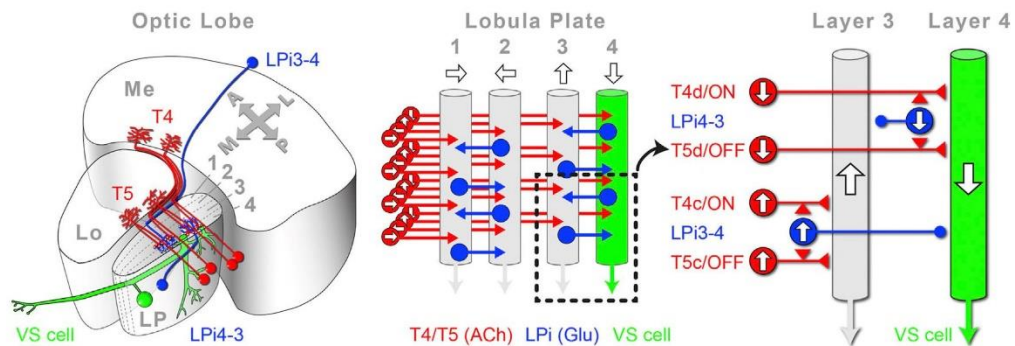


**Figure 7. Connectivity Model of the Lobula Plate**

Four subclasses of T4 and T5 cells (red) convey ON and OFF direction-selective input to the lobula plate. Both T4 and T5 cells signal front-to-back, back-to-front, upward, and downward motion and project according to their tuning to layers 1–4 (those encoding horizontal motion and targeting layers 1 and 2 are depicted only in the middle schematic for clarity). Lobula plate tangential cells (green) of the vertical system (VS) extend their dendrites in lobula plate layer 4, where they receive direct excitatory inputs from T4/T5 cells tuned to downward motion. In addition, LPI3–4 neurons (blue) obtain excitatory T4/T5 input during upward motion in layer 3 and convey a sign-inverted signal onto VS cells in the adjacent layer via an inhibitory glutamatergic synapse. This arrangement generates a fully motion-opponent response in VS cells. LPI4–3 neurons likely contribute to a complementary circuit in layers 1 and 2. A, anterior; P, posterior; M, medial; L, lateral.

certain natural stimulus statistics, or whether it reflects merely a bias of the driver line for an ON-selective LPI4–3 subgroup remains to be investigated. Some presynaptic swellings of the complementary LPI3–4 cells also exhibited polarity preference, but at present, it is unclear whether this indicates a similar T4/T5 selectivity on a cell-by-cell basis or stochastic sampling of inputs. The functional architecture of lobula plate layers 1 and 2 strongly resembles the one of layers 3 and 4 with a 90° directional tuning shift (Figure 7): motion-opponent HS cells with a preference for front-to-back motion ramify their dendrites exclusively in layer 1 (Schnell et al., 2010), while motion-opponent Hx cells that prefer back-to-front motion confine their dendrites to layer 2 (Wasserman et al., 2015). We therefore anticipate the existence of at least two complementary horizontal LPI cell types in those layers too. It thus seems that global motion information is processed initially in two segregated horizontal and vertical subsystems with little direct interaction. Rather than representing the cardinal directions in a clock- or counter-clockwise manner, the four lobula plate layers are arranged such that opposite directions are represented side by side. This functional organization might serve to facilitate efficient nearest-neighbor interactions of motion-opponent signals.

Similar to the fly lobula plate, the dorsal lateral geniculate nucleus (dLGN) in mammals relays direction-selective signals from the retina to higher brain centers (Cruz-Martín et al., 2014). Some fundamental parallels in the organization of the two brain regions seem to exist. Their input channels, T4/T5 neurons in flies and ON/OFF direction-selective ganglion cells in mammals, predominantly encode the four cardinal directions of motion up, down, left, and right (Maisak et al., 2013; Piscopo et al., 2013). The anatomical separation of the vertical and horizontal subsystems in flies seems to be mirrored, at least to a degree, in the dLGN, where opposing horizontal direction information resides in the superficial region of mouse dLGN, segregated from vertical motion (Marshall et al., 2012). Moreover, a feed-forward inhibitory

principle to generate motion opponency that we describe in the fly might also prevail in the dLGN, where directionally selective output neurons were suggested to integrate opposing signals from retinal ganglion cells (Levick et al., 1969; Oyster et al., 1971), possibly directly and indirectly via local inhibitory neurons (Cox et al., 1998; Singer, 1977; Wang et al., 2011). However, many mammalian dLGN neurons are also orientation selective, potentially obtaining this property by integrating opponent excitatory direction-selective input (Cruz-Martín et al., 2014; Marshall et al., 2012; Piscopo et al., 2013).

Associated with their proposed role as matched filters for sensing the optic flow generated by an animal's self-motion, in contrast to dLGN neurons, lobula plate tangential cells have large receptive fields, in some cases covering more than 100 degrees of visual space (Hopp et al., 2014; Joesch et al., 2008; Krapp and Hengstenberg, 1996; Schnell et al., 2010). Independent movement, e.g., originating from conspecifics or foliage, thus poses a challenge to the system by providing excitatory drive to tangential cells not associated with self-motion. Our experiments with intact and silenced LPI neurons support the idea that such inputs are attenuated by antagonistic signals from oppositely moving objects elsewhere in the visual scene (Figure 6D). Perhaps more importantly, different flight maneuvers generate ambiguous optic flow patterns in sub-parts of the receptive field. For instance, both lift and forward translation cause downward optic flow in the ventral visual field, while only the latter produces upward flow dorsally. Taking into account excitation only, a reliable distinction between those patterns, especially under varying stimulus intensities, i.e., contrasts as experienced in natural scenes, seems inconceivable. We have demonstrated (Figures 6E and 6F) that LPI cells strongly reduce such ambiguities, most likely by cancelling the excitation caused in one part of the dendrite by inhibition in another part. Motion opponency is thus reminiscent of other neural opponency mechanisms. In the classical example of color opponency, neural comparison discriminates

sensory signals that are ambiguous at the level of photoreceptors in terms of wavelength and stimulus intensity. Notably, while color vision requires at least two separate measurements at any point in space, motion opponency disambiguates different optic flow-fields derived from the same photoreceptor responses. Given that wide-field motion-sensitive neurons in various other systems are also motion opponent (Collett and Blest, 1966; Duffy and Wurtz, 1991; Ibbotson, 1991; Wylie et al., 1998), we suggest that such a mechanism might be universally required to increase sensitivity and selectivity for optic flow-fields associated with self-motion. Similar neural comparators might be widely used for the extraction of equally complex sensory features.

## EXPERIMENTAL PROCEDURES

### Flies

Details about all fly stocks and genotypes can be found in the [Supplemental Experimental Procedures](#).

### Immunostaining

Brains were dissected in phosphate-buffered saline and were fixed in 4% PFA with 0.1% TritonX or, for anti-vGlut and anti-GAD1, with Bouin's fixative. Brains were subsequently washed and sequentially stained with primary and fluorophore-conjugated secondary antibodies. 2% normal goat serum was added to all primary and secondary antibody solutions. Brains were optically sectioned with a Leica TCS SP5 confocal microscope. Brains expressing GRASP components were fixed and stained against the neuropile marker bruchpilot. Afterward, native GRASP fluorescence was visualized. For more details, please refer to the [Supplemental Experimental Procedures](#).

### Multicolor Stochastic Labeling

Stochastic single-cell labeling was carried out using "MultiColor FlipOut" (MCFO) (Nern et al., 2015), a multicolor adaptation of the "flip-out" approach (Struhl and Basler, 1993).

### Transcript Profiling

The transcript profiling protocol was modified from the method described previously (Takemura et al., 2011). For details, please see the [Supplemental Experimental Procedures](#), Table S1, and Figure S4.

### Two-Photon Calcium Imaging

Two-photon imaging was performed on a custom-built microscope, as previously described (Maisak et al., 2013). Images were acquired at a frame rate of 1.88 Hz.

### Electrophysiology, Optogenetic Stimulation, and Pharmacology

Electrophysiological and optogenetic experiments were performed as described previously (Mauss et al., 2014). Picrotoxinin (PTX; Sigma P8390) was dissolved in dimethylsulfoxide at 50 mM and was kept as a stock at  $-20^{\circ}\text{C}$ . For experiments, PTX was diluted in external solution to 25  $\mu\text{M}$  and washed in (10 min) and out (30 min) at 2 ml/min.

### Visual Stimulation

Custom-built LED arenas were used for visual stimulation in calcium imaging and electrophysiology experiments. The arenas covered  $\sim 170^{\circ}$  and  $90^{\circ}$  in azimuth and elevation, respectively, and allowed refresh rates of 550 Hz and 16 intensity levels (Maisak et al., 2013). Identical visual stimuli were presented in three to five trials in every experiment, usually in a randomized sequence. Please refer to the [Supplemental Experimental Procedures](#) for more details.

### Physiological Data Analysis

Data from VS cell recordings and LPI calcium imaging experiments were evaluated using custom-written analysis scripts in Matlab. Details can be found in the [Supplemental Experimental Procedures](#).

### Modeling

Stimuli were calculated at  $1^{\circ}$  spatial and 10 ms temporal resolution. Every stimulus frame was convolved with a radial Gaussian function of  $5^{\circ}$  half-width and down-sampled to an array of  $40 \times 40$  photoreceptors, corresponding to an angular separation of  $5^{\circ}$  between neighboring receptors. Please see the [Supplemental Experimental Procedures](#) for detailed parameters of the model.

## SUPPLEMENTAL INFORMATION

[Supplemental Information](#) includes Supplemental Experimental Procedures, four figures, and one table and can be found with this article online at <http://dx.doi.org/10.1016/j.cell.2015.06.035>.

## AUTHOR CONTRIBUTIONS

A.S.M. performed and analyzed electrophysiological recordings. K.P. carried out and analyzed immunostainings (except multicolor labeling and TNT-E expression), transcript profiling, and GRASP experiments. A.A. performed and analyzed two-photon calcium imaging experiments. A.B. did computer simulations. G.M.R. and A.N. generated the LPI driver lines and performed multicolor stochastic labeling. A.S.M. and A.B. designed the study. A.S.M., A.A., and A.B. wrote the paper with the help of all authors.

## ACKNOWLEDGMENTS

We would like to thank Barry Dickson (Janelia) for sharing unpublished fly lines; Matthias Meier, Etienne Serbe, and Jürgen Haag for help with two-photon calcium imaging; Christoph Kapfer for advice on fixation procedures; Georg Ammer and Wolfgang Essbauer for tetanus toxin staining; Aljoscha Leonhardt, Armin Bahl, and Tabea Schilling for experimental help; Wolfgang Essbauer, Christian Theile, Michael Sauter, and Renate Gleich for technical assistance; and Jürgen Haag for critically reading the manuscript. We thank the Janelia Fly-Light Project Team (especially Jennifer Jeter) for assistance with MCFO sample preparation and imaging. We would also like to acknowledge Karin Nordström (Uppsala University) for sharing unpublished results. We acknowledge the Developmental Studies Hybridoma Bank for antibodies and the Bloomington Drosophila Stock Center for flies. A.A. was funded by an EMBO Long-Term Fellowship. This work was supported by the Max-Planck-Society, the Deutsche Forschungsgemeinschaft (CRC 870), and HHMI.

Received: January 13, 2015

Revised: April 1, 2015

Accepted: May 18, 2015

Published: July 16, 2015

## REFERENCES

- Akerboom, J., Chen, T.-W., Wardill, T.J., Tian, L., Marvin, J.S., Mutlu, S., Calderón, N.C., Esposti, F., Borghuis, B.G., Sun, X.R., et al. (2012). Optimization of a GCaMP calcium indicator for neural activity imaging. *J. Neurosci.* *32*, 13819–13840.
- Bahl, A., Ammer, G., Schilling, T., and Borst, A. (2013). Object tracking in motion-blind flies. *Nat. Neurosci.* *16*, 730–738.
- Bausenwein, B., and Fischbach, K.F. (1992). Activity labeling patterns in the medulla of *Drosophila melanogaster* caused by motion stimuli. *Cell Tissue Res.* *270*, 25–35.
- Bausenwein, B., Dittrich, A.P., and Fischbach, K.F. (1992). The optic lobe of *Drosophila melanogaster*. II. Sorting of retinotopic pathways in the medulla. *Cell Tissue Res.* *267*, 17–28.
- Borst, A., and Egelhaaf, M. (1990). Direction selectivity of blowfly motion-sensitive neurons is computed in a two-stage process. *Proc. Natl. Acad. Sci. USA* *87*, 9363–9367.
- Borst, A., Egelhaaf, M., and Haag, J. (1995). Mechanisms of dendritic integration underlying gain control in fly motion-sensitive interneurons. *J. Comput. Neurosci.* *2*, 5–18.

- Borst, A., Haag, J., and Reiff, D.F. (2010). Fly motion vision. *Annu. Rev. Neurosci.* *33*, 49–70.
- Brotz, T.M., and Borst, A. (1996). Cholinergic and GABAergic receptors on fly tangential cells and their role in visual motion detection. *J. Neurophysiol.* *76*, 1786–1799.
- Clark, D.A., Bursztyn, L., Horowitz, M.A., Schnitzer, M.J., and Clandinin, T.R. (2011). Defining the computational structure of the motion detector in *Drosophila*. *Neuron* *70*, 1165–1177.
- Collett, T.S., and Blest, A.D. (1966). Binocular, directionally selective neurones, possibly involved in the optomotor response of insects. *Nature* *212*, 1330–1333.
- Cox, C.L., Zhou, Q., and Sherman, S.M. (1998). Glutamate locally activates dendritic outputs of thalamic interneurons. *Nature* *394*, 478–482.
- Cruz-Martín, A., El-Danaf, R.N., Osakada, F., Sriram, B., Dhande, O.S., Nguyen, P.L., Callaway, E.M., Ghosh, A., and Huberman, A.D. (2014). A dedicated circuit links direction-selective retinal ganglion cells to the primary visual cortex. *Nature* *507*, 358–361.
- Denk, W., Strickler, J.H., and Webb, W.W. (1990). Two-photon laser scanning fluorescence microscopy. *Science* *248*, 73–76.
- Duffy, C.J., and Wurtz, R.H. (1991). Sensitivity of MST neurons to optic flow stimuli. I. A continuum of response selectivity to large-field stimuli. *J. Neurophysiol.* *65*, 1329–1345.
- Egelhaaf, M., Borst, A., and Reichardt, W. (1989). Computational structure of a biological motion-detection system as revealed by local detector analysis in the fly's nervous system. *J. Opt. Soc. Am. A* *6*, 1070–1087.
- Egelhaaf, M., Borst, A., and Pilz, B. (1990). The role of GABA in detecting visual motion. *Brain Res.* *509*, 156–160.
- Eichner, H., Joesch, M., Schnell, B., Reiff, D.F., and Borst, A. (2011). Internal structure of the fly elementary motion detector. *Neuron* *70*, 1155–1164.
- Euler, T., Detwiler, P.B., and Denk, W. (2002). Directionally selective calcium signals in dendrites of starburst amacrine cells. *Nature* *418*, 845–852.
- Feinberg, E.H., Vanhoven, M.K., Bendesky, A., Wang, G., Fetter, R.D., Shen, K., and Bargmann, C.I. (2008). GFP Reconstitution Across Synaptic Partners (GRASP) defines cell contacts and synapses in living nervous systems. *Neuron* *57*, 353–363.
- Freifeld, L., Clark, D.A., Schnitzer, M.J., Horowitz, M.A., and Clandinin, T.R. (2013). GABAergic lateral interactions tune the early stages of visual processing in *Drosophila*. *Neuron* *78*, 1075–1089.
- Hausen, K. (1976). Functional characterization and anatomical identification of motion sensitive neurons in the lobula plate of the blowfly *Calliphora erythrocephala*. *Z. Naturforsch. C* *31*, 629–633.
- Hausen, K. (1984). The lobula-complex of the fly: Structure, function and significance in visual behaviour. *Photoreception and Vision in Invertebrates* *74*, 523–559.
- Hausen, K., Wolburg-Buchholz, W., and Ribi, W.A. (1980). The synaptic organization of visual interneurons in the lobula complex of flies. A light and electron microscopical study using silver-intensified cobalt-impregnations. *Cell Tissue Res.* *208*, 371–387.
- Hopp, E., Borst, A., and Haag, J. (2014). Subcellular mapping of dendritic activity in optic flow processing neurons. *J. Comp. Physiol. A Neuroethol. Sens. Neural Behav. Physiol.* *200*, 359–370.
- Ibbotson, M.R. (1991). Wide-field motion-sensitive neurons tuned to horizontal movement in the honeybee, *Apis mellifera*. *J. Comp. Physiol. A* *168*, 91–102.
- Jenett, A., Rubin, G.M., Ngo, T.T., Shepherd, D., Murphy, C., Dionne, H., Pfeiffer, B.D., Cavallaro, A., Hall, D., Jeter, J., et al. (2012). A GAL4-driver line resource for *Drosophila* neurobiology. *Cell Rep* *2*, 991–1001.
- Joesch, M., Plett, J., Borst, A., and Reiff, D.F. (2008). Response properties of motion-sensitive visual interneurons in the lobula plate of *Drosophila melanogaster*. *Curr. Biol.* *18*, 368–374.
- Joesch, M., Schnell, B., Raghu, S.V., Reiff, D.F., and Borst, A. (2010). ON and OFF pathways in *Drosophila* motion vision. *Nature* *468*, 300–304.
- Joesch, M., Weber, F., Eichner, H., and Borst, A. (2013). Functional specialization of parallel motion detection circuits in the fly. *J. Neurosci.* *33*, 902–905.
- Kim, J.S., Greene, M.J., Zlateski, A., Lee, K., Richardson, M., Turaga, S.C., Purcaro, M., Balkam, M., Robinson, A., Behabadi, B.F., et al.; EyeWireds (2014). Space-time wiring specificity supports direction selectivity in the retina. *Nature* *509*, 331–336.
- Krapp, H.G., and Hengstenberg, R. (1996). Estimation of self-motion by optic flow processing in single visual interneurons. *Nature* *384*, 463–466.
- Levick, W.R., Oyster, C.W., and Takahashi, E. (1969). Rabbit lateral geniculate nucleus: sharpener of directional information. *Science* *165*, 712–714.
- Liu, W.W., and Wilson, R.I. (2013). Glutamate is an inhibitory neurotransmitter in the *Drosophila* olfactory system. *Proc. Natl. Acad. Sci. USA* *110*, 10294–10299.
- Maisak, M.S., Haag, J., Ammer, G., Serbe, E., Meier, M., Leonhardt, A., Schilling, T., Bahl, A., Rubin, G.M., Nern, A., et al. (2013). A directional tuning map of *Drosophila* elementary motion detectors. *Nature* *500*, 212–216.
- Marder, E., and Paupardin-Tritsch, D. (1978). The pharmacological properties of some crustacean neuronal acetylcholine, gamma-aminobutyric acid, and L-glutamate responses. *J. Physiol.* *280*, 213–236.
- Marshel, J.H., Kaye, A.P., Nauhaus, I., and Callaway, E.M. (2012). Anterior-posterior direction opponency in the superficial mouse lateral geniculate nucleus. *Neuron* *76*, 713–720.
- Mauss, A.S., Meier, M., Serbe, E., and Borst, A. (2014). Optogenetic and pharmacologic dissection of feedforward inhibition in *Drosophila* motion vision. *J. Neurosci.* *34*, 2254–2263.
- Nern, A., Pfeiffer, B.D., and Rubin, G.M. (2015). Optimized tools for multicolor stochastic labeling reveal diverse stereotyped cell arrangements in the fly visual system. *Proc. Natl. Acad. Sci. USA* *112*, E2967–E2976.
- Oyster, C.W., Takahashi, E., and Levick, W.R. (1971). Information processing in the rabbit visual system. *Doc. Ophthalmol.* *30*, 161–204.
- Pfeiffer, B.D., Jenett, A., Hammonds, A.S., Ngo, T.-T.B., Misra, S., Murphy, C., Scully, A., Carlson, J.W., Wan, K.H., Lavery, T.R., et al. (2008). Tools for neuroanatomy and neurogenetics in *Drosophila*. *Proc. Natl. Acad. Sci. USA* *105*, 9715–9720.
- Piscopo, D.M., El-Danaf, R.N., Huberman, A.D., and Niell, C.M. (2013). Diverse visual features encoded in mouse lateral geniculate nucleus. *J. Neurosci.* *33*, 4642–4656.
- Reichardt, W. (1987). Evaluation of optical motion information by movement detectors. *J. Comp. Physiol. A Neuroethol. Sens. Neural Behav. Physiol.* *161*, 533–547.
- Reiff, D.F., Plett, J., Mank, M., Griesbeck, O., and Borst, A. (2010). Visualizing retinotopic half-wave rectified input to the motion detection circuitry of *Drosophila*. *Nat. Neurosci.* *13*, 973–978.
- Rister, J., Pauls, D., Schnell, B., Ting, C.Y., Lee, C.H., Sinakevitch, I., Morante, J., Strausfeld, N.J., Ito, K., and Heisenberg, M. (2007). Dissection of the peripheral motion channel in the visual system of *Drosophila melanogaster*. *Neuron* *56*, 155–170.
- Sato, H., Daw, N.W., and Fox, K. (1991). An intracellular recording study of stimulus-specific response properties in cat area 17. *Brain Res.* *544*, 156–161.
- Schnell, B., Joesch, M., Forstner, F., Raghu, S.V., Otsuna, H., Ito, K., Borst, A., and Reiff, D.F. (2010). Processing of horizontal optic flow in three visual interneurons of the *Drosophila* brain. *J. Neurophysiol.* *103*, 1646–1657.
- Schnell, B., Raghu, S.V., Nern, A., and Borst, A. (2012). Columnar cells necessary for motion responses of wide-field visual interneurons in *Drosophila*. *J. Comp. Physiol. A Neuroethol. Sens. Neural Behav. Physiol.* *198*, 389–395.
- Scott, E.K., Raabe, T., and Luo, L. (2002). Structure of the vertical and horizontal system neurons of the lobula plate in *Drosophila*. *J. Comp. Neurol.* *454*, 470–481.
- Shinomiya, K., Karuppudurai, T., Lin, T.Y., Lu, Z., Lee, C.H., and Meinertzhagen, I.A. (2014). Candidate neural substrates for off-edge motion detection in *Drosophila*. *Curr. Biol.* *24*, 1062–1070.



- Silies, M., Gohl, D.M., Fisher, Y.E., Freifeld, L., Clark, D.A., and Clandinin, T.R. (2013). Modular use of peripheral input channels tunes motion-detecting circuitry. *Neuron* 79, 111–127.
- Singer, W. (1977). Control of thalamic transmission by corticofugal and ascending reticular pathways in the visual system. *Physiol. Rev.* 57, 386–420.
- Single, S., Haag, J., and Borst, A. (1997). Dendritic computation of direction selectivity and gain control in visual interneurons. *J. Neurosci.* 17, 6023–6030.
- Struhl, G., and Basler, K. (1993). Organizing activity of wingless protein in *Drosophila*. *Cell* 72, 527–540.
- Sweeney, S.T., Brodie, K., Keane, J., Niemann, H., and O’Kane, C.J. (1995). Targeted expression of tetanus toxin light chain in *Drosophila* specifically eliminates synaptic transmission and causes behavioral defects. *Neuron* 14, 341–351.
- Takemura, S.Y., Karuppururai, T., Ting, C.Y., Lu, Z., Lee, C.H., and Meinertzhagen, I.A. (2011). Cholinergic circuits integrate neighboring visual signals in a *Drosophila* motion detection pathway. *Curr. Biol.* 21, 2077–2084.
- Takemura, S.Y., Bharioke, A., Lu, Z., Nern, A., Vitaladevuni, S., Rivlin, P.K., Katz, W.T., Olbris, D.J., Plaza, S.M., Winston, P., et al. (2013). A visual motion detection circuit suggested by *Drosophila* connectomics. *Nature* 500, 175–181.
- Tuthill, J.C., Nern, A., Holtz, S.L., Rubin, G.M., and Reiser, M.B. (2013). Contributions of the 12 neuron classes in the fly lamina to motion vision. *Neuron* 79, 128–140.
- van Santen, J.P., and Sperling, G. (1985). Elaborated Reichardt detectors. *J. Opt. Soc. Am. A* 2, 300–321.
- Wang, X., Vaingankar, V., Soto Sanchez, C., Sommer, F.T., and Hirsch, J.A. (2011). Thalamic interneurons and relay cells use complementary synaptic mechanisms for visual processing. *Nat. Neurosci.* 14, 224–231.
- Wasserman, S.M., Aptekar, J.W., Lu, P., Nguyen, J., Wang, A.L., Keles, M.F., Grygoruk, A., Krantz, D.E., Larsen, C., and Frye, M.A. (2015). Olfactory neuro-modulation of motion vision circuitry in *Drosophila*. *Curr. Biol.* 25, 467–472.
- Wertz, A., Borst, A., and Haag, J. (2008). Nonlinear integration of binocular optic flow by DNOVS2, a descending neuron of the fly. *J. Neurosci.* 28, 3131–3140.
- Wylie, D.R., Bischof, W.F., and Frost, B.J. (1998). Common reference frame for neural coding of translational and rotational optic flow. *Nature* 392, 278–282.

# Supplemental Figures

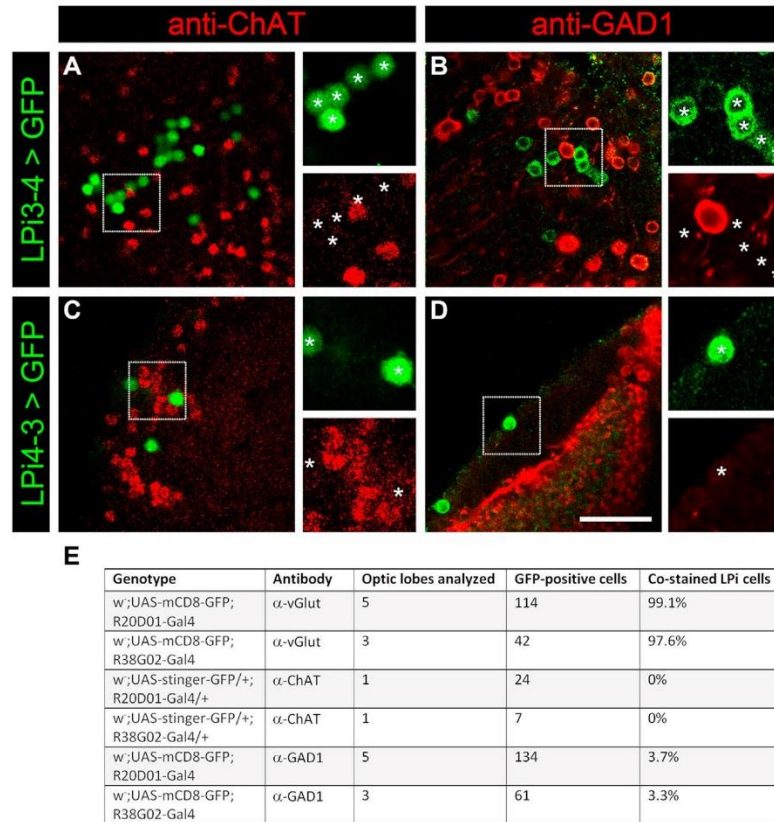


**Figure S1. Neurotransmitter Phenotype of LPI Neurons, Related to Figure 2**

(A–D) Immunostaining of brains expressing GFP in LPI3-4 (A and B) and LPI4-3 neurons (C and D) with antibodies against choline acetyltransferase (ChAT) and glutamic acid decarboxylase 1 (GAD1) does not show co-localization, indicating that LPI cells are neither cholinergic nor GABAergic.

(E) Quantification of neurotransmitter marker co-localization with GFP-expressing LPI neurons.

Scale bar 20  $\mu$ m (10  $\mu$ m for magnified views from demarcated boxes). Genotypes: (A) w ; UAS-stinger-GFP/+ ; R20D01-Gal4/+ , (B) w ; UAS-mCD8-GFP/+ ; R20D01-Gal4/+ , (C) w ; UAS-stinger-GFP/+ ; R38G02-Gal4/+ , (D) w ; UAS-mCD8-GFP/+ ; R38G02-Gal4/+ .

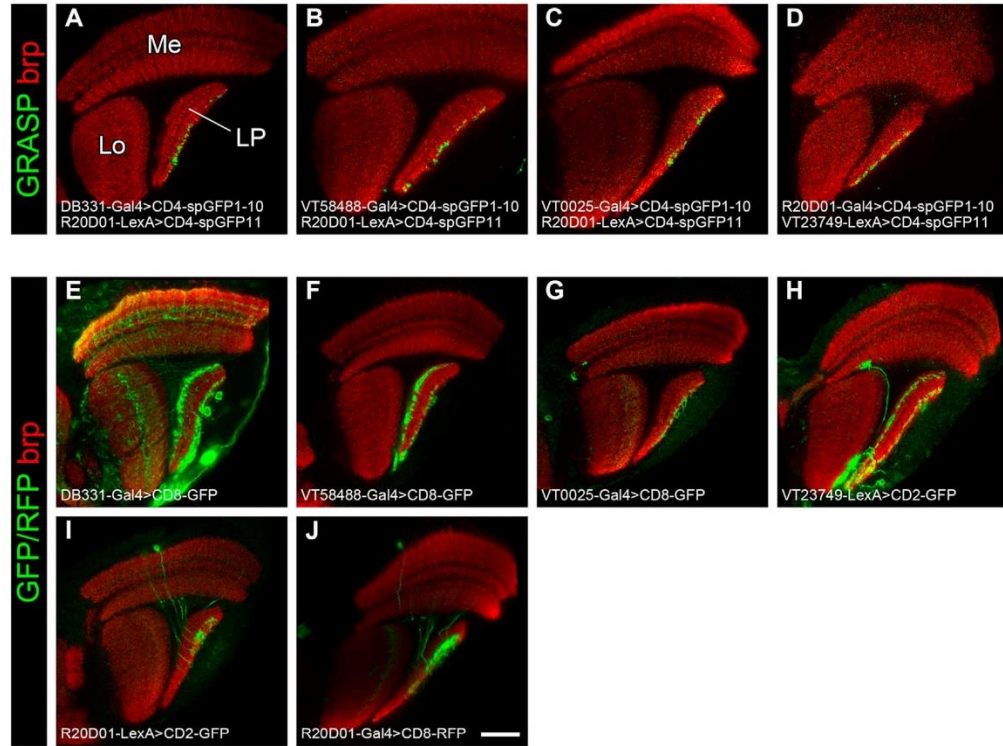


**Figure S2. Membrane Contact between LPI3-4 and VS Cells Labeled by GRASP, Related to Figure 2**

(A–D) GRASP signal is detected in lobula plate (LP) layer 4 using four different LPI3-4/VS cell driver line combinations (Lo, lobula; Me, medulla). (D) is the same confocal image as shown in Figure 2D.

(E–J) Expression patterns of the individual Gal4 and LexA lines used for GRASP experiments.

Scale bar 20  $\mu$ m. Genotypes: (A) DB331-Gal4/+; lexAop-CD4-spGFP11, UAS-CD4-spGFP1-10/R20D01-LexA/+; +, (B) w<sup>-</sup>; lexAop-CD4-spGFP11, UAS-CD4-spGFP1-10/R20D01-LexA; VT58488-Gal4/+; +, (C) w<sup>-</sup>; lexAop-CD4-spGFP11, UAS-CD4-spGFP1-10/R20D01-LexA; VT0025-Gal4/+; +, (D) w<sup>-</sup>; lexAop-CD4-spGFP11, UAS-CD4-spGFP1-10/VT23749-LexA; R20D01-Gal4/+; +, (E) DB331-Gal4; UAS-mCD8-GFP/+; +, (F) w<sup>-</sup>; UAS-mCD8-GFP/+; +; VT58488-Gal4/+; +, (G) w<sup>-</sup>; UAS-mCD8-GFP/+; +; VT0025-Gal4/+; +, (H) w<sup>-</sup>; VT23749-LexA/+; +; lexAop-CD2-GFP/+; +, (I) w<sup>-</sup>; R20D01-LexA/+; +; lexAop-CD2-GFP/+; +, (J) w<sup>-</sup>; UAS-mCD8-RFP/+; +; R20D01-Gal4/+; +.

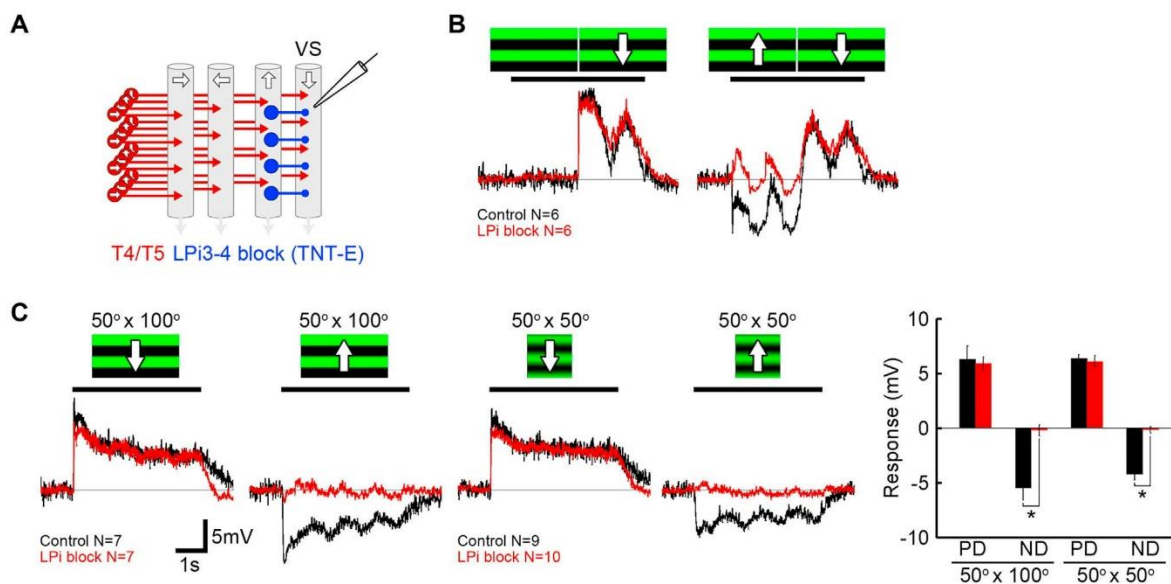


**Figure S3. VS Cell Preferred Direction Responses to Moving Gratings Are Not Affected by the Absence of Null Direction Inhibition, Related to Figure 5**

(A) Schematic to illustrate the experimental approach to probe LPI3-4 cell function by whole cell voltage recordings from VS cells. LPI3-4 output is silenced by TNT-E expression (genotypes as in Figure 5 and 6)

(B) Stimulation with a still grating followed by 2 s downward motion and stimulation with 2 s upward followed by 2 s downward grating motion, moving gratings presented at 1 Hz temporal frequency. For both stimulus conditions, preferred direction excitation is indistinguishable between the control and LPI3-4 block condition, showing that preceding inhibitory stimulus history does not affect the gain of the depolarizing output of tangential cells on a timescale of several seconds.

(C) Stimulation with moving gratings of two sizes: 50° x 100° (square-wave grating) and 50° x 50° (sine-wave grating, data taken from Figure 4B). Gratings were presented at 1 Hz temporal frequency. While null direction responses are selectively abolished in LPI3-4, preferred direction depolarization is identical in both experimental conditions, irrespective of the stimulus window size.

Significant differences were established using a two-tailed Wilcoxon rank-sum test with \* indicating  $p < 0.001$ . Data are represented as mean  $\pm$  SEM.

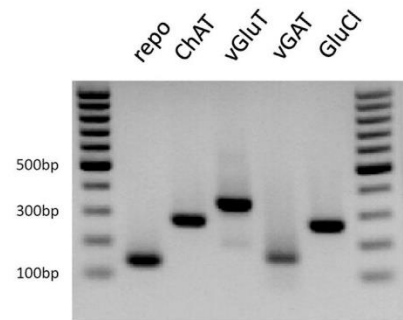


**Figure S4. PCR Amplification of Transcripts Isolated from Whole Heads, Related to Experimental Procedures**

Functionality of gene-specific primers used to detect transcript expression in individual neurons was tested on RNA isolated from heads of Canton S flies. The PCR products detected in the gel match their expected sizes (see [Table S1, Supplemental Experimental Procedures](#)).

Cell

Supplemental Information

## **Neural Circuit to Integrate**

## **Opposing Motions in the Visual Field**

Alex S. Mauss, Katarina Pankova, Alexander Arenz, Aljoscha Nern, Gerald M. Rubin,  
and Alexander Borst

## SUPPLEMENTAL EXPERIMENTAL PROCEDURES

**Flies.** Flies were raised at 25°C and 60% humidity on standard cornmeal agar medium at a 12 h light/dark cycle. The following fly strains were used: *Canton-S wildtype*, *R20D01-Gal4<sup>attP2</sup>* (LPi3-4), *R38G02-Gal4<sup>attP2</sup>* (LPi4-3), *R42F06-Gal4<sup>attP2</sup>* (T4/T5), *R20D01-LexA<sup>attP40</sup>* (LPi3-4), *DB331-Gal4* on X (courtesy of R. Stocker) (Joesch et al., 2008), *VT58488-Gal4<sup>attP2</sup>*, *VT0025-Gal4<sup>attP2</sup>*, *VT23749-LexA<sup>attP40</sup>*, recombined *lexAop-CD4-spGFP11*, *UAS-CD4-spGFP1-10* on 2<sup>nd</sup> (Gordon and Scott, 2009), *UAS-mCD8-GFP* on 2<sup>nd</sup> (all VT, GRASP and CD8-GFP lines courtesy of Barry Dickson), *UAS-synaptotagmin-HA* on 2<sup>nd</sup> (*UAS-syt-HA*, courtesy of Andreas Prokop) (Löhr et al., 2002; Robinson et al., 2002), multicolor flip-out line MCFO-7 (Nern et al., 2015), *UAS-Channelrhodopsin2-H134R-mCherry* on 2<sup>nd</sup> (*UAS-ChR2-H134R*, courtesy of Stefan Pulver) (Mattis et al., 2012; Nagel et al., 2005; Pulver et al., 2009), *norpA<sup>7</sup>* on X (dysfunctional phototransduction mutant EE5) (Hotta and Benzer, 1970), *UAS-stinger-GFP* on 2<sup>nd</sup>, *UAS-GCaMP5G<sup>attP40</sup>* (Akerboom et al., 2012), *UAS-TNT-E* on 2<sup>nd</sup> (Sweeney et al., 1995). If not otherwise indicated, flies were obtained from the Bloomington stock center.

### Genotypes for experiments

#### Figure 1

- (A) *w<sup>-</sup>*; *UAS-synaptotagmin-HA*, *UAS-mCD8-GFP/+*; *R20D01-Gal4/+*  
(B) *w<sup>-</sup>*; *UAS-synaptotagmin-HA*, *UAS-mCD8-GFP/+*; *R38G02-Gal4/+*  
(C–E) *R57C10-Flp2::PEST<sup>attP18</sup>*; +; *pJFRC201-10XUAS-FRT>STOP>FRT-myr::smGFP-HA<sup>VK0005</sup>*, *pJFRC240-10XUAS-FRT>STOP>FRT-myr::smGFP-V5-THS-10XUAS-FRT>STOP>FRT-myr::smGFP-FLAG<sup>su(Hw)attP1</sup>*, *pJFRC210-10XUAS-FRT>STOP>FRT-myr::smGFP-OLLAS<sup>attP2</sup>/R20D01-Gal4*  
(F–H) *R57C10-Flp2::PEST<sup>attP18</sup>*; +; *pJFRC201-10XUAS-FRT>STOP>FRT-myr::smGFP-HA<sup>VK0005</sup>*, *pJFRC240-10XUAS-FRT>STOP>FRT-myr::smGFP-V5-THS-10XUAS-FRT>STOP>FRT-myr::smGFP-FLAG<sup>su(Hw)attP1</sup>*, *pJFRC210-10XUAS-FRT>STOP>FRT-myr::smGFP-OLLAS<sup>attP2</sup>/R38G02-Gal4*  
(J) *pBPhsFlp2::PEST<sup>attP3</sup>*/+; *OL-KD (29C07-KDGeneswitch-4)<sup>attP40</sup>*/+; *R57C10-GAL4<sup>attP2</sup>*, *tubP-KDRT>GAL80-6-KDRT<sup>VK00027</sup>*/+*pJFRC201-10XUAS-FRT>STOP>FRT-myr::smGFP-HA<sup>VK0005</sup>*, *pJFRC240-10XUAS-FRT>STOP>FRT-myr::smGFP-V5-THS-10XUAS-FRT>STOP>FRT-myr::smGFP-FLAG<sup>su(Hw)attP1</sup>*

#### Figure 2

- (A) *w<sup>-</sup>*; *UAS-stinger-GFP/+*; *R20D01-Gal4/+*  
(B) *w<sup>-</sup>*; *UAS-stinger-GFP/+*; *R38G02-Gal4/+*  
(C, left) *w<sup>-</sup>*; *UAS-mCD8-GFP/+*; *R20D01-Gal4/+*  
(C, right) *DB331-Gal4*; *UASmCD8-GFP/+*  
(D) *w<sup>-</sup>*; *lexAop-CD4-spGFP11*, *UAS-CD4-spGFP1-10/VT23749-LexA*; *R20D01-Gal4/+*  
(E, red trace) *norpA<sup>7</sup>*; *UAS-ChR2-H134R*; *R42F06-Gal4*  
(E–H) *norpA<sup>7</sup>*; *UAS-ChR2-H134R*; *R20D01-Gal4*

#### Figure 3

- w<sup>-</sup>*; *UAS-GCaMP5G*; *R20D01-Gal4*  
*w<sup>-</sup>*; *UAS-GCaMP5G*; *R38G02-Gal4*

**Figure 4 to 6**

*w<sup>+</sup>* ; + ; *R20D01-Gal4*

*w<sup>+</sup>* ; *UAS-TNT-E* ; +

*w<sup>+</sup>* ; *UAS-TNT-E* ; *R20D01-Gal4*

**Immunostaining.** Brains were dissected in PBS and fixed in 4% PFA with 0.1% TritonX for 25 min at room temperature with the exception of anti-vGlut and anti-GAD1 stainings for which brains were fixed in Bouin's fixative (Gregory, 1980) for 5 min at room temperature. Brains were subsequently washed 3-4 times in 0.5% PBT. The primary antibodies used were mouse anti-bruchpilot (nc82, Developmental Studies Hybridoma Bank, 1:200), rabbit anti-GFP (Torrey Pines Biolabs, 1:500), rat anti-HA (Roche, 1:200), chicken anti-GFP (Rockland, 1:500), mouse anti-ChAT (courtesy of P. Salvaterra, 1:200) (Takagawa and Salvaterra, 1996), rabbit anti-vGlut (courtesy of A. DiAntonio, 1:200) (Daniels et al., 2004), rabbit anti-GAD1 (courtesy of F.R. Jackson, 1:200) (Featherstone et al., 2000) and rabbit anti-Tetanus Toxin (Statens Serum Institut, 1:5000). The secondary antibodies all used at 1:500 were goat anti-chicken Alexa Fluor 488, goat anti-rabbit Alexa Fluor 488, goat anti-rabbit Alexa Fluor 568, goat anti-mouse Alexa Fluor 568, goat anti-rat Alexa Fluor 568 (Life Technologies) and goat anti-mouse ATTO 647N (Rockland). 2% normal goat serum was added to all primary and secondary antibody solutions. Brains were mounted (IMM; ibidi) and optically sectioned with a Leica TCS SP5 confocal microscope. Brains expressing GRASP components were fixed, stained against the neuropile marker bruchpilot and mounted as described above. Afterwards, native GRASP fluorescence was visualized.

**Multicolor stochastic labeling.** "Multicolor FlpOut" (MCFO) labeling was carried out as described (Nern et al., 2015). Briefly, low level FLP recombinase expression was used to excise FRT-flanked transcriptional terminators from UAS reporter constructs carrying HA, V5 and FLAG epitope tags, respectively. Epitope tags were visualized by indirect immunofluorescence and images acquired on a Zeiss LSM 710 confocal microscope with a 63x 1.4 NA objective. Images were processed using Janelia Workstation and NeuronAnnotator software (Janelia Fly Light Scientific Computing Team, unpublished). The latter is a modified version of V3aaD (Peng et al., 2010). The images shown are reoriented substack projections generated using NeuronAnnotator and exported as TIFF-format screen shots. Manual segmentation of neurons from MCFO samples was carried out using Fluorender (<http://www.sci.utah.edu/software/fluorender.html>). The VS cell shown in Figures 1J and 1J' was labeled with a method that combines MCFO with a second recombinase system to obtain sparse labeling of optic lobe neurons from a "pan-neuronal" GAL4 driver ("Two-recombinase MCFO", for details see Nern et al. 2015).

**Transcript profiling.** The transcript profiling protocol was modified from the method described previously (Takemura et al., 2011). Lobula plate tangential cells were isolated from the line *DB331-Gal4* ; *UAS-mCD8-GFP/+*. Flies were dissected and cells were exposed using the same procedure as for the electrophysiology experiments. For the LPi cells isolation, flies with the genotype *w<sup>-</sup>* ; *UAS-mCD8-GFP/+* ; *R20D01-Gal4/+* were decapitated and their heads were fixed on a plastic holder with wax. Subsequently, retina and lamina were removed and the medulla was digested with 2 mg/ml Protease Type XIV (Sigma). GFP-expressing somata were harvested using custom-pulled capillaries and kept at -80°C. Five cells were collected into the same tube in order to increase the amount of mRNA for detection. cDNA synthesis



reaction was performed using SuperScript III First-Strand Synthesis SuperMix (Life Technologies). Reactions were primed with random hexamers and carried out exactly as directed by the manufacturer's instructions. Synthesized cDNA was amplified by nested PCR on FlexCycler (Analytik Jena) using DreamTaq Green PCR Master Mix (Thermo Scientific) and gene-specific primers (Table S1). The PCR amplification programs for the first and second round of PCR were as described previously (Takemura et al., 2011). In order to distinguish between PCR products amplified from genomic DNA and cDNA, primers were designed such that they amplified gene regions containing an intron. Size of PCR products was analyzed by agarose gel electrophoresis. For every cDNA synthesis, two control gene sequences were PCR amplified: *mouse CD8* transgene was included as a positive control and glial marker *repo* as a negative control. Functionality of primers used was tested on RNA obtained from heads of Canton S flies. Total RNA was isolated using TRIzol Reagent (Life Technologies), purified with RNeasy Mini Kit (Qiagen) and treated with DNase I, Amplification Grade (Life Technologies). cDNA synthesis and PCR amplification were performed as described above and the expected size of PCR products was confirmed by agarose gel electrophoresis (Figure S4).

**Two-photon calcium imaging.** Two-photon imaging was performed on a custom-built microscope as previously described (Maisak et al., 2013). Images were acquired at a frame rate of 1.88 Hz.

**Electrophysiology.** Electrophysiological experiments were performed as previously described (Mauss et al., 2014). For all experiments 1d old female flies kept at 25°C were used. For optogenetic experiments, yeast paste containing 1 mM all-trans-retinal (ATR, R2500; Sigma Aldrich) was fed to freshly eclosed flies. Using a plastic holder and bees wax, flies were attached beneath a recording chamber with the back of their heads inserted into a small cutout in the bottom of the chamber consisting of thin foil. Under external solution, a window was cut into the head capsule on one side using a hypodermic needle to expose the brain. Further dissection and recordings were performed under a Zeiss Axiovert 10 microscope. Under polarized light contrast, the glial sheath was digested locally by applying a stream of 0.5 mg/ml Collagenase IV (Gibco) through a cleaning micropipette (~5 µm opening) (Maimon et al., 2010). Whole cell recordings were established with patch electrodes of 5–8 MΩ resistance. Signals were recorded using a BA-1S bridge amplifier (npi Electronics), low-pass filtered at 3 kHz, and digitized at 10 kHz via an analog/digital converter (PCI-DAS6025; Measurement Computing). All physiological data were acquired in Matlab (R2010b; Mathworks) using the data acquisition toolbox. Normal external solution contained the following (in mM): 103 NaCl, 3 KCl, 5 TES, 10 trehalose, 10 glucose, 3 sucrose, 26 NaHCO<sub>3</sub>, 1 NaH<sub>2</sub>PO<sub>4</sub>, 1.5 CaCl<sub>2</sub>, and 4 MgCl<sub>2</sub>, pH7.3–7.35, ~280mOsmol/kg. External solution was carboxygenated (95% O<sub>2</sub>/5% CO<sub>2</sub>) and constantly perfused over the preparation at 2 ml/min. Internal solution, adjusted to pH 7.26 with 1N KOH, contained the following: 140 K-aspartate, 10 HEPES, 4 Mg-ATP, 0.5 Na-GTP, 1 EGTA, 1 KCl, and 0.1 Alexa Fluor 488 hydrazide salt (~265 mOsmol/kg).

**Pharmacology.** Picrotoxinin (PTX; Sigma P8390) was dissolved in dimethylsulfoxide at 50 mM and kept as a stock at -20°C. For experiments, PTX was diluted in external solution to 25 µM and washed in (10 min) and out (30 min) at 2 ml/min.

**Optogenetic stimulation.** Optogenetic stimulation was performed as previously described (Mauss et al., 2014). Light pulses were delivered by a Lambda DG-4 Plus wavelength switcher (Sutter) with a 300W

Xenon Arc lamp via the epifluorescence light path of the microscope through a 40x/0.8 NA water-immersion objective (LUMPlan FI; Olympus). Intensities were measured with a power meter (Thorlabs PM100D) under the objective in air and irradiance per  $\text{mm}^2$  estimated, as indicated in Figure 2. Light stimuli were triggered via the data acquisition software with voltage steps. A stimulus trial consisted of eight light pulses interleaved by 5 s.

**Visual stimulation.** Custom-built LED arenas were used for visual stimulation in calcium imaging and electrophysiology experiments. The arenas were engineered and modified based upon Reiser and Dickinson (2008), covered approx.  $170^\circ$  and  $90^\circ$  in azimuth and elevation, respectively, and allowed refresh rates of 550 Hz and 16 intensity levels (Maisak et al., 2013). Identical visual stimuli were presented in 3-5 trials in every experiment, usually in a randomized sequence. Patterns were smoothed by sub-maximal intensity steps so that 4 to 10 frames, depending on the pattern, corresponded to progression across one LED, i.e. pixel. For calcium imaging, stimuli were presented over the whole arena. For the direction tuning (Figure 3C and 3D), square-wave gratings with a spatial wavelength of  $24^\circ$  were shown running at  $24^\circ/\text{s}$  (corresponding to a temporal frequency of 1 Hz) in 12 directions separated by angles of  $30^\circ$ . Subsequently shown directions differed by  $150^\circ$  to avoid stimulating neighboring directions in direct succession. For the velocity tuning (Figure 3E and 3F), square-wave gratings with a spatial wavelength of  $24^\circ$  running in the preferred direction were presented at temporal frequencies from 0.05 to 10 Hz. Vertically running ON and OFF edges were presented at a velocity of  $30^\circ/\text{s}$  (Figure 3G and 3H). To probe visual VS cell responses in control and LPI block experiments, visual stimuli (except edges and expanding flow fields) were presented fronto-dorsally on the ipsilateral side, to account for GAL4 expression in the LPI3-4 driver line predominantly in cells covering the dorsal visual field. Grating stimuli had the following parameters. Figure 4B: sine-wave grating,  $20^\circ$  spatial wavelength, 1 Hz temporal frequency,  $50^\circ \times 50^\circ$  rectangular window; Figure 5A: square-wave grating,  $24^\circ$  spatial wavelength, 1 Hz temporal frequency,  $50^\circ$  diameter round window; Figure 5B: square-wave grating,  $24^\circ$  spatial wavelength, 1 Hz temporal frequency,  $50^\circ$  elevation  $\times$   $100^\circ$  azimuth rectangular window; and Figure 5C to E: sine-wave grating,  $24^\circ$  spatial wavelength, dynamic motion,  $50^\circ \times 50^\circ$  rectangular window. Horizontal edges (Figure 4C) subtended the full arena and moved vertically at a velocity of  $22.5^\circ/\text{s}$ . Four different random motion noise stimuli (Figure 6A) were tested each generated with the same parameters. Each consisted of 100 small squares ( $4 \times 4$  pixels, bright on dark) independently moving in x and y with random trajectories according to a Gaussian velocity distribution ( $\mu = 0^\circ/\text{s}$ ,  $\sigma = 20^\circ/\text{s}$ ). To simulate forward translation (Figure 6B), four random expanding flow fields were generated with the same parameters: 24 objects/s (1 cm half-size, bright on dark) approaching the observer at 10 cm/s and passing at a lateral distance of 10 cm. The angular displacement from the focus of expansion ( $\sim 34^\circ$  azimuth,  $\sim 0^\circ$  elevation) can be described by  $\tan^{-1}(d/vt)$  and the angular increase in size of each object by  $2 \cdot \tan^{-1}(l/\sqrt{d^2+vt^2})$ , with  $d$  denoting lateral distance,  $l$  the object half-size,  $v$  the approach velocity and  $t$  the time to passing. The looming square (Figure 6C) simulated a dark object of 5 cm on a collision course approaching at 10 cm/s. The time-varying angular size  $\theta(t)$  can be described by  $2 \cdot \tan^{-1}(l/vt)$ , with  $l$  denoting the object half-size,  $v$  the approach velocity and  $t$  the time to collision. All patterns except for Figure 5B were shown at full arena contrast.

**Physiological data analysis.** Data from LPi calcium imaging and VS cell recording experiments were evaluated using custom-written analysis scripts in Matlab. *Two-photon calcium imaging:* Time series of relative fluorescence changes ( $\Delta F/F$ ) were calculated from the raw image series. Regions of interest (ROIs) were selected by hand with a diameter of about 1-2  $\mu\text{m}$ , encompassing single putative presynaptic boutons. For every ROI, calcium signals were averaged over 3-5 stimulus repetitions. Visual responses were calculated as the peak amplitude of the average calcium signal during presentation of the respective stimulus subtracted by the preceding baseline calculated from the average of the 2 frames before stimulus presentation. These ROI responses were normalized to the maximum response of this ROI, averaged across ROIs within flies, and then averaged across flies. Only for edge selectivity, single ROIs were considered separately, and their selectivity for ON or OFF edges was quantified using a contrast selectivity index, calculated as  $\text{CSI} = (R_{\text{ON}} - R_{\text{OFF}})/(R_{\text{ON}} + R_{\text{OFF}})$ , with  $R_{\text{ON}}$  and  $R_{\text{OFF}}$  being the baseline subtracted responses to ON and OFF edges, respectively. *Electrophysiology:* To evaluate VS cell responses to optogenetic LPi3-4 stimulation (recorded cells identified anatomically by dye-labeling), eight trials for each cell and condition were averaged and taken for analysis. Those were then averaged across cells and plotted with shaded area as SEM (Figures 2E–2G), or baseline-subtracted minima taken for quantification (Figure 2H). To probe visual tangential cell responses (Figures 4 to 6), cells were selected for robust downward motion responses and after the recording session their VS cell identity could be confirmed by anatomy in most cases. Neurons with lateral receptive fields ( $\sim 90^\circ$  azimuth) were discarded right away and three out of eight UAS control flies with both weak preferred and null direction responses were not included in the analysis. Resting membrane potentials of included VS cells (corrected for the experimentally measured liquid junction potential of 11.5 mV) in Gal4 control, UAS control and LPi block flies amounted to  $-51 \text{ mV} \pm 0.4$ ,  $-50 \text{ mV} \pm 0.5$ , and  $-50 \text{ mV} \pm 0.3$  SEM, respectively. Measurements associated with Figure 4, Figures 5A and 5B and Figure S3 were down-sampled to 1 kHz and those associated with Figure 5C and Figure 6 to 0.1 kHz. Responses to four stimuli repetitions were averaged for each cell. In the case of ‘motion noise’ and ‘expanding flow field’ patterns, responses to four trials and four independent patterns (randomly generated with same parameters) were averaged. For quantification, except for edges and looming squares, the membrane potential during 4 s motion was measured and a 1 s baseline prior to motion onset subtracted. To quantify responses to full field edges, a 2 s time window within 4 s stimulation was chosen, in which the edges progressed through the upper half of the arena projecting to the dorsal visual field of the lobula plate, which contains the LPi3-4 cells targeted by the *R20D01-Gal4* driver line (Figure 4A). To quantify responses to the looming stimulus, an arbitrary 2 s response time window was chosen (indicated in Figure 6F). Plotted quantified values in all figures correspond to the mean  $\pm$  SEM. Significant differences were established using a two-tailed Wilcoxon rank-sum test in Matlab.

**Modeling.** Stimuli were calculated at  $1^\circ$  spatial and 10 ms temporal resolution. Every stimulus frame was convolved with a radial Gaussian function of  $5^\circ$  half-width and down-sampled to an array of  $40 \times 40$  photoreceptors, corresponding to an angular separation of  $5^\circ$  between neighboring receptors. Signals of lamina cells L1 and L2 were calculated by a high-pass filter (time constant 250 ms) plus 10% of the input (Eichner et al., 2011). L1 and L2 signals were processed separately in ON (L1) and OFF (L2) pathways (Joesch et al., 2010): The ON (L1) signal was obtained by half-wave rectifying the signal at a threshold of 0, the OFF (L2) signal was inverted and half-wave rectified at a threshold of 0.05. These signals were

then low- and high-pass filtered within each pathway with time constants of 100 and 300 ms, respectively. To obtain the responses of the 4 groups of T4 and T5 cells (one for each direction), low- and high-pass filtered signals from neighboring columns were multiplied accordingly (e.g. T4a = low-pass left \* high-pass right, T4b = low-pass right \* high-pass left, etc.). T4 and T5 signals were then half-wave rectified with a threshold of 0.005. The signal of VS cells in control flies was calculated as the spatial sum of all 40x40 T4d and T5d cells (i.e. downward tuned) minus the sum of all T4c and T5c cells (i.e. upward tuned). To simulate the condition of LPi block, the VS cell signal was calculated without subtraction of T4c and T5c cells.

**Table S1. Primer pairs used for the PCR amplification of gene-specific sequences, Related to Experimental Procedures**

Gene	First-round primers (5' - 3')	Nested primers (5' - 3')	Expected nested PCR product size	
			Template: DNA	Template: cDNA
mouse CD8	–	F: AAGGTGGACCTGGTATGTGAAGTG R: ACCGAGTTGCTGATGACTGAG	266 bp	266 bp
Repo (CG31240)	F: GAAGCAGCAGCAAGAAGAAGG R: CACGGGATTCGCTCAGATTCA	F: GGCATCAAGAAGAAGAAGACG R: GATTCGCTCAGATTCAGCTTG	552 bp	137 bp
ChAT (CG12345)	F: ACCGGGAAATGCTTCAGGAG R: GTCCACACTCTTGGAGGCTT	F: GCAATCAACGCAATCTGGAGC R: GGAACAGGAGTGCTCATAGCA	336 bp	272 bp
vGluT (CG9887)	F: TCCCGGCCAACAAGATATTC R: AACTTGTGCTTGAGGAACG	F: TGCATCTCTTCGTGCCATTCC R: GTATGCTGATGGCCGGATGTT	807 bp	339 bp
vGAT (CG8394)	F: GCCCGTATAGCAGCAGATGT R: CAGCAAACGGACGGCTTTAG	F: GCGATACGATGAACATGCC R: CAGCAAACGGACGGCTTTAG	223 bp	151 bp
GluCl $\alpha$ (CG7535)	F: GACGGATGAACGCCTCAAGT R: TTCTCCAGTGTGAAGCGAGG	F: TCGAACGAGAAGGAGGGACA R: RTGTGAAGCGAGGTAGGTGT	533 bp	265 bp

## SUPPLEMENTAL REFERENCES

- Akerboom, J., Chen, T.-W., Wardill, T., Tian, L., Marvin, J., Mutlu, S., Calderón, N., Esposti, F., Borghuis, B., Sun, X., *et al.* (2012). Optimization of a GCaMP calcium indicator for neural activity imaging. *J Neurosci* 32, 13819-13840.
- Daniels, R., Collins, C., Gelfand, M., Dant, J., Brooks, E., Krantz, D., and DiAntonio, A. (2004). Increased expression of the *Drosophila* vesicular glutamate transporter leads to excess glutamate release and a compensatory decrease in quantal content. *J Neurosci* 24, 10466-10474.
- Eichner, H., Joesch, M., Schnell, B., Reiff, D., and Borst, A. (2011). Internal structure of the fly elementary motion detector. *Neuron* 70, 1155-1164.
- Featherstone, D.E., Rushton, E.M., Hilderbrand-Chae, M., Phillips, A.M., Jackson, F.R., and Broadie, K. (2000). Presynaptic glutamic acid decarboxylase is required for induction of the postsynaptic receptor field at a glutamatergic synapse. *Neuron* 27, 71-84.
- Gordon, M.D., and Scott, K. (2009). Motor control in a *Drosophila* taste circuit. *Neuron* 61, 373-384.
- Gregory, G.E. (1980). The bodian protargol technique. In *Neuroanatomical Techniques: Insect Nervous System*, N.J. Strausfeld, and T.A. Miller, eds. (Springer Verlag New York), pp. 75-95.
- Hotta, Y., and Benzer, S. (1970). Genetic dissection of the *Drosophila* nervous system by means of mosaics. *Proc Natl Acad Sci U S A* 67, 1156-1163.
- Joesch, M., Plett, J., Borst, A., and Reiff, D. (2008). Response properties of motion-sensitive visual interneurons in the lobula plate of *Drosophila melanogaster*. *Curr Biol* 18, 368-374.
- Joesch, M., Schnell, B., Raghun, S., Reiff, D., and Borst, A. (2010). ON and OFF pathways in *Drosophila* motion vision. *Nature* 468, 300-304.
- Löhr, R., Godenschwege, T., Buchner, E., and Prokop, A. (2002). Compartmentalization of central neurons in *Drosophila*: a new strategy of mosaic analysis reveals localization of presynaptic sites to specific segments of neurites. *J Neurosci* 22, 10357-10367.
- Maimon, G., Straw, A., and Dickinson, M. (2010). Active flight increases the gain of visual motion processing in *Drosophila*. *Nat Neurosci* 13, 393-399.
- Maisak, M.S., Haag, J., Ammer, G., Serbe, E., Meier, M., Leonhardt, A., Schilling, T., Bahl, A., Rubin, G.M., Nern, A., *et al.* (2013). A directional tuning map of *Drosophila* elementary motion detectors. *Nature* 500, 212-216.
- Mattis, J., Tye, K., Ferenczi, E., Ramakrishnan, C., O'Shea, D., Prakash, R., Gunaydin, L., Hyun, M., Fenno, L., Gradinaru, V., *et al.* (2012). Principles for applying optogenetic tools derived from direct comparative analysis of microbial opsins. *Nature Methods* 9, 159-172.
- Mauss, A.S., Meier, M., Serbe, E., and Borst, A. (2014). Optogenetic and pharmacologic dissection of feedforward inhibition in *Drosophila* motion vision. *J Neurosci* 34, 2254-2263.
- Nagel, G., Brauner, M., Liewald, J., Adeishvili, N., Bamberg, E., and Gottschalk, A. (2005). Light activation of channelrhodopsin-2 in excitable cells of *Caenorhabditis elegans* triggers rapid behavioral responses. *Curr Biol* 15, 2279-2284.
- Nern, A., Pfeiffer, B.D., and Rubin, G.M. (2015). Optimized tools for multicolor stochastic labeling reveal diverse stereotyped cell arrangements in the fly visual system. *Proc Natl Acad Sci U S A* 112, E2967-2976.

- Peng, H., Ruan, Z., Long, F., Simpson, J.H., and Myers, E.W. (2010). V3D enables real-time 3D visualization and quantitative analysis of large-scale biological image data sets. *Nat Biotechnol* 28, 348-353.
- Pulver, S., Pashkovski, S., Hornstein, N., Garrity, P., and Griffith, L. (2009). Temporal dynamics of neuronal activation by Channelrhodopsin-2 and TRPA1 determine behavioral output in *Drosophila* larvae. *J Neurophysiol* 101, 3075-3088.
- Reiser, M., and Dickinson, M. (2008). A modular display system for insect behavioral neuroscience. *J Neurosci Methods* 167, 127-139.
- Robinson, I., Ranjan, R., and Schwarz, T. (2002). Synaptotagmins I and IV promote transmitter release independently of Ca(2+) binding in the C(2)A domain. *Nature* 418, 336-340.
- Struhl, G., and Basler, K. (1993). Organizing activity of wingless protein in *Drosophila*. *Cell* 72, 527-540.
- Sweeney, S., Broadie, K., Keane, J., Niemann, H., and O'Kane, C. (1995). Targeted expression of tetanus toxin light chain in *Drosophila* specifically eliminates synaptic transmission and causes behavioral defects. *Neuron* 14, 341-351.
- Takagawa, K., and Salvaterra, P. (1996). Analysis of choline acetyltransferase protein in temperature sensitive mutant flies using newly generated monoclonal antibody. *Neurosci Res* 24, 237-243.
- Takemura, S.Y., Karuppururai, T., Ting, C.Y., Lu, Z., Lee, C.H., and Meinertzhagen, I. (2011). Cholinergic circuits integrate neighboring visual signals in a *Drosophila* motion detection pathway. *Curr Biol* 21, 2077-2084.

## **2.2 RNA-SEQ TRANSCRIPTOME ANALYSIS OF DIRECTION-SELECTIVE T<sub>4</sub>/T<sub>5</sub> NEURONS IN *DROSOPHILA***

The article “RNA-seq transcriptome analysis of direction-selective T<sub>4</sub>/T<sub>5</sub> neurons in *Drosophila*” (<https://doi.org/10.1371/journal.pone.0163986>) was originally published in the journal PloS ONE in September 2016. The following authors contributed to this work: Katarina Pankova conceived and performed the experiments and wrote the manuscript. Alexander Borst revised the manuscript.

RESEARCH ARTICLE

# RNA-Seq Transcriptome Analysis of Direction-Selective T4/T5 Neurons in *Drosophila*

Katarina Pankova<sup>1,2\*</sup>, Alexander Borst<sup>1</sup>

**1** Max Planck Institute of Neurobiology, Martinsried, Germany, **2** Graduate School of Systemic Neurosciences, LMU Munich, Munich, Germany

\* [pankova@neuro.mpg.de](mailto:pankova@neuro.mpg.de)



**OPEN ACCESS**

**Citation:** Pankova K, Borst A (2016) RNA-Seq Transcriptome Analysis of Direction-Selective T4/T5 Neurons in *Drosophila*. PLoS ONE 11(9): e0163986. doi:10.1371/journal.pone.0163986

**Editor:** Brian D. McCabe, EPFL, SWITZERLAND

**Received:** July 31, 2016

**Accepted:** September 16, 2016

**Published:** September 29, 2016

**Copyright:** © 2016 Pankova, Borst. This is an open access article distributed under the terms of the [Creative Commons Attribution License](https://creativecommons.org/licenses/by/4.0/), which permits unrestricted use, distribution, and reproduction in any medium, provided the original author and source are credited.

**Data Availability Statement:** RNA-seq data are available from the NCBI GEO archive under accession code GSE77198.

**Funding:** This work was supported by the Max Planck Society. The funder had no role in study design, data collection and analysis, decision to publish, or preparation of the manuscript.

**Competing Interests:** The authors have declared that no competing interests exist.

## Abstract

Neuronal computation underlying detection of visual motion has been studied for more than a half-century. In *Drosophila*, direction-selective T4/T5 neurons show supralinear signal amplification in response to stimuli moving in their preferred direction, in agreement with the prediction made by the Hassenstein-Reichardt detector. Nevertheless, the molecular mechanism explaining how the Hassenstein-Reichardt model is implemented in T4/T5 cells has not been identified yet. In the present study, we utilized cell type-specific transcriptome profiling with RNA-seq to obtain a complete gene expression profile of T4/T5 neurons. We analyzed the expression of genes that affect neuronal computational properties and can underlie the molecular implementation of the core features of the Hassenstein-Reichardt model to the dendrites of T4/T5 neurons. Furthermore, we used the acquired RNA-seq data to examine the neurotransmitter system used by T4/T5 neurons. Surprisingly, we observed co-expression of the cholinergic markers and the vesicular GABA transporter in T4/T5 neurons. We verified the previously undetected expression of vesicular GABA transporter in T4/T5 cells using VGAT-LexA knock-in line. The provided gene expression dataset can serve as a useful source for studying the properties of direction-selective T4/T5 neurons on the molecular level.

## Introduction

Processing of visual cues and detecting the direction of motion in particular is critical for the survival of many organisms. In *Drosophila*, visual motion processing begins at the level of photoreceptors in retina that use histamine as their neurotransmitter [1]. Photoreceptor signals are segregated into parallel ON- and OFF-channels represented at the cellular level by glutamatergic L1 neurons (ON-channel) and cholinergic L2 neurons (OFF-channel) [2,3,4,5]. The identified downstream components of the ON motion vision pathway are Mi1 and Tm3 neurons which synapse on the T4 neurons [6,7,8,9]. In the OFF motion vision pathway the L2 neurons provide input to Tm1, Tm2, Tm4 and Tm9 cells that in turn connect with T5 neurons [4,7,8,10,11,12]. The neurotransmitter used by Tm1, Tm2, and Tm9 cells is acetylcholine



NMDA receptors [23], opening of rectifying electrical synapses [24] and deactivation of inhibitory currents [25]. As the present knowledge about expression of genes that could determine the computational properties of T4/T5 neurons is limited [11], the implementation of the HR model of direction-selectivity at the molecular level on the dendrites of T4/T5 neurons is still an unresolved issue.

Here, we provide a complete transcriptional profile of all protein-encoding genes in T4/T5 neurons. We examine expression levels of the identified neurotransmitter receptors and gap junction proteins in order to characterize the input T4/T5 neurons receive from their presynaptic partners. Furthermore, we analyze the expression of voltage-gated and non-gated ion channels that may underlie the mechanism for coincidence detection in the T4/T5 neurons. Unexpectedly, our RNA-seq data reveals that T4/T5 neurons co-express vesicular transporters for acetylcholine and GABA. In addition to cholinergic markers, T4/T5 neurons also produce GABA-degrading enzyme GABA transaminase. We confirm the co-expression of the vesicular GABA transporter (VGAT) and acetylcholine-synthesizing enzyme ChAT in all T4/T5 neurons using the transgenic VGAT-LexA knock-in line (Simpson 2016; *J Neurogenetics*, in revision) and immunostaining with antibody against ChAT.

## Materials and Methods

### Fly stocks

Flies were raised on standard cornmeal-agar food at 25°C. The following stocks were used: 10xUAS-unc84::2xGFP (provided by F. Schnorrer) [26], GMRSS00324 (R59E08-AD; R42F06-DBD) (provided by A. Nern) [27], R42F06-Gal4 (provided by G. Rubin) [15], UAS-mCD8::GFP (BDSC #5130) [28], VGAT-LexA (provided by J. Simpson) (Simpson 2016; *J Neurogenetics*, in revision) and LexAop-myr::mCherry (provided by B. Dickson) [29].

### Immunoprecipitation of nuclei

The following protocol was modified from the previously described procedure [26]. 300  $\mu$ l of Dynabeads Protein G magnetic beads (Thermo Fisher Scientific) were incubated with 10  $\mu$ l of the monoclonal anti-GFP antibody (Sigma-Aldrich, G6539) for 30 minutes at 4°C. Afterwards, beads were washed three times with 0.1% PBT. Approximately 50–60 ml of flies with the genotype *w<sup>+</sup>; R59E08-AD/+; R42F06-DBD/10xUAS-UNC-84::2xGFP* were anesthetized by CO<sub>2</sub> and frozen in liquid nitrogen. Flies were decapitated by vigorous vortexing. Heads were smashed using Dounce grinder (Sigma-Aldrich) with loose pestle in ice-cold buffer (10 mM  $\beta$ -glycerophosphate, 2 mM MgCl<sub>2</sub>, 0.5% Igepal). The homogenate was passed through a 180  $\mu$ m nylon net filter (Millipore) and filtrate was smashed again in Dounce grinder with tight pestle. After additional filtering through a 20  $\mu$ m nylon net filter (Millipore), the homogenate was brought to 50 ml with sucrose buffer (10 mM  $\beta$ -glycerophosphate, 2 mM MgCl<sub>2</sub>, 25 mM KCl, 250 mM sucrose) and the antibody-preincubated magnetic beads were added. The binding reaction was carried out at 4°C for 30 min and was followed by five washes of the bead-bound nuclei with sucrose buffer. The bead-bound nuclei were imaged on a Leica TCS SP8 laser-scanning confocal microscope with DAPI (1  $\mu$ g/ml) as a nuclear marker. In total, 636 DAPI-positive nuclei were manually counted, out of which 597 (94%) were GFP-positive.

### RNA isolation and RNA-seq

RNA from bead-bound nuclei was extracted with Trizol reagent (Thermo Fisher Scientific). Total RNA from two biological replicates (0.7  $\mu$ g and 0.8  $\mu$ g) was submitted to EMBL Genomics Core Facility, Heidelberg, Germany. A cDNA library was generated using TruSeq

Stranded mRNA LT Sample Prep Kit (Illumina) and single-end sequenced on Illumina HiSeq 2000 to 51 bp read length. TopHat (v2.1.0) [30] was used to align untrimmed reads to the annotated genome of *D. melanogaster* (FlyBase r6.04). Alignment was carried out with default settings, except for excluding reads that mapped to more than one genomic position. In two biological replicates, 90% and 87% of total reads were uniquely mapped, resulting in a total of 154 and 119 million aligned reads. Reads mapping to gene exons were counted with the 'featureCounts' software (Rsubread package v1.12.6) [31] in R (v3.0.2). Read counts per gene were normalized by total exon length of a gene and the sum of reads assigned to all exons to generate the reads per kilobase per million reads mapped (RPKM) values (S1 Table).

## Immunohistochemistry

Fly brains were dissected in PBS and fixed in 4% PFA with 0.1% TritonX for 25 minutes. Brains were washed in 0.3% PBT and incubated first with primary (24–72h) and then secondary (24–48h) antibodies in 0.3% PBT supplemented with 5% NGS at 4°C. Brains were mounted in Vectashield mounting medium (Vector Laboratories) and imaged on Leica TCS SP5 laser-scanning confocal microscope. We used the following antibodies: rabbit anti-GFP (Torrey Pines, 1:400), mouse anti-nc82 (DSHB, deposited by E. Buchner, 1:200), rat anti-RFP, (Chromotek 5F8, 1:50), mouse anti-ChAT (DSHB, deposited by P. Salvaterra, 1:50), goat anti-rabbit Alexa 488 (Thermo Fisher Scientific, 1:200), goat anti-rat Alexa 568 (Thermo Fisher Scientific, 1:200) and goat anti-mouse Alexa 647 (Thermo Fisher Scientific, 1:200).

## Results

### RNA-seq data

We performed RNA-seq of the mRNA extracted from immunoprecipitated GFP-tagged nuclei of T4/T5 neurons [26]. Cell type-specificity of our approach was achieved by using a split Gal4 line with expression restricted to T4/T5 neurons [27] (Fig 2A) and the high purity (94%) of the isolated GFP-labelled nuclei (Fig 2B). Two independent biological replicates showed high correlation of their expression values (Fig 2C), confirming the reproducibility of the obtained RNA-seq results. The genome-wide expression levels in T4/T5 neurons were within the range 0–4770 RPKM (S1 Table). We plotted all analyzed expression levels on an arbitrary color scale with the minimum at 0 and maximum at 100 RPKM, arguing that 95% of the genes in T4/T5 neurons have an expression value within these limits.

### Neurotransmitter receptors and gap junction proteins in T4/T5 neurons

We analyzed expression of the identified membrane receptors for all known neurotransmitters in *Drosophila* (Fig 3). In addition, we considered the possibility that T4/T5 neurons may receive input via electrical synapses and, therefore, examined expression of the known gap junction proteins as well (Fig 3). RNA-seq results showed that four subunits of nicotinic acetylcholine receptor ( $D\alpha 2$ ,  $D\alpha 7$ ,  $D\beta 1$  and  $D\beta 2$ ) had high expression levels. In addition, the muscarinic acetylcholine receptor mAChR-A was strongly expressed, while the other muscarinic receptor, mAChR-B, showed lower expression levels. Among the identified glutamate receptors, we observed strong expression of the glutamate-gated chloride channel GluCl $\alpha$  which has been shown to mediate the hyperpolarizing action of glutamate in fly neurons [32,33,34]. We detected high expression levels of the ionotropic glutamate receptor subunits CG3822 and CG11155. Despite the very weak expression of the functional subunits of the NMDA receptor Nmdar1 and Nmdar2, we found that a related gene, Nmda1 that encodes a protein associated

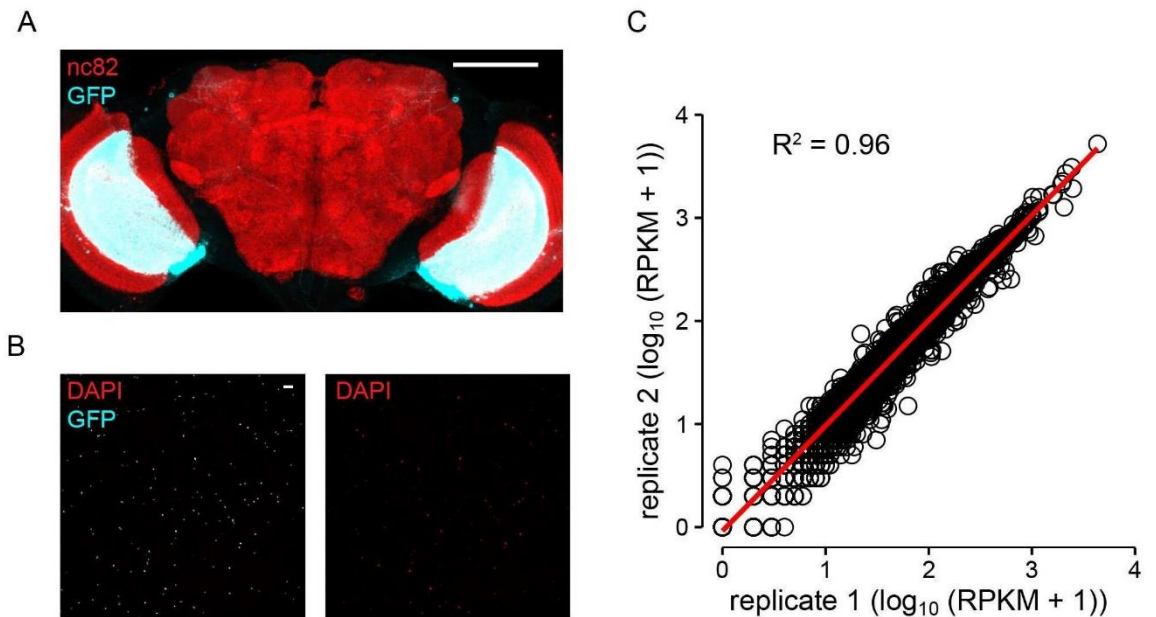


**Fig 2. Specificity and reproducibility of RNA-Seq.** (A) Expression pattern of the split Gal4 line labelling specifically T4/T5 neurons. In the central brain, the expression is—with an exception of a single pair of neurons—absent. The fly genotype was *w<sup>1118</sup>; R59E08-AD/+; R42F06-DBD/UAS-mCD8::GFP*. The anti-GFP staining is shown in cyan and anti-nc82 staining is in red. Scale bar: 100  $\mu$ m. (B) The immunoprecipitated GFP-tagged nuclei (cyan) were labelled with DAPI (red) to quantify the number of nuclei without GFP expression and as a result, the proportion of nuclei belonging to cells other than T4/T5. Scale bar: 30  $\mu$ m. (C) Correlation of RPKM values of the two biological replicates plotted on a logarithmic scale. Linear regression (red line) accounts for 96% of the variation among the two replicates. doi:10.1371/journal.pone.0163986.g002

with the NMDA receptor is strongly expressed. *Nmda1* gene has not been fully described yet and it is not clear whether it has functional role in neurotransmission.

Our RNA-Seq results showed presence of transcripts also for ionotropic GABA receptor subunits *Rdl*, *Lcch3* and *CG8916* as well as metabotropic GABA receptors *GABA-B-R1* and

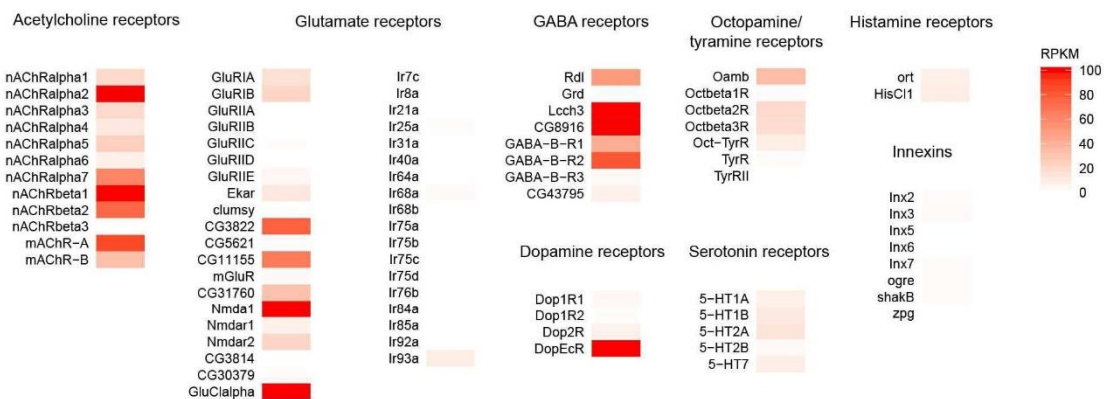


**Fig 3. Expression of neurotransmitter receptors and gap junction proteins in T4/T5 neurons.** Gene expression levels of the identified receptors for acetylcholine, glutamate, GABA, dopamine, octopamine, tyramine, serotonin and histamine as well as the innexin proteins are plotted as mean RPKM values using a color scale with the minimum at 0 and maximum at 100 RPKM. doi:10.1371/journal.pone.0163986.g003

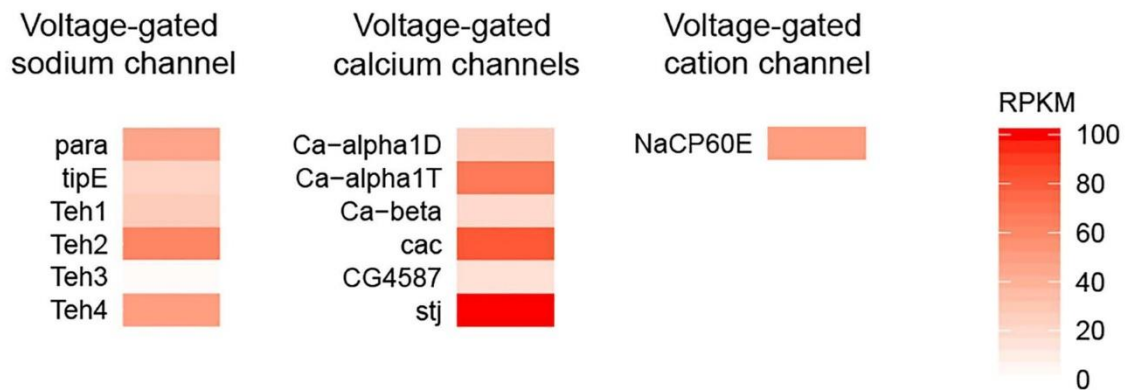


**Fig 4. Expression of voltage-gated sodium and calcium channels in T4/T5 neurons.** RPKM values of the identified structural and modulatory subunits of voltage-gated sodium and calcium channels are plotted on a color scale ranging from 0 to 100 RPKM.

doi:10.1371/journal.pone.0163986.g004

GABA-B-R2. None of the known receptors for serotonin, histamine or tyramine were expressed in T4/T5 neurons. Amongst the octopamine receptors, we detected low expression of Oamb, suggesting weak octopaminergic input to T4/T5 neurons. Dopamine-ecdysone receptor DopEcR was expressed at high levels in T4/T5 neurons. Nevertheless, presence of DopEcR does not necessarily imply that T4/T5 neurons receive dopaminergic input as DopEcR also serves as a detector of steroid hormones [35]. We did not detect expression of any gap junction proteins of the innexin family in the T4/T5 neurons.

### Ion channels in T4/T5 neurons

The whole *Drosophila* genome contains only one gene that encodes a voltage-gated sodium channel—named para—and five genes encoding auxiliary subunits that are known to modulate the gating of para. We found the voltage-gated sodium channel para to be expressed in T4/T5 neurons together with four out of the five identified modulatory subunits (Fig 4). All of the identified subunits of voltage-gated calcium channels were expressed in T4/T5 neurons as well (Fig 4). In addition, we also detected expression of the voltage-gated cation channel NaCP60E that is permeable for both, calcium and sodium (Fig 4).

Potassium channels can be divided based on their structure and function into three main groups: voltage-gated potassium channels, two-pore domain potassium channels and inwardly rectifying potassium channels. With the exception of Elk and KCNQ, all of the identified members of voltage-gated potassium channels were expressed in T4/T5 neurons (Fig 5). Expression of Shawl and SK was rather weak (Fig 5). Two-pore domain potassium channels have been shown to mediate leak potassium current as well as chemo- and mechano-sensation [36]. In T4/T5 neurons, two members of this family, CG1688 and Task7 were strongly expressed (Fig 5). None of the inwardly rectifying potassium channels was present in T4/T5 neurons (Fig 5).

### Neurotransmitter phenotype of T4/T5 neurons

T4/T5 neurons have previously been shown to use acetylcholine as their neurotransmitter [11,33]. Hence, our expectation was to confirm the cholinergic phenotype of these neurons. Indeed, we found the genes for the acetylcholine-synthesizing enzyme ChAT and the vesicular acetylcholine transporter (VACHT) to be expressed at high levels (Fig 6). Surprisingly,

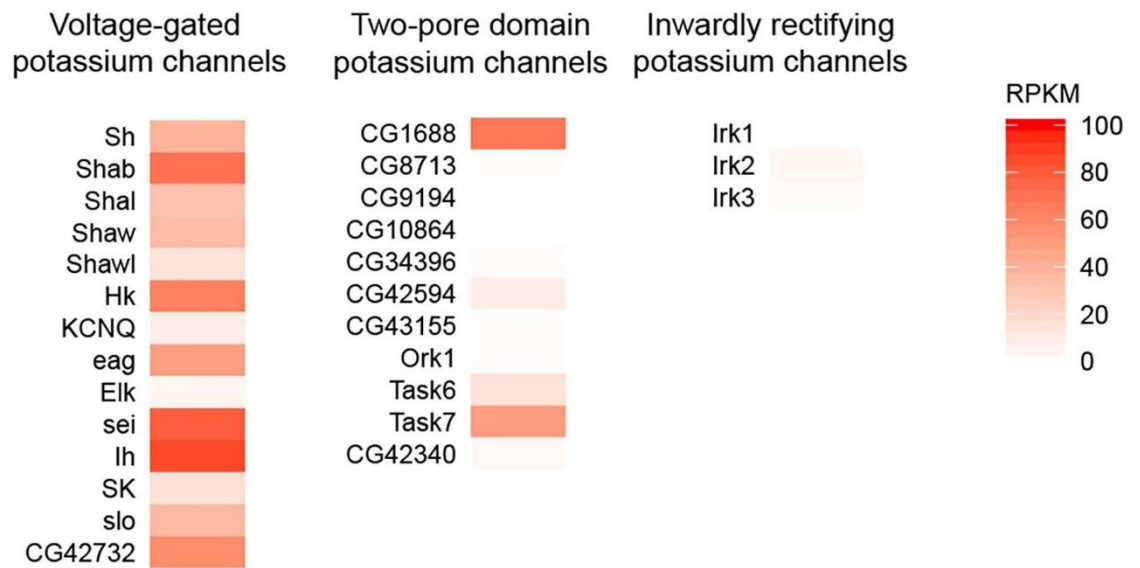


**Fig 5. Expression of potassium channels in T4/T5 neurons.** Expression levels of the identified members of the voltage-gated potassium channels, two-pore domain potassium channels and inwardly rectifying potassium channels are plotted as RPKM values on a color scale ranging from 0 to 100 RPKM.

doi:10.1371/journal.pone.0163986.g005

however, we also found the gene for the vesicular GABA transporter (VGAT) to be expressed in T4/T5 neurons (Fig 6A).

To prove the expression of VGAT in T4/T5 neurons by another line of evidence, we used a transgenic fly line VGAT-LexA that had the sequence for bacterial transcription factor LexA



**Fig 6. Neurotransmitter phenotype of T4/T5 neurons.** Expression values of the identified vesicular neurotransmitter transporters (A) and known markers of the cholinergic and GABAergic neurons (B) are plotted as RPKM levels on a color scale capturing the range 0–100 RPKM.

doi:10.1371/journal.pone.0163986.g006

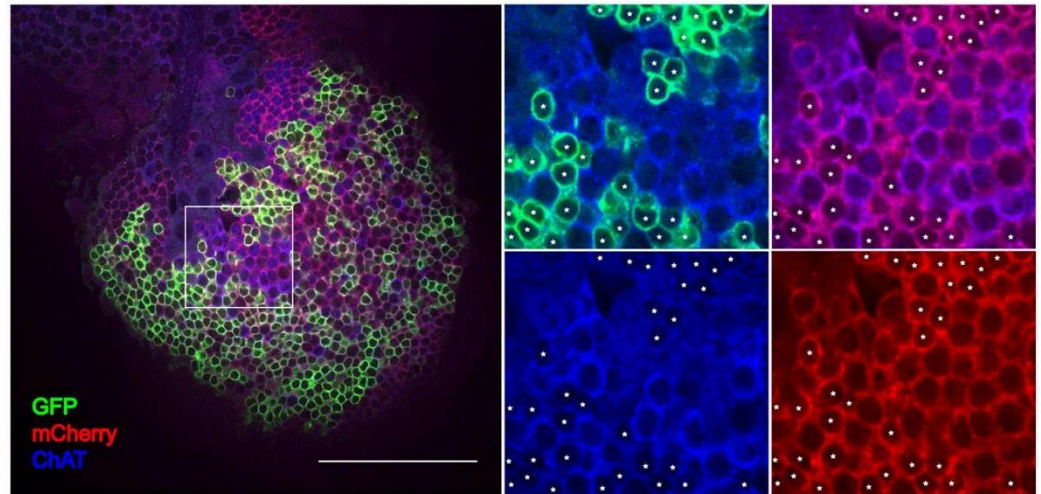


**Fig 7. Co-expression of ChAT and VGAT in T4/T5 neurons.** Optic lobe of a fly with genotype *w<sup>1118</sup>; VGAT-LexA/LexAop-myr::mCherry; R42F06-Gal4/UAS-mCD8::GFP* was immunostained with antibodies against GFP (green), mCherry (red) and ChAT (blue). Boxed area in the left picture is enlarged in four panels in the right. White asterisks mark the position of the GFP-labelled cell bodies of the T4/T5 neurons. Somatic membrane of the T4/T5 neurons co-localizes with anti-mCherry as well as with anti-ChAT immunostaining. Scale bar: 50  $\mu$ m.

doi:10.1371/journal.pone.0163986.g007

inserted into the first exon of the VGAT gene (Simpson 2016; J Neurogenetics, in revision). Utilizing two binary expression systems, Gal4/UAS [37] and LexA/lexAop [38], we labelled T4/T5 neurons with GFP and cells with an active VGAT locus with mCherry. The immunostaining revealed that T4/T5 neurons were indeed part of the VGAT-LexA expression pattern (Fig 7). The apparent co-expression of VAcHT and VGAT in T4/T5 neurons raises the possibility that T4/T5 neurons compose two different populations; one cholinergic and one expressing VGAT. To test this, we performed further staining against acetylcholine-synthesizing enzyme ChAT that showed that all of the VGAT-expressing T4 and T5 neurons were in addition cholinergic as well (Fig 7).

Besides the vesicular transporter VAcHT and acetylcholine-synthesizing enzyme ChAT, cholinergic neurons are characterized by the presence of the membrane choline transporter that is in *Drosophila* encoded by the gene CG7708. Our RNA-seq results confirmed the expression of all three cholinergic markers in the T4/T5 neurons (Fig 6). On the other hand, GABAergic neurons are characterized by the presence of GABA-synthesizing enzyme glutamate decarboxylase (Gad1), membrane GABA transporter (Gat) and GABA-degrading enzyme GABA transaminase (GabaT). We found that T4/T5 neurons did not express Gad1 and Gat but their expression of GabaT was comparable to that of cholinergic markers (Fig 6), suggesting that degradation of GABA is taking place in T4/T5 neurons.

## Discussion

### Comparison of expression data obtained with RNA-seq and RT-PCR

A low-throughput transcript profiling of selected 22 genes in T4/T5 neurons was already performed previously using RT-PCR amplification of mRNA from the isolated somata of either T4 or T5 neurons [11]. Shinomiya et al. [11] detected expression of ChAT and potassium channel slo in both, T4 and T5 neurons, muscarinic acetylcholine receptor mAChR-A in T5 cells

and mAChR-B in T4 cells, in agreement with our results (Figs 3, 5 and 6). However, transcripts for nicotinic subunit D $\beta$ 3 identified by RT-PCR in T4/T5 neurons [11] were not detected in our RNA-seq dataset (Fig 3). On the other hand, we observed strong expression of nicotinic receptor subunits D $\alpha$ 2, D $\beta$ 1, D $\beta$ 2 (Fig 3) and vesicular transporter VGAT (Fig 6) while none of these genes was identified as expressed in the RT-PCR assay [11]. These discrepancies are likely due to lower detection threshold caused by smaller amounts of input mRNA used in reported RT-PCR experiments and higher risk of contamination of the analyzed neurons with other cell types during the manual sampling of somata.

Our transcriptome analysis with RNA-seq pools T4 and T5 cells together as there is no available Gal4 line with the expression pattern restricted exclusively to either T4 or T5 neurons. The Gal4 lines used previously to target either T4 or T5 neurons [11,13,33] show expression also in other neuronal types in the central brain, therefore they are not suitable for the approach used in this study that involves immunoprecipitation of neuronal nuclei from the whole fly heads. As a consequence of the pooling of T4 and T5 cells together in our analysis, genes that are differentially expressed in T4 and T5 neurons might show weaker expression in our dataset although their expression is strong but restricted to either T4 or T5 cells. In addition, T4/T5 neurons comprise a total of eight subtypes that differ in their preferred direction, orientation of their dendrites and projection pattern of their axons. Although all these cell types likely perform the same dendritic computations, this diversity might still affect our transcriptome data.

## Molecular implementation of HR model

A major contribution of our transcriptome analysis of T4/T5 neurons is narrowing down the biological mechanisms that can apply the HR model of motion detection to the dendrites of the T4/T5 neurons. Depending on where the time delay in the HR model arises (Fig 1), different molecular processes underlying coincidence detection come into question. Inputs that are temporally offset already presynaptically to the dendrites of the T4/T5 neurons (Fig 1A) can be summed in a supralinear fashion by rectifying electrical synapses [24], deactivation of Kir conductance [25] or voltage-gated sodium or calcium channels [21,22]. As neither the electrical synapses nor the inwardly rectifying potassium channels are present in the T4/T5 neurons (Figs 3 and 5), we suggest that voltage-gated sodium and calcium channels (Fig 4) are the main candidates for the supralinear summation in this scenario.

Our results show that T4/T5 neurons are likely to receive cholinergic, glutamatergic and GABAergic input (Fig 3). For each of these neurotransmitters, both ionotropic as well as G-protein coupled receptors are expressed in the T4/T5 neurons. As the ionotropic and metabotropic neurotransmitter receptors have different activation dynamics, the temporal delay can indeed be generated by the two inputs synapsing on different types of receptors on the dendrites of T4/T5 neurons (Fig 1B). Supralinear dendritic summation by NMDA receptors in the T4/T5 neurons is not likely as the expression levels of the functional NMDA receptor subunits are rather low (Fig 3). A coincidence detection mechanism involving deactivation of KCNQ-mediated hyperpolarizing potassium current via muscarinic acetylcholine receptor signaling cascade has already been proposed to take place in T4/T5 neurons [11,39]. However, the weak expression of KCNQ in T4/T5 neurons makes the contribution of KCNQ currents to a supralinear signal amplification in T4/T5 neurons unlikely (Fig 5). As a potential substrate for the recently discovered null-direction suppression [18,19], T4/T5 neurons express GABA receptors as well as glutamate-binding hyperpolarizing GluCl $\alpha$  channel (Fig 3). Such inhibitory inputs could also shape the receptive field properties of T4/T5 neurons making them more sensitive to gratings orthogonal to their preferred orientation [14].

Dendritic signal propagation depends on the morphology of the dendrites as well as on their active and passive membrane properties. Possible differential temporal filtering in the dendritic compartments of T4/T5 cells (Fig 1C) can be caused by inhomogeneous distribution of ion channels mediating leak currents, low threshold potassium currents or hyperpolarization-activated potassium currents. We identify expression of candidate channels in the T4/T5 neurons that might mediate these currents such as leak potassium channels CG1688 and Task7, hyperpolarization-activated potassium channel Ih and low threshold-activated potassium channels Shab, Shaw [40], eag [41] and sei [42] (Fig 5).

### Co-existence of acetylcholine and GABA in T4 and T5 neurons?

GABAergic neurons in flies are traditionally characterized by the presence of glutamic acid decarboxylase Gad1, an enzyme responsible for GABA synthesis [43]. Mammalian neurons, however, can release GABA in absence of glutamate decarboxylase. This is achieved either by re-uptaking GABA from the extracellular space via GABA transporters [44] or by its synthesis with alternative pathways [45,46]. GABA transaminase (Gat) can convert succinic semialdehyde into GABA and vice versa [47], and is thought to participate in the degradation of GABA in most cells, not in its synthesis [48]. In T4/T5 neurons, the Gad1 and Gat are expressed very weakly (Fig 6B) and therefore their contribution to potential GABAergic transmission of T4/T5 neurons is questionable. On the other hand, Gat is expressed at the levels comparable to cholinergic markers (Fig 6B) suggesting that degradation of GABA is taking place in T4/T5 neurons. Alternatively, Gat might be the GABA synthesizing enzyme in the T4/T5 neurons.

T4/T5 neurons synthesize and release acetylcholine from their axons onto their postsynaptic partners, the lobula plate tangential cells [11,33]. In addition to axon terminals, T4 neurons also possess presynaptic neurotransmitter release sites in their dendrites [6]. The identified recipients of the dendritic synaptic input from T4 neurons are Mi9, C3 and other T4 neurons [6]. The functional role of dendritic synapses of T4 neurons has not been investigated yet, and neither has it been shown that these synapses are cholinergic. For comparison, in mouse retina, direction-selective starburst amacrine cells (SACs) co-release acetylcholine and GABA [49] and GABAergic SAC-SAC connections shape the velocity tuning and contrast range of SACs [50]. Whether this could be the role of GABAergic transmission in T4/T5 neurons remains to be investigated. In flies, there has been no evidence provided so far for the release of more than one neurotransmitter from a single neuron.

### Supporting Information

**S1 Table. RPKM values in T4/T5 neurons.**  
(XLSX)

### Acknowledgments

We would like to thank to B. Dickson, A. Nern, G. Rubin, F. Schnorrer, J. Simpson, Bloomington Drosophila Stock Centre and Developmental Studies Hybridoma Bank for flies and antibodies. We are grateful to J. Simpson for sharing the VGAT-LexA line prior to publishing. We would like to thank to A. Arenz, J. Pujol-Marti and I. Ribeiro for critically reading the manuscript. RNA-seq was performed by EMBL Genomics Core Facility, Heidelberg, Germany.

### Author Contributions

**Conceptualization:** KP.



**Formal analysis:** KP.

**Funding acquisition:** AB.

**Investigation:** KP.

**Visualization:** KP.

**Writing – original draft:** KP.

**Writing – review & editing:** KP AB.

## References

1. Hardie RC. A histamine-activated chloride channel involved in neurotransmission at a photoreceptor synapse. *Nature*. 1989 Jun 29; 339(6227):704–6. doi: [10.1038/339704a0](https://doi.org/10.1038/339704a0) PMID: [2472552](https://pubmed.ncbi.nlm.nih.gov/2472552/)
2. Joesch M, Schnell B, Raghu SV, Reiff DF, Borst A. ON and OFF pathways in *Drosophila* motion vision. *Nature*. 2010 Nov 11; 468(7321):300–4. doi: [10.1038/nature09545](https://doi.org/10.1038/nature09545) PMID: [21068841](https://pubmed.ncbi.nlm.nih.gov/21068841/)
3. Eichner H, Joesch M, Schnell B, Reiff DF, Borst A. Internal structure of the fly elementary motion detector. *Neuron*. 2011 Jun 23; 70(6):1155–64. doi: [10.1016/j.neuron.2011.03.028](https://doi.org/10.1016/j.neuron.2011.03.028) PMID: [21689601](https://pubmed.ncbi.nlm.nih.gov/21689601/)
4. Takemura SY, Karuppudurai T, Ting CY, Lu Z, Lee CH, Meinertzhagen IA. Cholinergic circuits integrate neighboring visual signals in a *Drosophila* motion detection pathway. *Curr Biol*. 2011 Dec 20; 21(24):2077–84. doi: [10.1016/j.cub.2011.10.053](https://doi.org/10.1016/j.cub.2011.10.053) PMID: [22137471](https://pubmed.ncbi.nlm.nih.gov/22137471/)
5. Joesch M, Weber F, Eichner H, Borst A. Functional specialization of parallel motion detection circuits in the fly. *J Neurosci*. 2013 Jan 16; 33(3):902–5. doi: [10.1523/JNEUROSCI.3374-12.2013](https://doi.org/10.1523/JNEUROSCI.3374-12.2013) PMID: [23325229](https://pubmed.ncbi.nlm.nih.gov/23325229/)
6. Takemura SY, Bharioke A, Lu Z, Nern A, Vitaladevuni S, Rivlin PK, et al. A visual motion detection circuit suggested by *Drosophila* connectomics. *Nature*. 2013 Aug 8; 500(7461):175–81. doi: [10.1038/nature12450](https://doi.org/10.1038/nature12450) PMID: [23925240](https://pubmed.ncbi.nlm.nih.gov/23925240/)
7. Behnia R, Clark DA, Carter AG, Clandinin TR, Desplan C. Processing properties of ON and OFF pathways for *Drosophila* motion detection. *Nature*. 2014 Aug 28; 512(7515):427–30. doi: [10.1038/nature13427](https://doi.org/10.1038/nature13427) PMID: [25043016](https://pubmed.ncbi.nlm.nih.gov/25043016/)
8. Strother JA, Nern A, Reiser MB. Direct observation of ON and OFF pathways in the *Drosophila* visual system. *Curr Biol*. 2014 May 5; 24(9):976–83. doi: [10.1016/j.cub.2014.03.017](https://doi.org/10.1016/j.cub.2014.03.017) PMID: [24704075](https://pubmed.ncbi.nlm.nih.gov/24704075/)
9. Ammer G, Leonhardt A, Bahl A, Dickson BJ, Borst A. Functional specialization of neural input elements to the *Drosophila* ON motion detector. *Curr Biol*. 2015 Aug 31; 25(17):2247–53. doi: [10.1016/j.cub.2015.07.014](https://doi.org/10.1016/j.cub.2015.07.014) PMID: [26234212](https://pubmed.ncbi.nlm.nih.gov/26234212/)
10. Meier M, Serbe E, Maisak MS, Haag J, Dickson BJ, Borst A. Neural circuit components of the *Drosophila* OFF motion vision pathway. *Curr Biol*. 2014 Feb 17; 24(4):385–92. doi: [10.1016/j.cub.2014.01.006](https://doi.org/10.1016/j.cub.2014.01.006) PMID: [24508173](https://pubmed.ncbi.nlm.nih.gov/24508173/)
11. Shinomiya K, Karuppudurai T, Lin TY, Lu Z, Lee CH, Meinertzhagen IA. Candidate neural substrates for off-edge motion detection in *Drosophila*. *Curr Biol*. 2014 May 19; 24(10):1062–70. doi: [10.1016/j.cub.2014.03.051](https://doi.org/10.1016/j.cub.2014.03.051) PMID: [24768048](https://pubmed.ncbi.nlm.nih.gov/24768048/)
12. Serbe E, Meier M, Leonhardt A, Borst A. Comprehensive characterization of the major presynaptic elements to the *Drosophila* OFF motion detector. *Neuron*. 2016 Feb 17; 89(4):829–41. doi: [10.1016/j.neuron.2016.01.006](https://doi.org/10.1016/j.neuron.2016.01.006) PMID: [26853306](https://pubmed.ncbi.nlm.nih.gov/26853306/)
13. Maisak MS, Haag J, Ammer G, Serbe E, Meier M, Leonhardt A, et al. A directional tuning map of *Drosophila* elementary motion detectors. *Nature*. 2013 Aug 8; 500(7461):212–6. doi: [10.1038/nature12320](https://doi.org/10.1038/nature12320) PMID: [23925246](https://pubmed.ncbi.nlm.nih.gov/23925246/)
14. Fisher YE, Sillescu M, Clandinin TR. Orientation selectivity sharpens motion detection in *Drosophila*. *Neuron*. 2015 Oct 21; 88(2):390–402. doi: [10.1016/j.neuron.2015.09.033](https://doi.org/10.1016/j.neuron.2015.09.033) PMID: [26456048](https://pubmed.ncbi.nlm.nih.gov/26456048/)
15. Schnell B, Raghu SV, Nern A, Borst A. Columnar cells necessary for motion responses of wide-field visual interneurons in *Drosophila*. *J Comp Physiol A*. 2012 May; 198(5):389–95. doi: [10.1007/s00359-012-0716-3](https://doi.org/10.1007/s00359-012-0716-3) PMID: [22411431](https://pubmed.ncbi.nlm.nih.gov/22411431/)
16. Bahl A, Ammer G, Schilling T, Borst A. Object tracking in motion-blind flies. *Nat Neurosci*. 2013 Jun; 16(6):730–8. doi: [10.1038/nn.3386](https://doi.org/10.1038/nn.3386) PMID: [23624513](https://pubmed.ncbi.nlm.nih.gov/23624513/)
17. Hassenstein V, Reichardt W. [System theoretical analysis of time, sequence and sign analysis of the motion perception of the snout-beetle *Chlorophanus*]. *Z Naturforsch B*. 1956; 11b:513–524. German.
18. Haag J, Arenz A, Serbe E, Gabbiani F, Borst A. Complementary mechanisms create direction selectivity in the fly. *Elife*. 2016 Aug 9; 5:e17421. doi: [10.7554/eLife.17421](https://doi.org/10.7554/eLife.17421) PMID: [27502554](https://pubmed.ncbi.nlm.nih.gov/27502554/)

19. Leong JC, Esch JJ, Poole B, Ganguli S, Clandinin TR. Direction selectivity in *Drosophila* emerges from preferred-direction enhancement and null-direction suppression. *J Neurosci*. 2016 Aug 3; 36(31):8078–92. doi: [10.1523/JNEUROSCI.1272-16.2016](https://doi.org/10.1523/JNEUROSCI.1272-16.2016) PMID: [27488629](https://pubmed.ncbi.nlm.nih.gov/27488629/)
20. Borst A, Helmstaedter M. Common circuit design in fly and mammalian motion vision. *Nat Neurosci*. 2015 Aug; 18(8):1067–76. doi: [10.1038/nn.4050](https://doi.org/10.1038/nn.4050) PMID: [26120965](https://pubmed.ncbi.nlm.nih.gov/26120965/)
21. Larkum ME, Zhu JJ, Sakmann B. A new cellular mechanism for coupling inputs arriving at different cortical layers. *Nature*. 1999 Mar 25; 398(6725):338–41. doi: [10.1038/18686](https://doi.org/10.1038/18686) PMID: [10192334](https://pubmed.ncbi.nlm.nih.gov/10192334/)
22. Gabbiani F, Krapp HG, Koch C, Laurent G. Multiplicative computation in a visual neuron sensitive to looming. *Nature*. 2002 Nov 21; 420(6913):320–4. doi: [10.1038/nature01190](https://doi.org/10.1038/nature01190) PMID: [12447440](https://pubmed.ncbi.nlm.nih.gov/12447440/)
23. Schiller J, Schiller Y, Clapham DE. NMDA receptors amplify calcium influx into dendritic spines during associative pre- and postsynaptic activation. *Nat Neurosci*. 1998 Jun; 1(2):114–8. doi: [10.1038/363](https://doi.org/10.1038/363) PMID: [10195125](https://pubmed.ncbi.nlm.nih.gov/10195125/)
24. Edwards DH, Yeh SR, Krasne FB. Neuronal coincidence detection by voltage-sensitive electrical synapses. *Proc Natl Acad Sci U S A*. 1998 Jun 9; 95(12):7145–50. doi: [10.1073/pnas.95.12.7145](https://doi.org/10.1073/pnas.95.12.7145) PMID: [9618553](https://pubmed.ncbi.nlm.nih.gov/9618553/)
25. Wessel R, Kristan WB Jr, Kleinfeld D. Supralinear summation of synaptic inputs by an invertebrate neuron: dendritic gain is mediated by an "inward rectifier" K(+) current. *J Neurosci*. 1999 Jul 15; 19(14):5875–88. PMID: [10407027](https://pubmed.ncbi.nlm.nih.gov/10407027/)
26. Henry GL, Davis FP, Picard S, Eddy SR. Cell type-specific genomics of *Drosophila* neurons. *Nucleic Acids Res*. 2012 Oct; 40(19):9691–704. doi: [10.1093/nar/gks671](https://doi.org/10.1093/nar/gks671) PMID: [22855560](https://pubmed.ncbi.nlm.nih.gov/22855560/)
27. Schilling T, Borst A. Local motion detectors are required for the computation of expansion flow-fields. *Biol Open*. 2015 Jul 31; 4(9):1105–8. doi: [10.1242/bio.012690](https://doi.org/10.1242/bio.012690) PMID: [26231626](https://pubmed.ncbi.nlm.nih.gov/26231626/)
28. Lee T, Luo L. Mosaic analysis with a repressible cell marker for studies of gene function in neuronal morphogenesis. *Neuron*. 1999 Mar; 22(3):451–61. doi: [10.1016/S0896-6273\(00\)80701-1](https://doi.org/10.1016/S0896-6273(00)80701-1) PMID: [10197526](https://pubmed.ncbi.nlm.nih.gov/10197526/)
29. Diegelmann S, Bate M, Landgraf M. Gateway cloning vectors for the LexA-based binary expression system in *Drosophila*. *Fly (Austin)*. 2008 Jul-Aug; 2(4):236–9. PMID: [18776741](https://pubmed.ncbi.nlm.nih.gov/18776741/)
30. Kim D, Perteau G, Trapnell C, Pimentel H, Kelley R, Salzberg SL. TopHat2: accurate alignment of transcriptomes in the presence of insertions, deletions and gene fusions. *Genome Biol*. 2013 Apr 25; 14(4):R36. doi: [10.1186/gb-2013-14-4-r36](https://doi.org/10.1186/gb-2013-14-4-r36) PMID: [23618408](https://pubmed.ncbi.nlm.nih.gov/23618408/)
31. Liao Y, Smyth GK, Shi W. featureCounts: an efficient general-purpose program for assigning sequence reads to genomic features. *Bioinformatics*. 2014 Apr 1; 30(7):923–30. doi: [10.1093/bioinformatics/btt656](https://doi.org/10.1093/bioinformatics/btt656) PMID: [24227677](https://pubmed.ncbi.nlm.nih.gov/24227677/)
32. Liu WW, Wilson RI. Glutamate is an inhibitory neurotransmitter in the *Drosophila* olfactory system. *Proc Natl Acad Sci U S A*. 2013 Jun 18; 110(25):10294–9. doi: [10.1073/pnas.1220560110](https://doi.org/10.1073/pnas.1220560110) PMID: [23729809](https://pubmed.ncbi.nlm.nih.gov/23729809/)
33. Mauss AS, Meier M, Serbe E, Borst A. Optogenetic and pharmacologic dissection of feedforward inhibition in *Drosophila* motion vision. *J Neurosci*. 2014 Feb 5; 34(6):2254–63. doi: [10.1523/JNEUROSCI.3938-13.2014](https://doi.org/10.1523/JNEUROSCI.3938-13.2014) PMID: [24501364](https://pubmed.ncbi.nlm.nih.gov/24501364/)
34. Mauss AS, Pankova K, Arenz A, Nern A, Rubin GM, Borst A. Neural circuit to integrate opposing motions in the visual field. *Cell*. 2015 Jul 16; 162(2):351–62. doi: [10.1016/j.cell.2015.06.035](https://doi.org/10.1016/j.cell.2015.06.035) PMID: [26186189](https://pubmed.ncbi.nlm.nih.gov/26186189/)
35. Srivastava DP, Yu EJ, Kennedy K, Chatwin H, Reale V, Hamon M, et al. Rapid, nongenomic responses to ecdysteroids and catecholamines mediated by a novel *Drosophila* G-protein-coupled receptor. *J Neurosci*. 2005 Jun 29; 25(26):6145–55. doi: [10.1523/JNEUROSCI.1005-05.2005](https://doi.org/10.1523/JNEUROSCI.1005-05.2005) PMID: [15987944](https://pubmed.ncbi.nlm.nih.gov/15987944/)
36. Buckingham SD, Kidd JF, Law RJ, Franks CJ, Sattelle DB. Structure and function of two-pore-domain K+ channels: contributions from genetic model organisms. *Trends Pharmacol Sci*. 2005 Jul; 26(7):361–7. doi: [10.1016/j.tips.2005.05.003](https://doi.org/10.1016/j.tips.2005.05.003) PMID: [15939489](https://pubmed.ncbi.nlm.nih.gov/15939489/)
37. Brand AH, Perrimon N. Targeted gene expression as a means of altering cell fates and generating dominant phenotypes. *Development*. 1993 Jun; 118(2):401–15. PMID: [8223268](https://pubmed.ncbi.nlm.nih.gov/8223268/)
38. Lai SL, Lee T. Genetic mosaic with dual binary transcriptional systems in *Drosophila*. *Nat Neurosci*. 2006 May; 9(5):703–9. doi: [10.1038/nn1681](https://doi.org/10.1038/nn1681) PMID: [16582903](https://pubmed.ncbi.nlm.nih.gov/16582903/)
39. Delmas P, Brown DA. Pathways modulating neural KCNQ/M (Kv7) potassium channels. *Nat Rev Neurosci*. 2005 Nov; 6(11):850–62. doi: [10.1038/nrn1785](https://doi.org/10.1038/nrn1785) PMID: [16261179](https://pubmed.ncbi.nlm.nih.gov/16261179/)
40. Wei A, Covarrubias M, Butler A, Baker K, Pak M, Salkoff L. K+ current diversity is produced by an extended gene family conserved in *Drosophila* and mouse. *Science*. 1990 May 4; 248(4955):599–603. doi: [10.1126/science.2333511](https://doi.org/10.1126/science.2333511) PMID: [2333511](https://pubmed.ncbi.nlm.nih.gov/2333511/)

41. Srinivasan S, Lance K, Levine RB. Contribution of EAG to excitability and potassium currents in *Drosophila* larval motor neurons. *J Neurophysiol*. 2012 May; 107(10):2660–71. doi: [10.1152/jn.00201.2011](https://doi.org/10.1152/jn.00201.2011) PMID: [22323637](https://pubmed.ncbi.nlm.nih.gov/22323637/)
42. Martinson AS, van Rossum DB, Diatta FH, Layden MJ, Rhodes SA, Martindale MQ, et al. Functional evolution of Erg potassium channel gating reveals an ancient origin for IKr. *Proc Natl Acad Sci U S A*. 2014 Apr 15; 111(15):5712–7. doi: [10.1073/pnas.1321716111](https://doi.org/10.1073/pnas.1321716111) PMID: [24706772](https://pubmed.ncbi.nlm.nih.gov/24706772/)
43. Enell L, Hamasaka Y, Kolodziejczyk A, Nässel DR. gamma-Aminobutyric acid (GABA) signaling components in *Drosophila*: immunocytochemical localization of GABA(B) receptors in relation to the GABA (A) receptor subunit RDL and a vesicular GABA transporter. *J Comp Neurol*. 2007 Nov 1; 505(1):18–31. doi: [10.1002/cne.21472](https://doi.org/10.1002/cne.21472) PMID: [17729251](https://pubmed.ncbi.nlm.nih.gov/17729251/)
44. Tritsch NX, Oh WJ, Gu C, Sabatini BL. Midbrain dopamine neurons sustain inhibitory transmission using plasma membrane uptake of GABA, not synthesis. *Elife*. 2014 Apr 24; 3:e01936. doi: [10.7554/eLife.01936](https://doi.org/10.7554/eLife.01936) PMID: [24843012](https://pubmed.ncbi.nlm.nih.gov/24843012/)
45. Yoon BE, Woo J, Chun YE, Chun H, Jo S, Bae JY, et al. Glial GABA, synthesized by monoamine oxidase B, mediates tonic inhibition. *J Physiol*. 2014 Nov 15; 592(22):4951–68. doi: [10.1113/jphysiol.2014.278754](https://doi.org/10.1113/jphysiol.2014.278754) PMID: [25239459](https://pubmed.ncbi.nlm.nih.gov/25239459/)
46. Kim JI, Ganesan S, Luo SX, Wu YW, Park E, Huang EJ, et al. Aldehyde dehydrogenase 1a1 mediates a GABA synthesis pathway in midbrain dopaminergic neurons. *Science*. 2015 Oct 2; 350(6256):102–6. doi: [10.1126/science.aac4690](https://doi.org/10.1126/science.aac4690) PMID: [26430123](https://pubmed.ncbi.nlm.nih.gov/26430123/)
47. Bessman SP, Rossen J, Layne EC. Gamma-Aminobutyric acid-glutamic acid transamination in brain. *J Biol Chem*. 1953 Mar; 201(1):385–91. PMID: [13044808](https://pubmed.ncbi.nlm.nih.gov/13044808/)
48. Balazs R, Machiyama Y, Hammond BJ, Julian T, Richter D. The operation of the gamma-aminobutyrate bypath of the tricarboxylic acid cycle in brain tissue in vitro. *Biochem J*. 1970 Feb; 116(3):445–61. PMID: [5435689](https://pubmed.ncbi.nlm.nih.gov/5435689/)
49. O'Malley DM, Sandell JH, Masland RH. Co-release of acetylcholine and GABA by the starburst amacrine cells. *J Neurosci*. 1992 Apr; 12(4):1394–408. PMID: [1556600](https://pubmed.ncbi.nlm.nih.gov/1556600/)
50. Ding H, Smith RG, Poleg-Polsky A, Diamond JS, Briggman KL. Species-specific wiring for direction selectivity in the mammalian retina. *Nature*. 2016 Jul 7; 535(7610):105–10. doi: [10.1038/nature18609](https://doi.org/10.1038/nature18609) PMID: [27350241](https://pubmed.ncbi.nlm.nih.gov/27350241/)

### **2.3 TRANSGENIC LINE FOR THE IDENTIFICATION OF CHOLINERGIC RELEASE SITES IN *DROSOPHILA MELANOGASTER***

The article “Transgenic line for the identification of cholinergic release sites in *Drosophila melanogaster*” (<https://doi.org/10.1242/jeb.149369>) was originally published in the Journal of Experimental Biology in April 2017. The following authors contributed to this work: Katarina Pankova conceived and performed the experiments and wrote the manuscript. Alexander Borst revised the manuscript.

METHODS & TECHNIQUES

# Transgenic line for the identification of cholinergic release sites in *Drosophila melanogaster*

Katarina Pankova<sup>1,2,\*</sup> and Alexander Borst<sup>1</sup>

## ABSTRACT

The identification of neurotransmitter type used by a neuron is important for the functional dissection of neuronal circuits. In the model organism *Drosophila melanogaster*, several methods for discerning the neurotransmitter systems are available. Here, we expanded the toolbox for the identification of cholinergic neurons by generating a new line FRT-STOP-FRT-VAcHT::HA that is a conditional tagged knock-in of the vesicular acetylcholine transporter (VAcHT) gene in its endogenous locus. Importantly, in comparison to already available tools for the detection of cholinergic neurons, the FRT-STOP-FRT-VAcHT::HA allele also allows for identification of the subcellular localization of the cholinergic presynaptic release sites in a cell-specific manner. We used the newly generated FRT-STOP-FRT-VAcHT::HA line to characterize the Mi1 and Tm3 neurons in the fly visual system and found that VAcHT is present in the axons of both cell types, suggesting that Mi1 and Tm3 neurons provide cholinergic input to the elementary motion detectors, the T4 neurons.

**KEY WORDS:** VAcHT, Acetylcholine, Neurotransmitter, Motion vision, Mi1 neurons, Tm3 neurons

## INTRODUCTION

Understanding of the information processing in neuronal circuits requires knowledge about connectivity and properties of the cells involved. The type of neurotransmitter released by a cell defines, to a large extent, the role of a cell and the range of logical operations that are performed within a circuit. Thus, the identification of the cellular neurotransmitter phenotype is of crucial importance for the functional dissection of neuronal circuits.

Various techniques have been described for the identification of neurotransmitter systems in the *Drosophila melanogaster* nervous system. The most common approach is the detection of neurotransmitter molecules (Monastirioti et al., 1995; Yuan et al., 2005; Kolodziejczyk et al., 2008), neurotransmitter-synthesizing enzymes (Takagawa and Salvaterra, 1996; Featherstone et al., 2000; Blanco et al., 2011) or vesicular neurotransmitter transporters (Kitamoto et al., 1998; Daniels et al., 2004; Greer et al., 2005; Romero-Calderón et al., 2008; Fei et al., 2010) with an antibody. In *Drosophila* neurons, the major disadvantage of this strategy is that

either cell bodies or larger neuropil areas are examined for the antibody staining. Because of the small diameter of the neuronal processes, reliable localization of the antibody staining within the individual neurites is beyond the resolution threshold of traditional confocal microscopy. Therefore, the markers that localize to the presynaptic regions and are not present ubiquitously in the cytoplasm or at the cytoplasmic membrane of soma cannot be easily detected in individual neurons.

The second approach for the identification of neurotransmitter phenotype is the detection of mRNA transcripts for neurotransmitter-synthesizing enzymes or neurotransmitter vesicular transporters. The *in situ* hybridization technique has been used to study gene expression mainly in fly embryos but also in other tissues, including the nervous system. Nevertheless, the demanding process of probe optimization poses a challenge and therefore this technique is not routinely used to assess neurotransmitter phenotype. With respect to the specificity and dynamic range, the current method of choice for transcript profiling is RNA-seq of a single cell or a homogeneous population of cells (Henry et al., 2012; Thomas et al., 2012). In addition, other techniques such as RT-PCR or gene expression microarrays have been successfully used to study gene expression in *Drosophila* neurons (Nagoshi et al., 2010; Takemura et al., 2011). Regardless of the specific technique, the cell-type-specific transcriptome profiling requires isolation of labeled somata, nuclei or ribosomes in sufficient quantity and purity, which is labor-intensive. Also, contamination of the analyzed sample with mRNA from other cell types may occur during this process.


The third approach relies on genetic labeling of neurons expressing the neurotransmitter-synthesizing enzymes or neurotransmitter vesicular transporters via insertion of a transgene into 5' UTR or a coding intron of the respective gene (Venken et al., 2011; Diao et al., 2015). When the inserted transgene is a transcription factor of a binary expression system such as Gal4/UAS (Brand and Perrimon, 1993) or LexA/lexAop (Lai and Lee, 2006), the complete expression pattern of a particular gene can be easily identified throughout the whole nervous system. Recently, a set of LexA knock-in lines for the neurotransmitter vesicular transporter genes was generated by ends-out homologous recombination (Simpson, 2016).

Acetylcholine is a major excitatory neurotransmitter in the *Drosophila* nervous system. Synthesis of acetylcholine is catalyzed by the enzyme choline acetyltransferase (ChAT) and its loading into synaptic vesicles is mediated by the vesicular acetylcholine transporter (VAcHT). Currently, the available tools for identification of the cholinergic neurons are ChAT antiserum (Takagawa and Salvaterra, 1996), ChAT Trojan-MiMIC driver lines (Venken et al., 2011; Diao et al., 2015) and VAcHT-LexA knock-in line (Simpson, 2016).

In the present study, we describe a newly generated FRT-STOP-FRT-VAcHT::HA allele for the reporting of the endogenous

<sup>1</sup>Max Planck Institute of Neurobiology, 82152 Martinsried, Germany. <sup>2</sup>Graduate School of Systemic Neurosciences, LMU Munich, 80539 Munich, Germany.

\*Author for correspondence (pankova@neuro.mpg.de)

 K.P., 0000-0002-7182-5486

This is an Open Access article distributed under the terms of the Creative Commons Attribution License (<http://creativecommons.org/licenses/by/3.0/>), which permits unrestricted use, distribution and reproduction in any medium provided that the original work is properly attributed.

expression of VACHT that not only identifies neurons with the cholinergic phenotype but also provides information about the subcellular localization of the cholinergic presynaptic release sites.

## MATERIALS AND METHODS

### Fly stocks and genotypes

The flies were raised on a standard cornmeal-agar food at 25°C. The following stocks were used: *yw*, *Act5C-cas9*, *lig4* (provided by F. Schnorrer, Max Planck Institute of Neurobiology, Germany) (Zhang et al., 2014), *UAS-FLP* (BDSC 4539 and 8208), *UAS-mCD8::GFP* (BDSC 5137) (Lee and Luo, 1999), *VT25965-Gal4* (T4/T5 line) (provided by B. Dickson, Janelia Research Campus, USA); *R20D01-Gal4* (LPI3-4 line) (BDSC 48889) (Jenett et al., 2012); *VT7747-AD*, *VT49371-DBD* (Mi1 line) (Ammer et al., 2015), *GMRSS00300-split Gal4* (Tm3 line) (provided by A. Nern, Janelia Research Campus, USA), *MB008B* (Aso et al., 2014), *MB112C* (Aso et al., 2014), *UAS-nsyb::GFP* (BDSC 6921) (Zhang et al., 2002) and *Act5C-Gal4* (BDSC 4414).

The genotypes of flies used in this study are detailed in Table 1.

### Generation of the FRT-STOP-FRT-VACHT::HA allele with the CRISPR/cas9 system

The target sites for CRISPR/cas9-induced cleavages in the *VACHT* gene were designed using a web-based software tool (<http://crispr.mit.edu/>; Hsu et al., 2013). The efficiency of individual guide RNAs (gRNAs) was tested in S2 cells stably expressing cas9 (provided by F. Schnorrer) (Böttercher et al., 2014) as described previously (Zhang et al., 2014). The CRISPR target sites used for genome editing were AGAGGAAGTCCCAAAGAAAC (TGG) and GGGCTATCGAT-ACAATCACG (AGG). The target-specific sequences were cloned into pU6-BbsI-gRNA plasmid (provided by M. Harrison, K. O'Connor-Giles and J. Wildonger; Addgene plasmid 45946) (Gratz et al., 2013) such that the first base of both sequences was replaced by G. The gRNA-expressing plasmids and the donor plasmid for the homology-directed repair were injected into fly embryos of the genotype *yw*, *Act5C-cas9*, *lig4*. The embryo injections were performed by BestGene Inc. (<https://www.thebestgene.com/>).

The donor fragment for the generation of FRT-STOP-FRT-VACHT::HA allele was assembled by PCR fusion of the following

sequences: (1) flippase recognition target (FRT)-flanked cassette containing transcriptional terminator (*hsp70Ab* polyadenylation signal) and the sequence for a screenable eye marker (*3xP3-DsRed-α1tub\_3'UTR*), synthesized *de novo*; (2) DNA fragment containing the Kozak sequence followed by an open reading frame (ORF) of the *VACHT* gene with the sequence for the HA tag inserted after the first 14 codons from translational start, synthesized *de novo*; and (3) two 1 kb homology arms flanking the CRISPR cleavage sites, amplified from genomic DNA of *yw*, *Act5C-cas9*, *lig4* flies. The resulting donor fragment consisted of the upstream homology arm fused to the FRT cassette, followed by the Kozak sequence, the ORF with tag sequence and the downstream homology arm. The donor fragment was blunt-end cloned into pJet1.2 vector (Thermo Fisher Scientific). The nucleotide sequence of the HA tag was TAC CCA TAC GAT GTT CCA GAT TAC GCT.

### Immunohistochemistry

Fly brains were dissected in PBS and fixed in 4% PFA with 0.1% Triton X for 25 min. Brains were washed in 0.3% PBT and incubated first with primary (24–72 h) and then secondary (24–48 h) antibodies in 0.3% PBT supplemented with 5% NGS. The brains were mounted in Vectashield mounting medium (Vector Laboratories) and imaged on a Leica TCS SP5 or SP8 laser-scanning confocal microscope. The following antibodies were used: rabbit anti-GFP (Torrey Pines TP401, 1:400), rat anti-HA (Sigma-Aldrich, clone 3F10, 1:100), mouse anti-ChAT (DSHB, deposited by P. Salvaterra, 1:50) (Takagawa and Salvaterra, 1996), goat anti-rabbit Alexa 488 (Thermo Fisher Scientific A-11008, 1:200), goat anti-rat Alexa 647 (Thermo Fisher Scientific A-21247, 1:200) and goat anti-mouse Alexa 647 (Thermo Fisher Scientific A-21235, 1:200).

## RESULTS AND DISCUSSION

Using CRISPR/cas9-based genome editing (Jinek et al., 2012; Gratz et al., 2013), we generated a new allele of the *VACHT* gene that carried an additional HA tag. This new allele was positioned in the original genomic locus of the *VACHT* gene and therefore its expression depended on the endogenous regulatory sequences of *VACHT*. The HA tag was placed after the first 14 amino acids from the N terminus, within the cytoplasmic domain of the VACHT protein. The position of the tag was chosen such that it would not interfere with protein folding or signaling sequences known to participate in the intracellular trafficking of VACHT (Fei et al., 2008).

Our aim was to restrict the expression of VACHT::HA to a population of neurons defined by the expression pattern of a Gal4 line of choice. Therefore, we included a transcriptional stop cassette into the 5' UTR of the *VACHT* gene that was flanked by two FRT sites (Fig. 1). The expression of the VACHT::HA was, as a result,

**Table 1. Genotypes of flies used in the study**

Experiment	Genotype
Adult viability	<i>w<sup>1118</sup>;yw</i> ; <i>Act5C-Gal4/UAS-FLP</i> ; <i>FRT-STOP-FRT-VACHT::HA/FRT-STOP-FRT-VACHT::HA</i>
Fig. 2A	<i>w<sup>1118</sup></i> ; <i>UAS-FLP/UAS-mCD8::GFP</i> ; <i>FRT-STOP-FRT-VACHT::HA/VT25965-Gal4</i>
Fig. 2B	<i>w<sup>1118</sup></i> ; <i>UAS-FLP/UAS-mCD8::GFP</i> ; <i>FRT-STOP-FRT-VACHT::HA/R20D01-Gal4</i>
Fig. 2C	<i>UAS-FLP/w<sup>1118</sup></i> ; <i>MB008B-split Gal4/UAS-mCD8::GFP</i> ; <i>MB008B-split Gal4/FRT-STOP-FRT-VACHT::HA</i>
Fig. 2D	<i>UAS-FLP/w<sup>1118</sup></i> ; <i>MB112C-split Gal4/UAS-mCD8::GFP</i> ; <i>MB112C-split Gal4/FRT-STOP-FRT-VACHT::HA</i>
Fig. 3A	<i>UAS-FLP/w<sup>1118</sup></i> ; <i>VT7747-AD/UAS-mCD8GFP</i> ; <i>VT49371-DBD/FRT-STOP-FRT-VACHT::HA</i>
Fig. 3B	<i>UAS-FLP/w<sup>1118</sup></i> ; <i>GMRSS00300-split Gal4/UAS-mCD8GFP</i> ; <i>GMRSS00300-split Gal4/FRT-STOP-FRT-VACHT::HA</i>
Fig. 3C	<i>UAS-FLP/w<sup>1118</sup></i> ; <i>VT7747-AD/UAS-nsyb::GFP</i> ; <i>VT49371-DBD/FRT-STOP-FRT-VACHT::HA</i>
Fig. 3D	<i>UAS-FLP/w<sup>1118</sup></i> ; <i>GMRSS00300-split Gal4/UAS-nsyb::GFP</i> ; <i>GMRSS00300-split Gal4/FRT-STOP-FRT-VACHT::HA</i>
Fig. 3E	<i>w<sup>1118</sup></i> ; <i>VT7747-AD/UAS-mCD8GFP</i> ; <i>VT49371-DBD/+</i>
Fig. 3F	<i>w<sup>1118</sup></i> ; <i>GMRSS00300-split Gal4/UAS-mCD8GFP</i> ; <i>GMRSS00300-split Gal4/+</i>

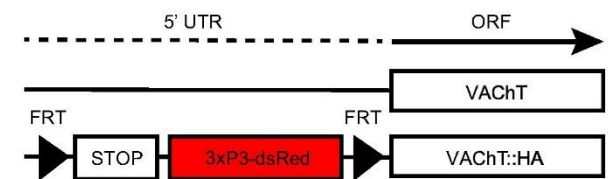


**Fig. 1. Original VACHT allele and FRT-STOP-FRT-VACHT::HA allele.** FRT-flanked transcriptional stop signal in the 5' UTR constrains the expression of VACHT::HA. Removal of the stop cassette requires FLP recombinase, introduced by the Gal4/UAS system. Expression of the VACHT::HA is therefore restricted to cells with active endogenous regulatory sequences of *VACHT* that are, in addition, part of the Gal4 expression pattern. The 3xP3-dsRed sequence encodes a screenable eye marker. ORF, open reading frame.

confined to cells that were expressing flippase (FLP) recombinase introduced by the Gal4/UAS system and contained an active endogenous promoter of *VAcHt*.

Disruption of both copies of the *VAcHt* gene causes lethality during embryonic or larval development (Kitamoto et al., 2000). We did not observe any adult flies homozygous for the newly generated FRT-STOP-FRT-*VAcHt*::HA allele, confirming that the stop cassette efficiently disrupts transcription of the *VAcHt*::HA. When the stop cassette was removed by expressing the FLP recombinase ubiquitously with Act5C-Gal4 driver line, the flies homozygous for FRT-STOP-FRT-*VAcHt*::HA allele were viable. This suggests that the tagged transporter *VAcHt*::HA can fully substitute the original *VAcHt* transporter at the synapse.

To test the functionality of the FRT-STOP-FRT-*VAcHt*::HA allele, we chose the T4/T5 neurons. T4/T5 neurons are the elementary motion detectors of the fly, sensitive to motion of bright (T4) and dark (T5) edges (Maisak et al., 2013). These cells have been shown previously to synthesize and release acetylcholine (Mauss et al., 2014; Shinomiya et al., 2014). In accordance with these prior findings, we detected *VAcHt*::HA in the axon terminals of the T4/T5 neurons in the lobula plate (Fig. 2A). A weaker HA signal was present also in the dendrites of T4/T5 neurons in medulla and lobula. This finding is in line with a previous study reporting existence of the dendritic presynaptic release sites in the T4 neurons (Takemura et al., 2013). To show that the expression of *VAcHt*::HA is absent in non-cholinergic neurons, we looked at the expression of

*VAcHt*::HA in the LPI3-4 neurons that have been previously identified as glutamatergic (Mauss et al., 2015). As expected, we could not detect any expression of the *VAcHt*::HA in the LPI3-4 neurons (Fig. 2B).

To demonstrate that FRT-STOP-FRT-*VAcHt*::HA allele reliably captures the endogenous expression pattern of the *VAcHt* gene in a variety of neuronal populations, we additionally examined the expression of *VAcHt*::HA in the mushroom body neurons. We detected *VAcHt*::HA in the Kenyon cells in  $\alpha/\beta$  lobes of the mushroom body (Fig. 2C) that have recently been shown to release acetylcholine (Barnstedt et al., 2016). On the contrary, we did not observe any HA signal in the GABAergic mushroom body output neurons  $\gamma$ 1pedc> $\alpha/\beta$  (Aso et al., 2014) (Fig. 2D).

Mi1 and Tm3 neurons synapse onto dendrites of T4 neurons (Takemura et al., 2013) and are involved in visual detection of the moving bright edges (Behnia et al., 2014; Ammer et al., 2015). Despite the functional characterization of the responses of Mi1 and Tm3 neurons (Behnia et al., 2014) and the reported effects of the synaptic silencing of Mi1 and Tm3 on the motion vision circuit (Ammer et al., 2015), the exact contribution of the Mi1 and Tm3 neurons to direction-selective responses of the T4 neurons is not clear (Maisak et al., 2013; Haag et al., 2016), nor is it known whether the synaptic input that Mi1 and Tm3 neurons provide to T4 neurons is excitatory or inhibitory. Therefore, we employed the newly generated FRT-STOP-FRT-*VAcHt*::HA allele to investigate the neurotransmitter system used by Mi1 and Tm3 neurons.

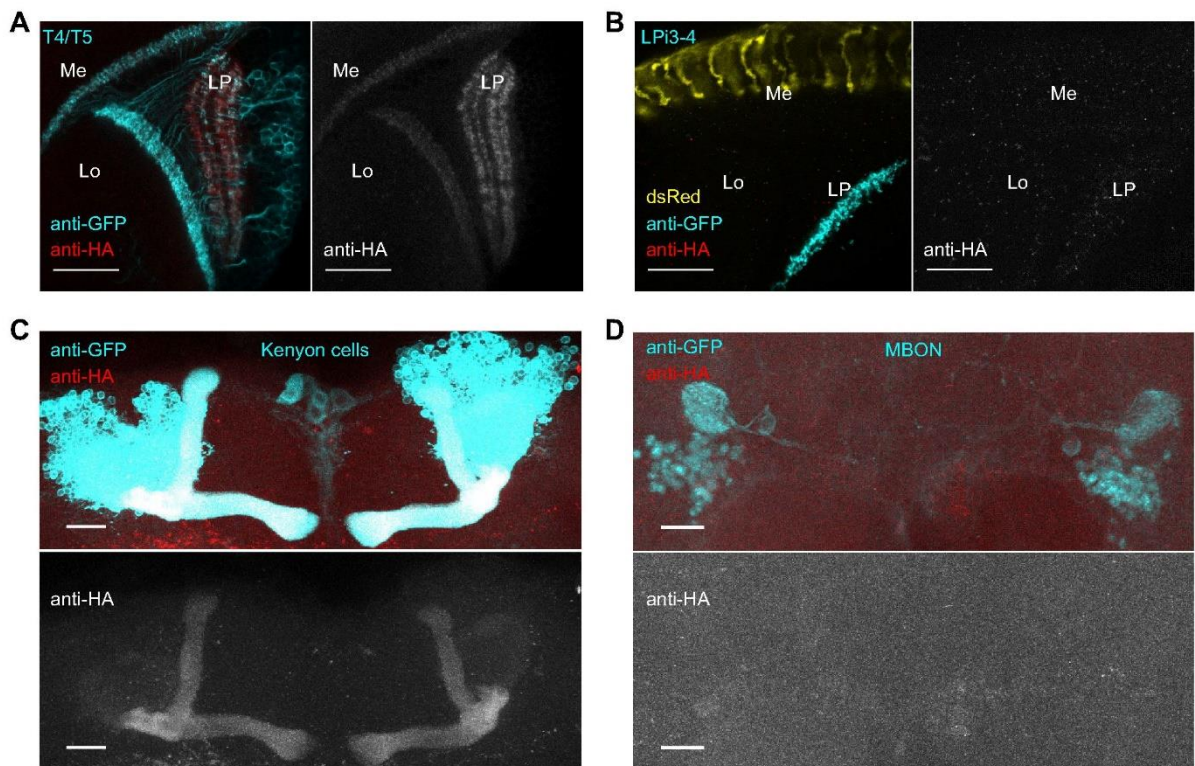


**Fig. 2. *VAcHt*::HA is detectable exclusively in the cholinergic neurons.** (A) The expression of *VAcHt*::HA in T4/T5 neurons is localized to the axons in the lobula plate and dendrites in the medulla and lobula. (B) In the LPI3-4 neurons, no expression of *VAcHt*::HA can be detected. The fluorescence of DsRed in the R7/R8 photoreceptor terminals in the medulla confirms the presence of the FRT-STOP-FRT-*VAcHt*::HA allele in the fly genome. (C) Kenyon cells in the  $\alpha/\beta$  lobes of the mushroom body show expression of *VAcHt*::HA. (D) No co-localization of the HA signal and GFP staining in the mushroom body output neurons (MBON)  $\gamma$ 1pedc> $\alpha/\beta$  can be detected. All scale bars: 20  $\mu$ m. Me, medulla; Lo, lobula; LP, lobula plate.

Using the FRT-STOP-FRT-VAcHT::HA line, we identified the Mi1 and Tm3 neurons as cholinergic. The expression of VAcHT::HA could be detected in all medullar and lobular layers where Mi1 and Tm3 neurons laterally extend their neurites (Fig. 3A,B). The VAcHT::HA signal was strongest for both the Mi1 and Tm3 neurons in the medullar layer 9/10, where Mi1 and Tm3 neurons synapse on the dendrites of T4 neurons (Takemura et al., 2013). In order to examine whether the localization of VAcHT::HA corresponds to the presynaptic release sites in the Mi1 and Tm3 neurons, we expressed a marker for presynaptic sites, the GFP-tagged neuronal synaptobrevin (*nsyb::GFP*) (Zhang et al., 2002), in Mi1 and Tm3 neurons. We observed that the subcellular localization of *nsyb::GFP* in both Mi1 and Tm3 neurons shows the same pattern as VAcHT::HA (Fig. 3C,D), confirming that the subcellular distribution of VAcHT::HA corresponds to the presynaptic release sites. The expression of *nsyb::GFP* in Mi1 and Tm3 neurons was stronger than the expression of VAcHT::HA and could be detected also in the neuronal fibers. This is likely due to overexpression of the *nsyb::GFP* transgene with the Gal4/UAS system. To prove the cholinergic phenotype of the Mi1 and Tm3 neurons by another line of evidence,

we stained fly brains with ChAT antiserum (Takagawa and Salvaterra, 1996) and looked at the presence of ChAT immunostaining in the cell bodies of Mi1 and Tm3 neurons. We detected the presence of ChAT immunoreactivity in the cell bodies of both Mi1 and Tm3 neurons (Fig. 3E,F), confirming that Mi1 and Tm3 neurons use acetylcholine as their neurotransmitter.

When using the FRT-STOP-FRT-VAcHT::HA allele, one important aspect to consider is choosing a Gal4 line with as specific an expression pattern as possible. Even very weak expression of the FLP can lead to genomic excision of the FRT-flanked transcriptional stop cassette and, as a result, to expression of the VAcHT::HA. As the expression level of VAcHT::HA depends on the endogenous regulatory sequences and not on the amount of Gal4 molecules present, it may occur that the expression of VAcHT::HA is stronger than that of Gal4-driven GFP. When using a Gal4 line containing cells with various strength of Gal4 expression, we noticed the presence of VAcHT::HA also in the neurons that were barely detectably labeled with GFP. We believe that this is the reason for the unspecific dotted pattern of the anti-HA staining in the optic lobe of the Tm3 line (Fig. 3B).

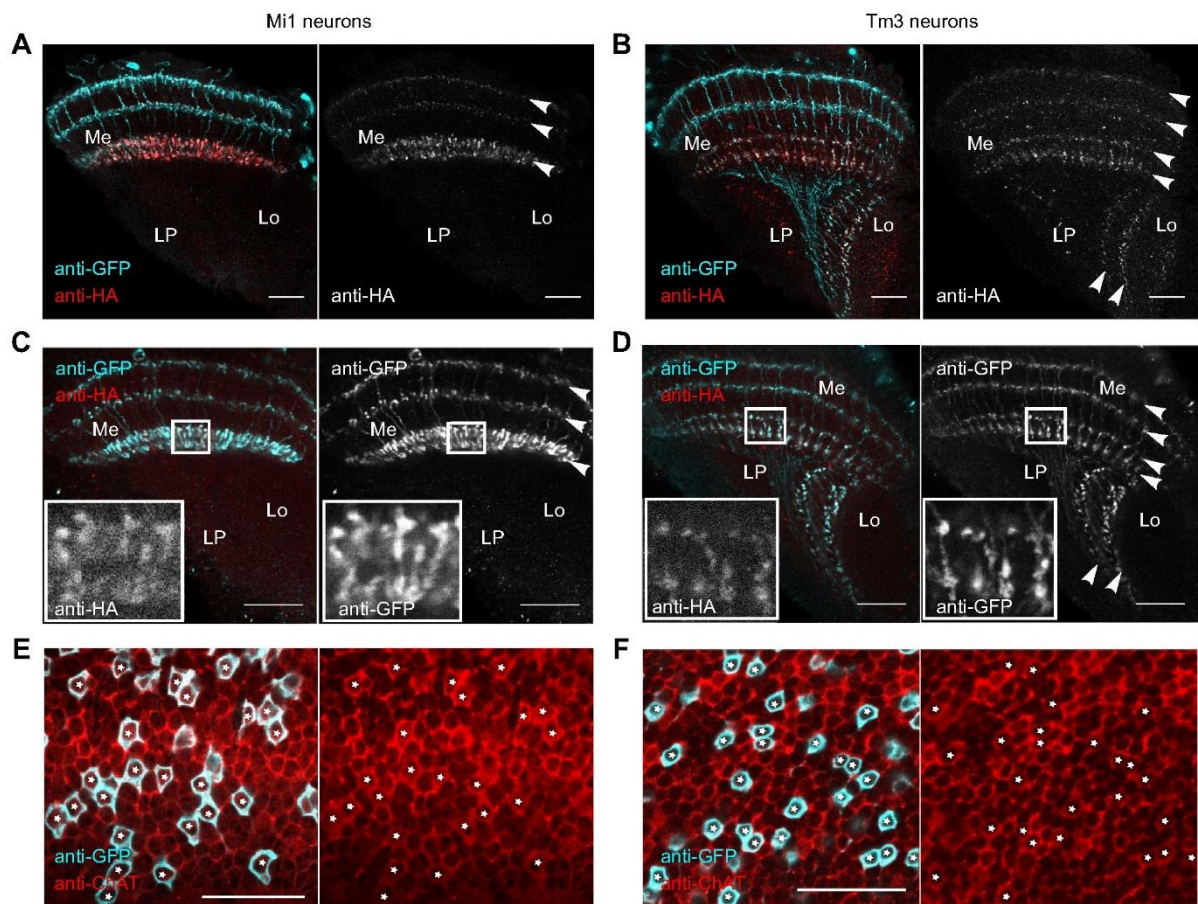


**Fig. 3. The Mi1 and Tm3 neurons are cholinergic.** The VAcHT::HA can be found in all layers of the medulla and lobula in which Mi1 (A) and Tm3 (B) neurons laterally extend their processes (white arrowheads). The subcellular localization of the presynaptic marker *nsyb::GFP* in the Mi1 (C) and Tm3 (D) neurons (white arrowheads) corresponds to that of VAcHT::HA. The insets in C and D show close-ups of the medulla regions containing presynaptic release sites of Mi1 and Tm3 neurons labeled by VAcHT::HA and *nsyb::GFP*. Anti-ChAT staining co-localizes with the GFP-labeled somatic cytoplasmic membrane of the Mi1 (E) and Tm3 (F) neurons. White asterisks mark the position of the GFP-labeled cell bodies of the Mi1 and Tm3 neurons. All scale bars: 20  $\mu$ m. Me, medulla; Lo, lobula; LP, lobula plate.



The decision about which approach to use for the identification of cholinergic neurons should be based on the driver line inspected. For the Gal4 lines with a narrow expression pattern and the split-Gal4 lines, the FRT-STOP-FRT-VAcHt::HA allele is the tool of choice. When using the FRT-STOP-FRT-VAcHt::HA allele, there is no need for further experiments to determine which neurites contain presynaptic release sites. In contrast, for the Gal4 lines with a broader expression pattern, the examined neurons should instead be tested for co-localization with the expression pattern of the ChAT Trojan-MiMIC driver line (Venken et al., 2011; Diao et al., 2015), the VAcHt-LexA knock-in line (Simpson, 2016) or with ChAT antisera (Takagawa and Salvaterra, 1996).

A previously reported method for synaptic tagging with recombination using bruchpilot protein as a general marker of presynaptic release sites (Chen et al., 2014) served as an inspiration for the generation of the transgenic allele described in this study. The combination of the conditionally tagged bruchpilot protein and the conditionally tagged VAcHt might enable enumeration of the total presynaptic release sites and cholinergic release sites simultaneously in a single neuron, assuming that a specific and sparse Gal4 line is provided.

#### Acknowledgements

We would like to thank B. Dickson, M. Harrison, A. Nern, K. O'Connor-Giles, F. Schnorrer, J. Wildonger, Bloomington *Drosophila* Stock Center and Developmental Studies Hybridoma Bank for the flies and reagents. Fly embryo injections were performed by BestGene Inc. We would like to thank W. Essbauer and M. Sauter for technical assistance.

#### Competing interests

The authors declare no competing or financial interests.

#### Author contributions

K.P. conceived and performed the experiments and wrote the manuscript. A.B. revised the manuscript.

#### Funding

This work was supported by the Max-Planck-Gesellschaft. Deposited in PMC for immediate release.

#### References

- Ammer, G., Leonhardt, A., Bahl, A., Dickson, B. J. and Borst, A. (2015). Functional specialization of neural input elements to the *Drosophila* ON motion detector. *Curr. Biol.* **25**, 2247–2253.
- Aso, Y., Hattori, D., Yu, Y., Johnston, R. M., Iyer, N. A., Ngo, T. T., Dionne, H., Abbott, L. F., Axel, R., Tanimoto, H. et al. (2014). The neuronal architecture of the mushroom body provides a logic for associative learning. *Elife* **3**, e04577.
- Barnstedt, O., Oswald, D., Felsenberg, J., Brain, R., Moszynski, J.-P., Talbot, C. B., Perrat, P. N. and Waddell, S. (2016). Memory-relevant mushroom body output synapses are cholinergic. *Neuron* **89**, 1237–1247.
- Behnia, R., Clark, D. A., Carter, A. G., Clandinin, T. R. and Desplan, C. (2014). Processing properties of ON and OFF pathways for *Drosophila* motion detection. *Nature* **512**, 427–430.
- Bianco, J., Pandey, R., Wasser, M. and Udolph, G. (2011). Orthodenticle is necessary for survival of a cluster of clonally related dopaminergic neurons in the *Drosophila* larval and adult brain. *Neural Dev.* **6**, 34.
- Böttcher, R., Hollmann, M., Merk, K., Nitschko, V., Obermaier, C., Philippou-Massier, J., Wieland, I., Gaul, U. and Förstemann, K. (2014). Efficient chromosomal gene modification with CRISPR/cas9 and PCR-based homologous recombination donors in cultured *Drosophila* cells. *Nucleic Acids Res.* **42**, e89.
- Brand, A. H. and Perrimon, N. (1993). Targeted gene expression as a means of altering cell fates and generating dominant phenotypes. *Development* **118**, 401–415.
- Chen, Y., Akin, O., Nern, A., Tsui, C. Y. K., Pecot, M. Y. and Zipursky, S. L. (2014). Cell-type-specific labeling of synapses *in vivo* through synaptic tagging with recombination. *Neuron* **81**, 280–293.
- Daniels, R. W., Collins, C. A., Gelfand, M. V., Dant, J., Brooks, E. S., Krantz, D. E. and DiAntonio, A. (2004). Increased expression of the *Drosophila* vesicular glutamate transporter leads to excess glutamate release and a compensatory decrease in quantal content. *J. Neurosci.* **24**, 10466–10474.
- Diao, F., Ironfield, H., Luan, H., Diao, F., Shropshire, W. C., Ewer, J., Marr, E., Potter, C. J., Landgraf, M. and White, B. H. (2015). Plug-and-play genetic access to *Drosophila* cell types using exchangeable exon cassettes. *Cell Rep.* **10**, 1410–1421.
- Featherstone, D. E., Rushton, E. M., Hilderbrand-Chae, M., Phillips, A. M., Jackson, F. R. and Brodie, K. (2000). Presynaptic glutamic acid decarboxylase is required for induction of the postsynaptic receptor field at a glutamatergic synapse. *Neuron* **27**, 71–84.
- Fei, H., Grygoruk, A., Brooks, E. S., Chen, A. and Krantz, D. E. (2008). Trafficking of vesicular neurotransmitter transporters. *Traffic* **9**, 1425–1436.
- Fei, H., Chow, D. M., Chen, A., Romero-Calderón, R., Ong, W. S., Ackerson, L. C., Maidment, N. T., Simpson, J. H., Frye, M. A. and Krantz, D. E. (2010). Mutation of the *Drosophila* vesicular GABA transporter disrupts visual figure detection. *J. Exp. Biol.* **213**, 1717–1730.
- Gratz, S. J., Cummings, A. M., Nguyen, J. N., Hamm, D. C., Donohue, L. K., Harrison, M. M., Wildonger, J. and O'Connor-Giles, K. M. (2013). Genome engineering of *Drosophila* with the CRISPR RNA-guided Cas9 nuclease. *Genetics* **194**, 1029–1035.
- Greer, C. L., Grygoruk, A., Patton, D. E., Ley, B., Romero-Calderon, R., Chang, H.-Y., Houshyar, R., Bainton, R. J., Diantonio, A. and Krantz, D. E. (2005). A splice variant of the *Drosophila* vesicular monoamine transporter contains a conserved trafficking domain and functions in the storage of dopamine, serotonin, and octopamine. *J. Neurobiol.* **64**, 239–258.
- Haag, J., Arenz, A., Serbe, E., Gabbiani, F. and Borst, A. (2016). Complementary mechanisms create direction selectivity in the fly. *Elife* **5**, e17421.
- Henry, G. L., Davis, F. P., Picard, S. and Eddy, S. R. (2012). Cell type-specific genomics of *Drosophila* neurons. *Nucleic Acids Res.* **40**, 9691–9704.
- Hsu, P. D., Scott, D. A., Weinstein, J. A., Ran, F. A., Konermann, S., Agarwala, V., Li, Y., Fine, E. J., Wu, X., Shalem, O. et al. (2013). DNA targeting specificity of RNA-guided Cas9 nucleases. *Nat. Biotechnol.* **31**, 827–832.
- Jennett, A., Rubin, G. M., Ngo, T.-T. B., Shepherd, D., Murphy, C., Dionne, H., Pfeiffer, B. D., Cavallaro, A., Hall, D., Jeter, J. et al. (2012). A GAL4-driver line resource for *Drosophila* neurobiology. *Cell Rep.* **2**, 991–1001.
- Jinek, M., Chylinski, K., Fonfara, I., Hauer, M., Doudna, J. A. and Charpentier, E. (2012). A programmable dual-RNA-guided DNA endonuclease in adaptive bacterial immunity. *Science* **337**, 816–821.
- Kitamoto, T., Wang, W. and Salvaterra, P. M. (1998). Structure and organization of the *Drosophila* cholinergic locus. *J. Biol. Chem.* **273**, 2706–2713.
- Kitamoto, T., Xie, X., Wu, C.-F. and Salvaterra, P. M. (2000). Isolation and characterization of mutants for the vesicular acetylcholine transporter gene in *Drosophila melanogaster*. *J. Neurobiol.* **42**, 161–171.
- Kolodziejczyk, A., Sun, X., Meinertzhagen, I. A. and Nässel, D. R. (2008). Glutamate, GABA and acetylcholine signaling components in the lamina of the *Drosophila* visual system. *PLoS ONE* **3**, e2110.
- Lai, S. L. and Lee, T. (2006). Genetic mosaic with dual binary transcriptional systems in *Drosophila*. *Nat. Neurosci.* **9**, 703–709.
- Lee, T. and Luo, L. (1999). Mosaic analysis with a repressible cell marker for studies of gene function in neuronal morphogenesis. *Neuron* **22**, 451–461.
- Maisak, M. S., Haag, J., Ammer, G., Serbe, E., Meier, M., Leonhardt, A., Schilling, T., Bahl, A., Rubin, G. M., Nern, A. et al. (2013). A directional tuning map of *Drosophila* elementary motion detectors. *Nature* **500**, 212–216.
- Mauss, A. S., Meier, M., Serbe, E. and Borst, A. (2014). Optogenetic and pharmacologic dissection of feedforward inhibition in *Drosophila* motion vision. *J. Neurosci.* **34**, 2254–2263.
- Mauss, A. S., Pankova, K., Arenz, A., Nern, A., Rubin, G. M. and Borst, A. (2015). Neural circuit to integrate opposing motions in the visual field. *Cell* **162**, 351–362.
- Monastirioti, M., Gorczyca, M., Rapus, J., Eckert, M., White, K. and Budnik, V. (1995). Octopamine immunoreactivity in the fruit fly *Drosophila melanogaster*. *J. Comp. Neurol.* **356**, 275–287.
- Nagoshi, E., Sugino, K., Kula, E., Okazaki, E., Tachibana, T., Nelson, S. and Rosbash, M. (2010). Dissecting differential gene expression within the circadian neuronal circuit of *Drosophila*. *Nat. Neurosci.* **13**, 60–68.
- Romero-Calderón, R., Uhlenbrock, G., Borycz, J., Simon, A. F., Grygoruk, A., Yee, S. K., Shyer, A., Ackerson, L. C., Maidment, N. T., Meinertzhagen, I. A. et al. (2008). A glial variant of the vesicular monoamine transporter is required to store histamine in the *Drosophila* visual system. *PLoS Genet.* **4**, e1000245.
- Simpson, J. H. (2016). Rationally subdividing the fly nervous system with versatile expression reagents. *J. Neurogenet.* **30**, 185–194.
- Shinomiya, K., Karuppudurai, T., Lin, T.-Y., Lu, Z., Lee, C.-H. and Meinertzhagen, I. A. (2014). Candidate neural substrates for off-edge motion detection in *Drosophila*. *Curr. Biol.* **24**, 1062–1070.
- Takagawa, K. and Salvaterra, P. (1996). Analysis of choline acetyltransferase protein in temperature sensitive mutant flies using newly generated monoclonal antibody. *Neurosci. Res.* **24**, 237–243.
- Takemura, S. Y., Karuppudurai, T., Ting, C. Y., Lu, Z., Lee, C. H. and Meinertzhagen, I. A. (2011). Cholinergic circuits integrate neighboring visual signals in a *Drosophila* motion detection pathway. *Curr. Biol.* **21**, 2077–2084.

- Takemura, S. Y., Bharioke, A., Lu, Z., Nern, A., Vitaladevuni, S., Rivlin, P. K., Katz, W. T., Olbris, D. J., Plaza, S. M., Winston, P. et al.** (2013). A visual motion detection circuit suggested by *Drosophila* connectomics. *Nature* **500**, 175-181.
- Thomas, A., Lee, P.-J., Dalton, J. E., Nomie, K. J., Stoica, L., Costa-Mattioli, M., Chang, P., Nuzhdin, S., Arbeitman, M. N. and Dierick, H. A.** (2012). A versatile method for cell-specific profiling of translated mRNAs in *Drosophila*. *PLoS ONE* **7**, e40276.
- Venken, K. J. T., Schulze, K. L., Haelterman, N. A., Pan, H., He, Y., Evans-Holm, M., Carlson, J. W., Levis, R. W., Spradling, A. C., Hoskins, R. A. et al.** (2011). MiMIC: a highly versatile transposon insertion resource for engineering *Drosophila melanogaster* genes. *Nat. Methods* **8**, 737-743.
- Yuan, Q., Lin, F., Zheng, X. and Sehgal, A.** (2005). Serotonin modulates circadian entrainment in *Drosophila*. *Neuron* **47**, 115-127.
- Zhang, X., Koolhaas, W. H. and Schnorrer, F.** (2014). A versatile two-step CRISPR- and RMCE-based strategy for efficient genome engineering in *Drosophila*. *G3* **4**, 2409-2418.
- Zhang, Y. Q., Rodesch, C. K. and Broadie, K.** (2002). Living synaptic vesicle marker: synaptotagmin-GFP. *Genesis* **34**, 142-145.

# 3 | DISCUSSION

## 3.1 MECHANISM UNDERLYING DIRECTION SELECTIVITY IN THE T4 AND T5 NEURONS

The HR model of direction selectivity assumes that the theoretical motion-detecting unit receives two excitatory inputs while the BL model, by contrast, requires presence of one excitatory and one inhibitory input (Figures 8 and 9). The power of the genome-wide transcriptome analysis of the T4 and T5 neurons is that it reveals information about the expression levels of all neurotransmitter receptors expressed, the excitatory as well as inhibitory ones. One of the hypotheses that the transcriptome analysis of the T4 and T5 neurons aimed to test was whether the T4 and T5 neurons only receive excitatory inputs. In such situation, the possibility that the T4 and T5 neurons follow the BL model of direction selectivity could be excluded. This, however, turned out not to be the case as the T4 and T5 neurons express depolarizing receptors for acetylcholine along with the hyperpolarizing receptors for GABA and glutamate.

Recent evidence revealed that the mechanism for direction selectivity in the T4 and T5 neurons is indeed a combination of both, the HR as well as the BL model (Fisher (b) et al., 2015; Haag et al., 2016; Leong et al., 2016; Strother et al., 2017). As the two major cell types providing input to T4 neurons, the Mi1 and Tm3 cells, were identified as cholinergic (Strother et al., 2017; Takemura et al., 2017; this dissertation), the question arises which neurons provide null direction inhibition to the T4 neurons. The possible candidates are the GABAergic Mi4 cells, glutamatergic Mi9 cells and the newly described GABAergic CT1 neurons (Strother et al., 2017, Takemura et al., 2017).

The identified input neurons to T5 neurons appear to be all cholinergic (Raghu et al., 2011; Shinomiya et al., 2014). This poses a question what the neuronal substrate for the inhibitory mechanism acting on the level

of T5 neurons (Leong et al., 2016) during null direction motion is. As the newly identified GABAergic CT1 neurons also possess presynaptic release sites in the lobular layer 1 where the dendrites of the T5 neurons are found (Takemura et al., 2017), the CT1 neurons are the likely candidates. The plausible molecular substrates for the null direction inhibition in the T4 and T5 neurons appear to be the GABA and the GluCl $\alpha$  receptor subunits (Strother et al., 2017; this dissertation). As the null direction inhibition is likely conveyed by a GABAergic neuron (Strother et al., 2017; Takemura et al., 2017), the depletion of GABAergic receptor subunits specifically in the T4 and T5 neurons should affect their direction tuning. Downregulation of the GluCl $\alpha$  in the T4 and T5 neurons has been shown to affect fly behavioral response to moving ON edges (Strother et al., 2017). The role of GluCl $\alpha$  in the direction tuning of the T4 and T5 cells has not been tested yet.

Both models of direction selectivity, the HR as well as BL, propose existence of a time delay in one of the inputs. However, the biophysical mechanism underlying this feature is still unresolved. The temporal offsets of the input neurons in both, the ON and OFF channels, have been measured by calcium imaging of axon terminals (Serbe et al., 2016; Arenz et al., 2017). Although delayed signal propagation is observable at the level of axon terminals of some input neurons, the implementation of the neuronal cell types to a theoretical model that is based solely on the measured differential temporal filtering of neurons is not fully consistent with the reported synaptic strength of the input neurons to T4 cells (Arenz et al., 2017; Strother et al., 2017; Takemura et al., 2017).

### **3.2 VGAT IN T4 AND T5 NEURONS**

The most surprising finding learned from the transcriptome analysis of the T4 and T5 neurons was the expression of VGAT in these cells. The expression of VGAT in the T4 and T5 neurons was further confirmed by showing that the T4 and T5 neurons are part of the expression pattern of the VGAT-LexA knock-in line (Simpson, 2016; this dissertation). Nevertheless, it is not clear what the role of VGAT in the T4 and T5 neurons is. To create hypotheses about the function of VGAT in the T4 and T5 neurons, first, it is necessary to understand where in the neurons VGAT localizes. The confinement of VGAT to axons or dendrites that contain synaptic vesicles would indicate a role in neurotransmission.

Previously reported antibody staining using VGAT antiserum did not detect presence of VGAT in the cell bodies of the T4 and T5 neurons (Mauss et al., 2014), suggesting that subcellular localization of VGAT might be restricted to their neuronal processes. To identify presence of VGAT in the neurites, two different approaches can be employed: generation of a conditional tagged VGAT knock-in line or detection of VGAT using a previously described antibody with super-resolution microscopy techniques.

### *3.2.1 Approach to generate a conditional knock-in of the VGAT gene*

Using the same strategy as described in this dissertation for the generation of the FRT-STOP-FRT-VChT::HA allele, a conditional tagged VGAT line may be generated as well. However, one attempt to produce such line with the CRISPR/Cas9 system already failed because of off-target breaks in the DNA which led to multiple unspecific insertions of the donor fragment and possibly also chromosomal rearrangements. To decrease the likelihood of the unspecific DNA cleavages, choosing an sgRNA with minimal number of the predicted off-targets should be the first step. Amongst other measures reported to suppress unwanted off-target breaks, for instance, the use of truncated sgRNA with only 18 nucleotides instead of 20 has been shown to increase the specificity of the CRISPR/Cas9-mediated cleavages in mammalian cells without sacrificing on-target editing efficiency (Fu et al., 2014). Also, the employment of nickase Cas9 to mediate two single-strand breaks in the adjacent sites instead of one double-break cleavage promotes higher specificity and has been shown to function in *Drosophila* (Port et al., 2014).

### *3.2.2 Approach to visualize VGAT using super-resolution microscopy*

Another possibility to characterize localization of VGAT in the T4 and T5 neurons requires immunostaining with an antibody against VGAT followed by detection of the staining inside of the neurites of the T4 and T5 cells using super-resolution microscopy techniques such as STORM or STED. As the diameter of the presynaptic active zone in *Drosophila* neurons is approximately 200nm (Maglione and Sigrist, 2013), in order to reliably localize the VGAT signal in the processes of a studied neuron, the required resolution in all three dimensions must be below 100nm and

must allow to reconstitute the thinnest neuronal branches as hollow tubes.

The STED microscopy offers significantly improved resolution compared to traditional confocal microscopy. Nevertheless, when used to image tissue blocks, the acquired resolution is often suboptimal due to high sensitivity of STED microscopy to light scattering. Despite reported improvements on the optical clearing of the samples (Ke et al., 2016), imaging of thin neurites in dense neuropils requires further optimization.

STORM microscopy has been demonstrated to provide resolution of up to 20nm in plane, however, the axial resolution is limited by the extent of the evanescent field illumination that reaches to 100–200 nm. Possible improvement can be achieved by employing ultra-thin tissue sectioning. In the sectioned tissue, the thickness of the slices determines the z-axis resolution. So far, slices of brain tissue with 70nm thickness were already obtained and imaged (Sigal et al., 2015). Although certainly achievable, the use of super-resolution techniques to detect the localization of VGAT in the T4 and T5 neurons requires establishment of new protocols for sample preparation.

### 3.2.3 Possible roles of VGAT

The expression of VGAT in the T4 and T5 neurons in the absence of GABA-synthesizing enzyme *Gad1* is intriguing and opens door for several hypotheses explaining the function of VGAT in these cells. In *Drosophila*, the only known function of VGAT is the transport of GABA into synaptic vesicles. In mammals, however, VGAT transports also glycine (Chaudhry et al., 1998) and in is capable of transporting  $\beta$ -alanine in an *in vitro* assay (Juge et al., 2013). Recent evidence implies that glycine might be a previously unrecognized neurotransmitter in fruit flies (Frenkel et al., 2017), nevertheless, it is not clear yet whether VGAT is involved in its transport into synaptic vesicles. The  $\beta$ -alanine has been shown to open *D. melanogaster* Rdl receptors expressed in oocytes (McGonigle and Lummis, 2010). In the fly brain,  $\beta$ -alanine localizes mainly to the glial cells in retina and lamina where it serves as a substrate for the conversion of histamine into carcinine (Borycz et al., 2002). There is no evidence for the synaptic function of  $\beta$ -alanine *in vivo* in the brain of a fruit fly.

The VGAT in T4 and T5 neurons might transport also GABA, provided that GABA is synthesized in the T4 and T5 neurons by other means than by glutamate decarboxylase Gad1. For instance, in the mammalian dopaminergic midbrain neurons, GABA is synthesized by aldehyde dehydrogenase in the absence of glutamate decarboxylase (Kim et al., 2015). Interestingly, aldehyde dehydrogenase (Aldh) is also expressed in the T4 and T5 neurons as revealed by the transcriptome analysis (this dissertation). GABA is also synthesized in the mammalian glial cells in the absence of glutamate decarboxylase by the enzyme monoamine oxidase B (Yoon et al., 2014). Although this enzyme has in *D. melanogaster* a predicted homologue based on the structural similarity, the CG5653 gene, this gene is not expressed in the T4 and T5 neurons (this dissertation). A hypothetical synthesis of GABA by GABA transaminase which normally degrades GABA was already suggested previously (Tritsch et al., 2014). The GABA transaminase is expressed in the T4 and T5 neurons (this dissertation) and presence of this enzymes speaks in favor of the hypothesis that GABA is present in the T4 and T5 cells. Nevertheless, it is not clear what role GABA transaminase has in the T4 and T5 neurons and whether it is involved in the metabolism of GABA. Detectable GABA immunoreactivity would confirm dual neurotransmitter phenotype of the T4 and T5 neurons. However, the cell bodies of the T4 and T5 neurons are not immunopositive for GABA (K. Pankova, unpublished observation). This, nevertheless, does not confirm the absence of GABA at the presynaptic release sites of the T4 and T5 neurons.

To speculate about a hypothetical role of the VGAT-mediated inhibitory output of the T4 and T5 neurons on the circuit level, first, it is necessary to establish whether VGAT localizes to the axons of the T4 and T5 neurons in the lobula plate or to their dendrites that also possess presynaptic release sites (Takemura et al., 2013; Takemura et al., 2017; this dissertation) or to both. The synaptic output of the T4 and T5 axons onto LPTCs and LPi neurons has been shown to be excitatory and cholinergic (Mauss et al., 2014; this dissertation), therefore, the potential recipient of the inhibition from the T4 and T5 neurons in the lobula plate must be some other neuronal type. As there is no electron microscopy-based reconstruction of neuronal connections in the lobula plate available, such hypothetical candidate neuron cannot be specified any further. On the other hand, if VGAT localizes to the dendrites of the T4 and T5 cells in the medulla and lobula, the neurons that might receive theoretical

inhibitory synaptic input from the T4 neurons are identified (Takemura et al., 2013; Takemura et al., 2017). The dendrites of the T4 neurons provide synaptic input to the TmY15, CT1, Mi9, C3 and other T4 cells (Takemura et al., 2013; Takemura et al., 2017). As VAcHT is present in the dendritic presynaptic release sites (this dissertation), some of the inputs that T4 cell dendrites provide to these neurons are certainly cholinergic.

When considering the number of similarities between the organization of the motion vision circuits in flies and mammals, the dendro-dendritic connections among the T4 cells are the most likely candidates for the hypothetical VGAT-mediated inhibition. The functional analogues of the T4 and T5 neurons in mammalian retina are starburst amacrine cells (SACs), the first direction-selective neurons in the mammalian retina (Euler et al., 2002). SACs have been shown to co-release two neurotransmitters: acetylcholine and GABA (O'Malley et al., 1992). Similar to T4 neurons, SACs also form dendro-dendritic synapses among themselves (Ding et al., 2016). The GABAergic SAC-SAC synapses shape the direction selectivity of SACs, although the effect of this inhibition is not very strong (Ding et al., 2016). Blocking of the GABAergic SAC-SAC transmission results in decreased direction selectivity of SACs under high-velocity and high-contrast conditions (Ding et al., 2016). Would that also be the case in the T4 and T5 neurons of *Drosophila*?

Interestingly, the direction tuning of the T4 and T5 neurons with blocked synaptic output including their dendro-dendritic connections was measured for a range of velocities (Haag et al., 2016) (Figure 10).

Despite the authors' conclusion that no differences in the direction tuning could be found (Haag et al., 2016), a close comparison of the response properties of the T4 and T5 neurons with dendro-dendritic signaling intact and blocked differs when high velocity stimuli are presented. Nevertheless, the contribution of the VGAT-mediated inhibition to these differences is in the light of current evidence still just a speculation.

### **3.3 INHIBITORY ROLE OF GLUTAMATE IN NEURONAL CIRCUITS**

The substrate for the inhibitory action of glutamate in fruit flies is the glutamate-gated chloride channel that is encoded by the *GluCl $\alpha$*  gene (Cully et al., 1996). The *GluCl* receptors appear to be unique to nervous systems of invertebrates and are not found in mammals. Since the first



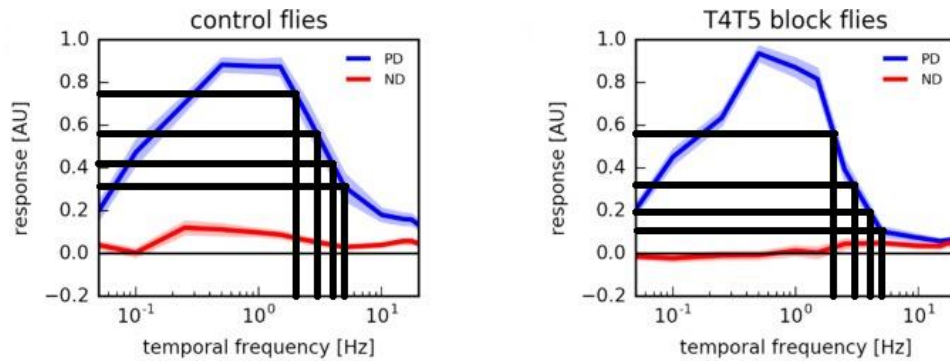


**Figure 10. Direction tuning of the T4 and T5 neurons.** (Adapted from Haag et al., 2016). Responses properties of the axons of T4T5 neurons in the lobula plate layer 3 to grating moving at various velocities either upward (preferred direction, PD) or downward (null direction, ND) measured using a calcium indicator. The responses of the control flies to high velocities PD stimuli are larger than those of the T4T5 block flies, suggesting that synapses among the T4T5 neurons might be necessary to retain direction-selectivity at higher velocities.

demonstration of the inhibitory function of glutamate in the olfactory system of fruit flies (Liu et al., 2013), the inhibitory role of glutamate has been indicated also in the LPTCs and T4 and T5 neurons in the neuronal circuit for motion vision (Mauss et al., 2014; Strother et al., 2017; this dissertation).

From the evolutionary perspective, the two different effects of glutamate at the synapse in invertebrates, depolarizing and hyperpolarizing, may provide a possibility to easily exchange the sign of the signal transduced to the postsynaptic neuron. Switching the expression to the particular type of glutamate receptor in the postsynaptic neurons might be a more flexible way of changing the computation performed by a circuit compared to altering the enzymatic machinery involved in neurotransmitter synthesis and transport in the presynaptic neuron.

Another possible advantage for the existence of a neurotransmitter capable of exerting two different effects, depolarization as well as hyperpolarization, might be the increased range of computations performed on a dendrite with differentially distributed excitatory and inhibitory glutamate-gated receptors. Moreover, having another inhibitory neurotransmitter in addition to GABA in the fruit fly nervous system may increase the range and flexibility of synaptic inhibition (Liu et al., 2013).

Despite the lack of GluCl receptors in mammals, the hyperpolarizing effect of glutamate has also been reported to take place in mammalian retina. The mammalian photoreceptors release glutamate as a response to light decrements. The presence of ionotropic glutamate-gated channels on the OFF bipolar neurons explains their depolarization as a response to light decrements (DeVries and Schwartz, 1999; DeVries, 2000). Nevertheless, the more interesting is the mechanism that conveys the information about light increments. The binding of glutamate to the metabotropic receptors on the ON bipolar cells leads to the activation of a second messenger cascade that triggers closure of the non-selective cation channel TRPM1 (Nawy and Jahr, 1990; Masu et al., 1995; Koike et al., 2010). As there is less glutamate released from photoreceptors as a response to light increments, the TRPM1 cation channels open and cause depolarization of the ON bipolar cell. Thus, the inhibitory role of glutamate in the mammalian ON bipolar cells is mediated counterintuitively via channel closure, not its opening. The inhibitory function of glutamate acting via metabotropic receptors has not been demonstrated in fruit flies, yet.

### **3.4 PROS AND CONS OF THE FRT-STOP-FRT-VACHT::**HA** ALLELE**

The previously reported approaches to detect acetylcholine-releasing neurons include ChAT antiserum (Takagawa and Salvaterra, 1996), ChAT Trojan-MiMIC driver lines (Venken et al., 2011; Diao et al., 2015) or the VAcHT-LexA knock-in line (Simpson, 2016). Despite the different working principles, these three tools function in a very similar manner: they all visualize the complete expression pattern of the cholinergic neurons in a fly brain. The neurons of interest to be tested for the cholinergic phenotype are labelled using a binary expression system with transgene such as GFP. Then, the co-localization (or lack of it) of the GFP signal with the expression pattern of the cholinergic neurons determines whether the neurons of interest are cholinergic or not. In practice, the major issue is that the labelling of the cholinergic neurons with the aforementioned tools is often ambiguous and for the weakly labelled neurons it is hard to judge whether they belong to the cholinergic expression pattern or not. In such cases, the FRT-STOP-FRT-VAcHT::**HA** allele can be particularly helpful. To use the FRT-STOP-FRT-VAcHT::**HA** allele in an experiment, the allele needs to be combined with a GAL4 line, UAS-FLP construct and a reporter gene construct such as UAS-GFP.

In order to understand the role of any neuron in a neuronal circuit, it is necessary to identify which of its neuronal branches are dendritic and which are axonal. To address this question, a commonly used approach in *D. melanogaster* is the expression of tagged proteins participating at the neurotransmitter release sites such as HA-tagged synaptotagmin (Robinson et al., 2002) or GFP-tagged n-synaptobrevin (Zhang et al., 2002). The advantage of the FRT-STOP-FRT-VACHT::HA allele in comparison to the other approaches to detect acetylcholine-releasing neurons is that it enables direct visualization of the cholinergic release sites in a single experiment, without the need to further determine which branches of the examined neuron release neurotransmitter.

A drawback of using the FRT-STOP-FRT-VACHT::HA allele is that it can lead to uncertainties when using GAL4 lines with broad expression patterns. The problematic are cases when the GAL4 expression pattern includes weakly expressing neurons or neurons that express GAL4 only transiently during development. For an illustration, let us consider a hypothetical situation in which a neuron with FRT-STOP-FRT-VACHT::HA allele expresses two UAS constructs, UAS-GFP and UAS-FLP. In extreme scenario, this neuron produces only one protein molecule from each of the UAS constructs. The expression of the GFP would be impossible to visualize because the amount of the protein produced is too low. However, if the one molecule of FLP flips the stop cassette out, the amount of VACHT::HA in the neuron (assuming the neuron is cholinergic) would be easily detectable. Indeed, in practice, we observed presence of HA tag in several GAL4 lines in neurons with barely detectable expression of GFP. For this reason, a care should be taken that the GAL4 line tested has an expression pattern as narrow as possible. Otherwise, it may happen that the tested neuron is falsely identified as cholinergic because of the VACHT::HA localized in the branches of an adjacent, weakly labelled neuron.

The FRT-STOP-FRT-VACHT::HA line described in this work expresses a red fluorescent protein dsRed in all photoreceptors using the P3 promoter of the rhodopsin genes. The 3xP3-DsRed sequence is commonly used as a marker of the successful integration of a transgenic sequence into host genome. Once the transformants are identified, the 3xP3-DsRed sequence can be removed from genome assuming that it is flanked by excisable transposase or recombinase recognition sites. The FRT-STOP-FRT-VACHT::HA allele was not designed to have the 3xP3-DsRed sequence

removed. Nevertheless, this had no observable effects on the FLP-mediated recombination events and the functionality of the allele.

### 3.5 CONCLUSION

The important breakthrough in the field of *Drosophila* motion vision research came with the demonstration that the two conceptually different theoretical models of direction selectivity, the HR and the BL model, act together to ensure the direction-selective response properties of the T4 and T5 neurons. This termination of dichotomy in the field was documented by several lines of evidence provided by different labs (Fisher (b) et al., 2015; Haag et al., 2016; Leong et al., 2016; Strother et al., 2017; this dissertation).

Mapping of the neurons to the components of theoretical models requires information about both, the connectivity established by electron microscopy-based reconstructions as well as the functional characterization of the neuronal response properties. As the recent studies provided detailed characterization of the neurons in motion vision circuit on the structural and also functional level (Serbe et al., 2016, Yang et al., 2016; Arenz et al., 2017; Strother et al., 2017; Takemura et al., 2017; this dissertation), the current focus of research shifts more towards understanding of the computations that take place in this circuit on the molecular level. Conveniently, the rise of novel powerful techniques such as RNA-seq and CRISPR/Cas9-based genome editing greatly facilitates such efforts. Obtaining the transcriptome data from other neurons participating in the motion vision circuit as well as generating the cell type-specific tools to visualize and knock down receptors and channels involved in neuronal computations is necessary to gain deeper understanding of processes that underlie visual detection of motion in *D. melanogaster*.

## 4 | BIBLIOGRAPHY

**Adams, M. D., Celniker, S. E., Holt, R. A., Evans, C. A., Gocayne, J. D., Amanatides, P. G., Scherer, S. E., Li, P. W., Hoskins, R. A., Galle, R. F. et al.** (2000). The genome sequence of *Drosophila melanogaster*. *Science*, Mar 24;287(5461):2185-95.

**Alderson, T.** (1965). Chemically induced delayed germinal mutation in *Drosophila*. *Nature*, Jul 10;207(993):164-167.

**Ammer, G., Leonhardt, A., Bahl, A., Dickson, B. J. and Borst, A.** (2015). Functional specialization of neural input elements to the *Drosophila* ON motion detector. *Curr Biol*, Aug 31;25(17):2247-53.

**Arenz, A., Drews, M. S., Richter, F. G., Ammer, G. and Borst, A.** (2017). The temporal tuning of the *Drosophila* motion detectors is determined by the dynamics of their input elements. *Curr Biol*, Apr 3;27(7):929-944.

**Balazs, R., Machiyama, Y., Hammond, B. J., Julian, T. and Richter, D.** (1970). The operation of the gamma-aminobutyrate bypath of the tricarboxylic acid cycle in brain tissue in vitro. *Biochem J*, Feb; 116(3):445-61.

**Barlow, H. B. and Levick, W.R.** (1965). The mechanism of directionally selective units in the rabbit's retina. *J. Physiol.* Jun;178(3):477-504.

**Barrangou, R., Fremaux, C., Deveau, H., Richards, M., Boyaval, P., Moineau, S., Romero, D. A. and Horvath, P.** (2007). CRISPR provides acquired resistance against viruses in prokaryotes. *Science*, Mar 23;315(5819):1709-12.

**Behnia, R., Clark, D. A., Carter, A. G., Clandinin, T. R. and Desplan, C.** (2014). Processing properties of ON and OFF pathways for *Drosophila* motion detection. *Nature*, Aug 28;512(7515):427-30.

**Besson, M. T., Soustelle, L. and Birman, S.** (1999). Identification and structural characterization of two genes encoding glutamate transporter

homologues differently expressed in the nervous system of *Drosophila melanogaster*. *FEBS Lett*, Jan 25;443(2):97-104.

**Borst, A. and Helmstaedter, M.** (2015). Common circuit design in fly and mammalian motion vision. *Nat Neurosci*, Aug;18(8):1067-76.

**Borycz, J., Borycz, J. A., Loubani, M. and Meinertzhagen, I. A.** (2002). tan and ebony genes regulate a novel pathway for transmitter metabolism at fly photoreceptor terminals. *J Neurosci*, Dec 15;22(24):10549-57.

**Brand, A. H. and Perrimon, N.** (1993). Targeted gene expression as a means of altering cell fates and generating dominant phenotypes. *Development*, Jun;118(2):401-15.

**Burg, M. G., Sarthy, P. V., Koliantz, G. and Pak, W. L.** (1993). Genetic and molecular identification of a *Drosophila* histidine decarboxylase gene required in photoreceptor transmitter synthesis. *EMBO J*, Mar;12(3):911-9.

**Cao, G., Platisa, J., Pieribone, V. A., Raccuglia, D., Kunst, M. and Nitabach, M. N.** (2013). Genetically targeted optical electrophysiology in intact neural circuits. *Cell*, Aug 15;154(4):904-13.

**Chase, B. A. and Kankel, D. R.** (1987). A genetic analysis of glutamatergic function in *Drosophila*. *J Neurobiol*, Jan;18(1):15-41.

**Chaudhry, F. A., Reimer, R. J., Bellocchio, E. E., Danbolt, N. C., Osen, K. K., Edwards, R. H. and Storm-Mathisen, J.** (1998). The vesicular GABA transporter, VGAT, localizes to synaptic vesicles in sets of glycinergic as well as GABAergic neurons. *J Neurosci*, 1998 Dec 1;18(23):9733-50.

**Chen, T. W., Wardill, T. J., Sun, Y., Pulver, S. R., Renninger, S. L., Baohan, A., Schreiter, E. R., Kerr, R. A., Orger, M. B., Jayaraman, V. et al.** (2013). Ultrasensitive fluorescent proteins for imaging neuronal activity. *Nature*, Jul 18;499(7458):295-300.

**Chen, W. F., Maguire, S., Sowcik, M., Luo, W., Koh, K. and Sehgal, A.** (2015). A neuron-glia interaction involving GABA transaminase contributes to sleep loss in sleepless mutants. *Mol Psychiatry*, Feb;20(2):240-51.

**Chiang, A. S., Lin, C. Y., Chuang, C. C., Chang, H. M., Hsieh, C. H., Yeh, C. W., Shih, C. T., Wu, J. J., Wang, G. T., Chen, Y. C. et al.** (2011). Three-

dimensional reconstruction of brain-wide wiring networks in *Drosophila* at single-cell resolution. *Curr Biol*, Jan 11;21(1):1-11.

**Corey, J. L., Quick, M. W., Davidson, N., Lester, H. A. and Guastella, J.** (1994). A cocaine-sensitive *Drosophila* serotonin transporter: cloning, expression, and electrophysiological characterization. *Proc Natl Acad Sci U S A*, Feb 1;91(3):1188-92.

**Cully, D. F., Paress, P. S., Liu, K. K., Schaeffer, J. M. and Arena, J. P.** (1996). Identification of a *Drosophila melanogaster* glutamate-gated chloride channel sensitive to the antiparasitic agent avermectin. *J Biol Chem*, Aug 16;271(33):20187-91.

**Daniels, R. W., Collins, C. A., Gelfand, M. V., Dant, J., Brooks, E. S., Krantz, D. E. and DiAntonio, A.** (2004). Increased expression of the *Drosophila* vesicular glutamate transporter leads to excess glutamate release and a compensatory decrease in quantal content. *J Neurosci*, Nov 17;24(46):10466-74.

**Demchyshyn, L. L., Pristupa, Z. B., Sugamori, K. S., Barker, E. L., Blakely, R. D., Wolfgang, W. J., Forte, M. A. and Niznik, H. B.** (1994). Cloning, expression, and localization of a chloride-facilitated, cocaine-sensitive serotonin transporter from *Drosophila melanogaster*. *Proc Natl Acad Sci U S A*, May 24;91(11):5158-62.

**DeVries, S. H. and Schwartz, E. A.** (1999). Kainate receptors mediate synaptic transmission between cones and 'Off' bipolar cells in a mammalian retina. *Nature*, 397(6715):157-60.

**DeVries, S. H. (2000).** Bipolar cells use kainate and AMPA receptors to filter visual information into separate channels. *Neuron*, 28(3):847-56.

**Diao, F., Ironfield, H., Luan, H., Diao, F., Shropshire, W. C., Ewer, J., Marr, E., Potter, C. J., Landgraf, M. and White, B. H.** (2015). Plug-and-play genetic access to *Drosophila* cell types using exchangeable exon cassettes. *Cell Rep*, Mar 3;10(8):1410-21

**Ding, H., Smith, R. G., Poleg-Polsky, A., Diamond, J. S. and Briggman, K. L.** (2016). Species-specific wiring for direction selectivity in the mammalian retina. *Nature*, Jul 7;535(7610):105-10.

**Eichner, H., Joesch, M., Schnell, B., Reiff, D. F. and Borst, A.** (2011). Internal structure of the fly elementary motion detector. *Neuron*, Jun 23; 70(6):1155-64

- Euler, T., Detwiler, P. B. and Denk, W. (2002).** Directionally selective calcium signals in dendrites of starburst amacrine cells. *Nature*, Aug 22;418(6900):845-52.
- Fei, H., Chow, D. M., Chen, A., Romero-Calderón, R., Ong, W. S., Ackerson, L. C., Maidment, N. T., Simpson, J. H., Frye, M. A. and Krantz, D. E. (2010).** Mutation of the *Drosophila* vesicular GABA transporter disrupts visual figure detection. *J Exp Biol*, May;213(Pt 10):1717-30.
- Featherstone, D. E., Rushton, E. M., Hilderbrand-Chae, M., Phillips, A. M., Jackson, F. R. and Broadie, K. (2000).** Presynaptic glutamic acid decarboxylase is required for induction of the postsynaptic receptor field at a glutamatergic synapse. *Neuron*, Jul;27(1):71-84.
- Fischbach, K. F. and Dittrich, A. P. (1989).** The optic lobe of *Drosophila melanogaster*. I. A Golgi analysis of wild-type structure. *Cell Tissue Res*, 258:441-475.
- Fisher (a), Y. E., Leong, J. C., Sporar, K., Ketkar, M. D., Gohl, D. M., Clandinin, T. R. and Silies, M. A. (2015).** Class of visual neurons with wide-field properties is required for local motion detection. *Curr Biol*, Dec 21;25(24):3178-89.
- Fisher (b), Y. E., Silies, M. and Clandinin, T. R. (2015).** Orientation selectivity sharpens motion detection in *Drosophila*. *Neuron*, Oct 21;88(2):390-402.
- Frenkel, L., Muraro, N. I., Beltrán González, A. N., Marcora, M. S., Bernabó, G., Hermann-Luibl, C., Romero, J. I., Helfrich-Förster, C., Castaño, E. M., Marino-Busjle, C. et al. (2017).** Organization of circadian behavior relies on glycinergic transmission. *Cell Rep*, Apr 4;19(1):72-85.
- Friggi-Grelin, F., Coulom, H., Meller, M., Gomez, D., Hirsh, J. and Birman, S. (2003).** Targeted gene expression in *Drosophila* dopaminergic cells using regulatory sequences from tyrosine hydroxylase. *J Neurobiol*, Mar;54(4):618-27.
- Fu, Y., Sander, J. D., Reyon, D., Cascio, V. M., Joung, J. K. (2014).** Improving CRISPR-Cas nuclease specificity using truncated guide RNAs. *Nat Biotechnol*, Mar;32(3):279-84.



- Gisselmann, G., Pusch, H., Hovemann, B. T. and Hatt, H.** Two cDNAs coding for histamine-gated ion channels in *D. melanogaster*. *Nat Neurosci*, Jan;5(1):11-2.
- Greer, C. L., Grygoruk, A., Patton, D. E., Ley, B., Romero-Calderon, R., Chang, H. Y., Houshyar, R., Bainton, R. J., Diantonio, A. and Krantz, D.E.** (2005). A splice variant of the *Drosophila* vesicular monoamine transporter contains a conserved trafficking domain and functions in the storage of dopamine, serotonin, and octopamine. *J Neurobiol*, Sep 5;64(3):239-58.
- Golic, K. G. and Lindquist, S.** (1989). The FLP recombinase of yeast catalyzes site-specific recombination in the *Drosophila* genome. *Cell*, Nov 3;59(3):499-509.
- Golic, K. G.** (1991). Site-specific recombination between homologous chromosomes in *Drosophila*. *Science*, May 17;252(5008):958-61.
- Gong, Y., Huang, C., Li, J. Z., Grewe, B. F., Zhang, Y., Eismann, S. and Schnitzer, M. J.** (2015). High-speed recording of neural spikes in awake mice and flies with a fluorescent voltage sensor. *Science*, Dec 11;350(6266):1361-6.
- Gratz, S. J., Cummings, A. M., Nguyen, J. N., Hamm, D. C., Donohue, L. K., Harrison, M. M., Wildonger, J. and O'Connor-Giles, K. M.** (2013). Genome engineering of *Drosophila* with the CRISPR RNA-guided Cas9 nuclease. *Genetics*, Aug;194(4):1029-35.
- Haag, J., Arenz, A., Serbe, E., Gabbiani, F. and Borst, A.** (2016). Complementary mechanisms create direction selectivity in the fly. *Elife*, Aug 9;5. pii: e17421.
- Haas, R., Marshall, T. L. and Rosenberry, T. L.** (1988). *Drosophila* acetylcholinesterase: demonstration of a glycoinositol phospholipid anchor and an endogenous proteolytic cleavage. *Biochemistry*, 27(1): 6453-6457.
- Hardie, R. C.** (1989). A histamine-activated chloride channel involved in neurotransmission at a photoreceptor synapse. *Nature*, Jun 29; 339(6227):704-6.
- Hassenstein, V. and Reichardt, W.** (1956). [System theoretical analysis of time, sequence and sign analysis of the motion perception of the snout-beetle *Chlorophanus*]. *Z Naturforsch B*. 1956; 11b:513-524. German.

- Jenett, A., Rubin, G. M., Ngo, T. T., Shepherd, D., Murphy, C., Dionne, H., Pfeiffer, B. D., Cavallaro, A., Hall, D., Jeter, J. et al. (2012).** A GAL4-driver line resource for *Drosophila* neurobiology. *Cell Rep*, 2012 Oct 25;2(4):991-1001.
- Jinek, M., Chylinski, K., Fonfara, I., Hauer, M., Doudna, J. A. and Charpentier, E. (2012).** A programmable dual-RNA-guided DNA endonuclease in adaptive bacterial immunity. *Science*, Aug 17;337(6096):816-21.
- Joesch, M., Plett, J., Borst, A. and Reiff, D. F. (2008).** Response properties of motion-sensitive visual interneurons in the lobula plate of *Drosophila melanogaster*. *Curr Biol*, Mar 11;18(5):368-74.
- Joesch, M., Schnell, B., Raghu, S. V., Reiff, D. F. and Borst, A. (2010).** ON and OFF pathways in *Drosophila* motion vision. *Nature*, Nov 11; 468(7321):300-4.
- Joesch, M., Weber, F., Eichner, H. and Borst, A. (2013).** Functional specialization of parallel motion detection circuits in the fly. *J Neurosci*, Jan 16; 33(3):902-5.
- Juge, N., Omote, H. and Moriyama, Y. (2013).** Vesicular GABA transporter (VGAT) transports  $\beta$ -alanine. *J Neurochem*, Nov;127(4):482-6.
- Kanamori, T., Togashi, K., Koizumi, H. and Emoto, K. (2015).** Dendritic remodeling: Lessons from invertebrate model systems. *Int Rev Cell Mol Biol*, 318:1-25.
- Karuppudurai, T., Lin, T. Y., Ting, C. Y., Pursley, R., Melnattur, K. V., Diao, F., White, B. H., Macpherson, L. J., Gallio, M., Pohida, T. et al. (2014).** A hard-wired glutamatergic circuit pools and relays UV signals to mediate spectral preference in *Drosophila*. *Neuron*, 2014 Feb 5;81(3):603-15.
- Ke, M. T., Nakai, Y., Fujimoto, S., Takayama, R., Yoshida, S., Kitajima, T. S., Sato, M. and Imai, T. (2016).** Super-resolution mapping of neuronal circuitry with an index-optimized clearing agent. *Cell Rep*, Mar 22;14(11):2718-32.
- Kidwell, M. G., Kidwell, J. F. and Sved, J. A. (1977).** Hybrid dysgenesis in *Drosophila melanogaster*: A syndrome of aberrant traits including mutation, sterility and male recombination. *Genetics*, Aug;86(4):813-33.

- Kim, J. I., Ganesan, S., Luo, S. X., Wu, Y. W., Park, E., Huang, E. J., Chen, L., Ding, J.B.** (2015) Aldehyde dehydrogenase 1a1 mediates a GABA synthesis pathway in midbrain dopaminergic neurons. *Science*, Oct 2; 350(6256):102-6.
- Kitamoto, T., Wang, W. and Salvaterra, P. M.** (1998). Structure and organization of the *Drosophila* cholinergic locus. *J Biol Chem*, Jan 30;273(5):2706-13.
- Koike, C., Obara, T., Uriu, Y., Numata, T., Sanuki, R., Miyata, K., Koyasu, T., Ueno, S., Funabiki, K., Tani, A. et al.** (2010). TRPM1 is a component of the retinal ON bipolar cell transduction channel in the mGluR6 cascade. *Proc Natl Acad Sci U S A*, Jan 5;107(1):332-7.
- Kolodziejczyk, A., Sun, X., Meinertzhagen, I. A. and Nässel, D. R.** (2008). Glutamate, GABA and acetylcholine signaling components in the lamina of the *Drosophila* visual system. *PLoS One*, May 7;3(5):e2110.
- Kvon, E. Z., Kazmar, T., Stampfel, G., Yáñez-Cuna, J. O., Pagani, M., Schernhuber, K., Dickson, B. J. and Stark, A.** (2014). Genome-scale functional characterization of *Drosophila* developmental enhancers in vivo. *Nature*, Aug 7;512(7512):91-5.
- Lemaitre, B., Nicolas, E., Michaut, L., Reichhart, J. M. and Hoffmann, J. A.** (1996). The dorsoventral regulatory gene cassette spätzle/Toll/cactus controls the potent antifungal response in *Drosophila* adults. *Cell*, Sep 20;86(6):973-83.
- Leong, J. C., Esch, J. J., Poole, B., Ganguli, S. and Clandinin, T. R.** (2016). Direction selectivity in *Drosophila* emerges from preferred-direction enhancement and null-direction suppression. *J Neurosci*, Aug 3;36(31):8078-92.
- Lewis, E.B.** (1978). A gene complex controlling segmentation in *Drosophila*. *Nature*, Dec 7;276(5688):565-70.
- Liu, W. W. and Wilson, R. I.** (2013). Glutamate is an inhibitory neurotransmitter in the *Drosophila* olfactory system. *Proc Natl Acad Sci U S A*, Jun 18;110(25):10294-9.
- Livingstone, M. S. and Tempel, B. L.** (1983). Genetic dissection of monoamine neurotransmitter synthesis in *Drosophila*. *Nature*, May 5-11;303(5912):67-70.
- Maisak, M. S., Haag, J., Ammer, G., Serbe, E., Meier, M., Leonhardt, A., Schilling, T., Bahl, A., Rubin, G. M., Nern, A. et al.** (2013). A

directional tuning map of *Drosophila* elementary motion detectors. *Nature*, Aug 8;500(7461):212-6.

**Maglione, M. and Sigrist, S. J.** (2013). Seeing the forest tree by tree: super-resolution light microscopy meets the neurosciences. *Nat Neurosci*, Jul;16(7):790-7.

**Malutan, T., McLean, H., Caveney, S. and Donly, C.** (2002). A high-affinity octopamine transporter cloned from the central nervous system of cabbage looper *Trichoplusia ni*. *Insect Biochem Mol Biol*, Mar 1;32(3):343-57.

**Martin, C. A. and Krantz, D. E.** (2014). *Drosophila melanogaster* as a genetic model system to study neurotransmitter transporters. *Neurochem Int*, Jul;73:71-88.

**Masu M, Iwakabe H, Tagawa Y, Miyoshi T, Yamashita M, Fukuda Y, Sasaki H, Hiroi K, Nakamura Y, Shigemoto R, et al.** (1995). Specific deficit of the ON response in visual transmission by targeted disruption of the mGluR6 gene. *Cell*, Mar 10;80(5):757-65.

**Mauss A. S., Meier, M., Serbe, E. and Borst, A.** (2014). Optogenetic and pharmacologic dissection of feedforward inhibition in *Drosophila* motion vision. *J Neurosci*, Feb 5;34(6):2254-63.

**Meinertzhagen, I. A. and O'Neil, S. D.** (1991). Synaptic organization of columnar elements in the lamina of the wild type in *Drosophila melanogaster*. *J Comp Neurol*, Mar 8;305(2):232-63.

**McGonigle, I. and Lummis, S. C.** (2010). Molecular characterization of agonists that bind to an insect GABA receptor. *Biochemistry*, Apr 6;49(13):2897-902.

**Monastirioti, M., Gorczyca, M., Rapus, J., Eckert, M., White, K. and Budnik, V.** (1995). Octopamine immunoreactivity in the fruit fly *Drosophila melanogaster*. *J Comp Neurol*, May 29;356(2):275-87.

**Monastirioti, M., Linn, C. E. and White, K.** (1996). Characterization of *Drosophila* tyramine beta-hydroxylase gene and isolation of mutant flies lacking octopamine. *J Neurosci*, Jun 15;16(12):3900-11.

**Morante, J. and Desplan, C.** (2008). The color-vision circuit in the medulla of *Drosophila*. *Curr Biol*, Apr 22;18(8):553-65.

**Muller, H. J.** (1927). Artificial transmutation of the gene. *Science*, Jul 22;66(1699):84-7.

- Nawy, S. and Jahr, C. E.** (1990). Suppression by glutamate of cGMP-activated conductance in retinal bipolar cells. *Nature*, Jul 19;346(6281):269-71.
- Neckameyer, W. S. and Cooper, R. L.** (1998). GABA transporters in *Drosophila melanogaster*: molecular cloning, behavior, and physiology. *Invert Neurosci*, ;3:279-94.
- Nüsslein-Volhard, C. and Wieschaus, E.** (1980). Mutations affecting segment number and polarity in *Drosophila*. *Nature*, Oct 30;287(5785):795-801.
- O'Malley, D. M., Sandell, J. H. and Masland, R. H.** (1992). Co-release of acetylcholine and GABA by the starburst amacrine cells. *J Neurosci*, Apr; 12(4):1394-408.
- Parikh, V., St Peters, M., Blakely, R. D. and Sarter, M.** (2013). The presynaptic choline transporter imposes limits on sustained cortical acetylcholine release and attention. *J Neurosci*, 33:2326-37.
- Pfeiffer, B. D., Jenett, A., Hammonds, A. S., Ngo, T. T., Misra, S., Murphy, C., Scully, A., Carlson, J. W., Wan, K. H., Laverly, T. R. et al.** (2008). Tools for neuroanatomy and neurogenetics in *Drosophila*. *Proc Natl Acad Sci U S A*, Jul 15;105(28):9715-20.
- Port, F., Chen, H. M., Lee, T. and Bullock, S. L.** (2014). Optimized CRISPR/Cas tools for efficient germline and somatic genome engineering in *Drosophila*. *Proc Natl Acad Sci U S A*, Jul 22;111(29):E2967-76.
- Pörzgen, P., Park, S. K., Hirsh, J., Sonders, M. S. and Amara, S. G.** (2001). The antidepressant-sensitive dopamine transporter in *Drosophila melanogaster*: a primordial carrier for catecholamines. *Mol Pharmacol*, Jan;59(1):83-95.
- Raghu, S., Reiff, D. F. and Borst, A.** (2011). Neurons with cholinergic phenotype in the visual system of *Drosophila*. *J Comp Neurol*, Jan 1;519(1):162-76.
- Reiff D. F., Plett, J., Mank, M., Griesbeck, O. and Borst, A.** (2010). Visualizing retinotopic half-wave rectified input to the motion detection circuitry of *Drosophila*. *Nat Neurosci*, Aug;13(8):973-8.
- Rivera-Alba, M., Vitaladevuni, S. N., Mishchenko, Y., Lu, Z., Takemura, S. Y., Scheffer, L., Meinertzhagen, I. A., Chklovskii, D. B. and de Polavieja, G. G.** (2011). Wiring economy and volume exclusion

determine neuronal placement in the *Drosophila* brain. *Curr Biol*, Dec 6;21(23):2000-5.

**Romero-Calderón, R., Uhlenbrock, G., Borycz, J., Simon, A. F., Grygoruk, A., Yee, S. K., Shyer, A., Ackerson, L. C., Maidment, N. T., Meinertzhagen, I. A. et al.** (2008). A glial variant of the vesicular monoamine transporter is required to store histamine in the *Drosophila* visual system. *PLoS Genet*, Nov;4(11):e1000245.

**Rubin, G. M. and Spradling, A. C.** (1982). Genetic transformation of *Drosophila* with transposable element vectors. *Science*, Oct 22;218(4570):348-53.

**Salvaterra, P. M. and McCaman, R. E.** (1985). Choline acetyltransferase and acetylcholine levels in *Drosophila melanogaster*: a study using two temperature-sensitive mutants. *J Neurosci*, Apr;5(4):903-10.

**Sarov, M., Barz, C., Jambor, H., Hein, M. Y., Schmied, C., Suchold, D., Stender, B., Janosch, S., KJ, V. V., Krishnan, R. T. et al.** (2016). A genome-wide resource for the analysis of protein localisation in *Drosophila*. *Elife*, Feb 20;5:e12068.

**Serbe, E., Meier, M., Leonhardt, A. and Borst, A.** (2016). Comprehensive characterization of the major presynaptic elements to the *Drosophila* OFF motion detector. *Neuron*, Feb 17;89(4):829-41.

**Schnell, B., Joesch, M., Forstner, F., Raghu, S. V., Otsuna, H., Ito, K., Borst, A. and Reiff, D. F.** (2010). Processing of horizontal optic flow in three visual interneurons of the *Drosophila* brain. *J Neurophysiol*, Mar;103(3):1646-57.

**Schnell, B., Raghu, S. V., Nern, A. and Borst, A.** (2012). Columnar cells necessary for motion responses of wide-field visual interneurons in *Drosophila*. *J Comp Physiol A*, May;198(5):389-95.

**Shinomiya, K., Karuppudurai, T., Lin, T. Y., Lu, Z., Lee, C. H. and Meinertzhagen, I. A.** (2014). Candidate neural substrates for off-edge motion detection in *Drosophila*. *Curr Biol*, May 19;24(10):1062-70.

**Sigal, Y. M., Speer, C. M., Babcock, H. P. and Zhuang, X.** (2015). Mapping synaptic input fields of neurons with super-resolution imaging. *Cell*. Oct 8;163(2):493-505.

**Simpson, J. H.** (2016). Rationally subdividing the fly nervous system with versatile expression reagents. *J Neurogenet*, Sep - Dec;30(3-4):185-194.

- Silies, M., Gohl, D. M., Fisher, Y. E., Freifeld, L., Clark, D. A. and Clandinin, T. R.** (2013). Modular use of peripheral input channels tunes motion-detecting circuitry. *Neuron*, Jul 10;79(1):111-27.
- Stenesen, D., Moehlman, A. T. and Krämer, H.** (2015). The carcinine transporter CarT is required in *Drosophila* photoreceptor neurons to sustain histamine recycling. *Elife*, Dec 14;4:e10972.
- Strother, J. A., Nern, A. and Reiser, M. B.** (2014). Direct observation of ON and OFF pathways in the *Drosophila* visual system. *Curr Biol*, May 5;24(9):976-83.
- Strother, J. A., Wu, S. T., Wong, A. M., Nern, A., Rogers, E. M., Le, J. Q., Rubin, G. M. and Reiser, M. B.** (2017). The emergence of directional selectivity in the visual motion pathway of *Drosophila*. *Neuron*, Apr 5;94(1):168-182.e10.
- Takagawa, K. and Salvaterra, P.** (1996). Analysis of choline acetyltransferase protein in temperature sensitive mutant flies using newly generated monoclonal antibody. *Neurosci Res*, Feb;24(3):237-43.
- Takemura, S. Y., Karuppururai, T., Ting, C. Y., Lu, Z., Lee, C. H. and Meinertzhagen, I. A.** (2011). Cholinergic circuits integrate neighboring visual signals in a *Drosophila* motion detection pathway. *Curr Biol*, Dec 20; 21(24):2077-84.
- Takemura, S. Y., Bharioke, A., Lu, Z., Nern, A., Vitaladevuni, S., Rivlin, P. K., Katz, W. T., Olbris, D. J., Plaza, S. M., Winston, P. et al.** (2013). A visual motion detection circuit suggested by *Drosophila* connectomics. *Nature*, Aug 8;500(7461):175-81.
- Takemura, S. Y., Nern, A., Chklovskii, D. B., Scheffer, L. K., Rubin, G. M. and Meinertzhagen, I. A.** (2017). The comprehensive connectome of a neural substrate for 'ON' motion detection in *Drosophila*. *Elife*, Apr 22;6. pii: e24394.
- Traiffort E, O'Regan S, Ruat M.** (2013). The choline transporter-like family SLC44: properties and roles in human diseases. *Mol Aspects Med*, 34:646-54.
- Tritsch, N. X., Oh, W. J., Gu, C. and Sabatini, B. L.** (2014). Midbrain dopamine neurons sustain inhibitory transmission using plasma membrane uptake of GABA, not synthesis. *Elife*, Apr 24; 3:e01936.

- Tuthill, J. C., Nern, A., Holtz, S. L., Rubin, G. M. and Reiser, M. B.** (2013). Contributions of the 12 neuron classes in the fly lamina to motion vision. *Neuron*, Jul 10;79(1):128-40.
- Tuthill, J. C., Nern, A., Rubin, G. M. and Reiser, M. B.** (2014). Wide-field feedback neurons dynamically tune early visual processing. *Neuron*, May 21;82(4):887-95.
- Venken, K. J., Schulze, K. L., Haelterman, N. A., Pan, H., He, Y., Evans-Holm, M., Carlson, J. W., Levis, R. W., Spradling, A. C., Hoskins, R. A. et al.** (2011). MiMIC: a highly versatile transposon insertion resource for engineering *Drosophila melanogaster* genes. *Nat Methods*, Sep;8(9):737-43.
- Wang, Z., Gerstein, M. and Snyder, M.** (2009). RNA-Seq: a revolutionary tool for transcriptomics. *Nat Rev Genet*, Jan; 10(1): 57-63.
- Wang, H., La Russa, M. and Qi, L. S.** (2016). CRISPR/Cas9 in genome editing and beyond. *Annu Rev Biochem*, Jun 2;85:227-64.
- Wernet, M. F., Perry, M. W. and Desplan, C.** (2015). The evolutionary diversity of insect retinal mosaics: common design principles and emerging molecular logic. *Trends Genet*, Jun;31(6):316-28.
- Yang, H. H., St-Pierre, F., Sun, X., Ding, X., Lin, M. Z. and Clandinin, T. R.** (2016). Subcellular imaging of voltage and calcium signals reveals neural processing in vivo. *Cell*, 2016 Jun 30;166(1):245-57.
- Yamaguchi, S., Wolf, R., Desplan, C. and Heisenberg, M.** (2008). Motion vision is independent of color in *Drosophila*. *Proc Natl Acad Sci U S A*, Mar 25;105(12):4910-5.
- Yamaguchi, S., Desplan, C. and Heisenberg, M.** (2010). Contribution of photoreceptor subtypes to spectral wavelength preference in *Drosophila*. *Proc Natl Acad Sci U S A*, Mar 23;107(12):5634-9.
- Yaniv, S. P. and Schuldiner, O.** (2016). A fly's view of neuronal remodeling. *Wiley Interdiscip Rev Dev Biol*, Sep;5(5):618-35.
- Yoon, B. E., Woo, J., Chun, Y. E., Chun, H., Jo, S., Bae, J. Y., An, H., Min, J. O., Oh, S. J., Han, K. S. et al.** (2014). Glial GABA, synthesized by monoamine oxidase B, mediates tonic inhibition. *J Physiol*, Nov 15;592(22):4951-68.
- Yuan, Q., Lin, F., Zheng, X. and Sehgal, A.** (2005). Serotonin modulates circadian entrainment in *Drosophila*. *Neuron*, Jul 7;47(1):115-27.



**Zheng, Y., Hirschberg, B., Yuan, J., Wang, A. P., Hunt, D. C., Ludmerer, S. W., Schmatz, D. M. and Cully, D. F.** (2002). Identification of two novel *Drosophila melanogaster* histamine-gated chloride channel subunits expressed in the eye. *J Biol Chem*, Jan 18;277(3):2000-5.

## Annex 1: LIST OF PUBLICATIONS

- 1) Mauss AS, Pankova K, Arenz A, Nern A, Rubin GM, Borst A. Neural circuit to integrate opposing motions in the visual field. *Cell*. 2015 Jul 16;162(2):351-62.
- 2) Pankova K, Borst A. RNA-seq transcriptome analysis of direction-selective T4/T5 neurons in *Drosophila*. *PLoS One*. 2016 Sep 29;11(9):e0163986.
- 3) Pankova K, Borst A. Transgenic line for the identification of cholinergic release sites in *Drosophila melanogaster*. *J Exp Biol*. 2017 Apr 15;220(Pt 8):1405-1410.

# Annex 2: CURRICULUM VITAE

## **CONTACT INFORMATION**

---

Name: Katarina Pankova  
Affiliation: Graduate School of System Neurosciences  
Ludwig Maximilian University, 80539 Munich, Germany  
Email: [pankova.katarina@gmail.com](mailto:pankova.katarina@gmail.com)

## **EDUCATION**

---

### **10/2010 – 08/2017 (expected)**

Fast-Track PhD student  
Graduate School of Systemic Neurosciences  
Ludwig Maximilian University, Munich, Germany

### **07/2013**

Student in the laboratory and lecture course Drosophila Neurobiology  
Cold Spring Harbor Laboratory, Cold Spring Harbor, USA

### **09/2006 - 06/2010**

BSc in Molecular Biology  
Charles University in Prague, Prague, Czech Republic

### **01/2008 - 06/2008**

Erasmus exchange program  
University of Aberdeen, Aberdeen, United Kingdom

## **RESEARCH EXPERIENCE**

---

**12/2011 – 01/2017**

Projects: Transsynaptic tracing with neurotropic viruses in *Drosophila*  
Neurotransmitters in the neuronal circuit for motion vision in  
*D. melanogaster*

A. Borst's lab, Max Planck Institute of Neurobiology, Martinsried,  
Germany

**11/2009 - 02/2010**

Undergraduate research project: Morphological analysis of the  
hippocampal neurons

I. Vida's lab, University of Glasgow, Glasgow, United Kingdom

**10/2008 - 06/2009**

Undergraduate research project: Mechanisms of invasiveness in tumor  
cells

J. Brabek's lab, Charles University in Prague, Czech Republic

## **CONFERENCES AND MEETINGS**

---

Munich Fly Retreat 2013, Ringberg, Germany – talk

GSN Retreat 2014, Spitzingsee, Germany – talk

Neurofly Meeting 2014, Heraklion, Crete – poster

Interact Meeting 2015, Munich, Germany – talk

GSN Retreat 2015, Chiemsee, Germany – poster

Neurobiology of *Drosophila* 2015, Cold Spring Harbor, USA – poster

Neurobiology of Mental Health 2016, Geneva, Switzerland – poster

## **PUBLICATIONS**

---

Pankova K, Borst A. Transgenic line for the identification of cholinergic release sites in *Drosophila melanogaster*. *J Exp Biol*. 2017 Apr 15;220(Pt 8):1405-1410.

Pankova K, Borst A. RNA-seq transcriptome analysis of direction-selective T4/T5 neurons in *Drosophila*. *PLoS One*. 2016 Sep 29;11(9):e0163986.

Mauss AS, Pankova K, Arenz A, Nern A, Rubin GM, Borst A. Neural circuit to integrate opposing motions in the visual field. *Cell*. 2015 Jul 16;162(2):351-62.

Pankova K, Rosel D, Novotny M, Brabek J. The molecular mechanisms of transition between mesenchymal and amoeboid invasiveness in tumor cells. *Cell Mol Life Sci*. 2010 Jan; 67(1):63-71. Review.

## **SCHOLARSHIPS AND AWARDS**

---

Erasmus program scholarship, 2008

Stipend for excellent study results, 2008

# **Annex 3: AFFIDAVIT/EIDESSTATTLICHE VERSICHERUNG**

I hereby confirm that the dissertation “Neurotransmitters in the neuronal circuit for motion vision in *Drosophila melanogaster*” is the result of my own work and that I have only used sources or materials listed and specified in the dissertation.

Hiermit versichere ich an Eides statt, dass ich die vorliegende Dissertation “Neurotransmitters in the neuronal circuit for motion vision in *Drosophila melanogaster*” selbstständig angefertigt habe, mich außer der angegebenen keiner weiteren Hilfsmittel bedient und alle Erkenntnisse, die aus dem Schrifttum ganz oder annähernd übernommen sind, als solche kenntlich gemacht und nach ihrer Herkunft unter Bezeichnung der Fundstelle einzeln nachgewiesen habe.

Munich, May 12<sup>th</sup>, 2017

.....

Katarina Pankova

## Annex 4: AUTHOR CONTRIBUTIONS

The author contributions to the publication “Neural circuit to integrate opposing motions in the visual field” by Alex S. Mauss, Katarina Pankova, Alexander Arenz, Aljoscha Nern, Gerald M. Rubin and Alexander Borst published in *Cell*, 2015 Jul 16;162(2):351-62 were as follows: A.S.M. performed and analyzed electrophysiological recordings. K.P. carried out and analyzed immunostainings (except multicolor labeling and TNT-E expression), transcript profiling, and GRASP experiments. A.A. performed and analyzed two-photon calcium imaging experiments. A.B. did computer simulations. G.M.R. and A.N. generated the LPi driver lines and performed multicolor stochastic labeling. A.S.M. and A.B. designed the study. A.S.M., A.A., and A.B. wrote the paper with the help of all authors.

The author contributions to the publication “RNA-seq transcriptome analysis of direction-selective T4/T5 neurons in *Drosophila*” by Katarina Pankova and Alexander Borst published in *PLoS One*, 2016 Sep 29;11(9):e0163986 were as follows: K.P. conceived and performed the experiments and wrote the manuscript. A.B. revised the manuscript.

The author contributions to the publication “Transgenic line for the identification of cholinergic release sites in *Drosophila melanogaster*” by Katarina Pankova and Alexander Borst published in *J Exp Biol*, 2017 Apr 15;220(Pt 8):1405-1410 were as follows: K.P. conceived and performed the experiments and wrote the manuscript. A.B. revised the manuscript.

I hereby certify that the information above is true and accurate.

Munich, May 12<sup>th</sup>, 2017 .....  
Katarina Pankova Alexander Borst